IMPROVING THE EFFICIENCY OF ABDOMINAL AORTIC ANEURYSM WALL STRESS COMPUTATIONS

By

Jaime Eduardo Zelaya, Jr.

A DISSERTATION

Presented to the Department of Biomedical Engineering
and the Oregon Health & Science University
School of Medicine
in partial fulfillment of
the requirements for the degree of

Doctor of Philosophy
In Biomedical Engineering

September 2014

School of Medicine

Oregon Health & Science University

CERTIFICATE OF APPROVAL

This is to certify that the Ph.D. dissertation of

Jaime Eduardo Zelaya, Jr.

has been approved

Sandra Rugonyi, Ph.D.
Associate Professor, Thesis Advisor

Amir-Farzin Azarbal, M.D.
Assistant Professor

George Giraud, M.D., Ph.D.
Professor

Mary M. Heinricher, Ph.D.
Professor

Monica T. Hinds, Ph.D.
Associate Professor

David B. Jacoby, M.D.
Director, MD/PhD Training Program
Chief, Pulmonary and Critical Care

For my mother, who is the most patient, kind, understanding, and wise person I know,

for God, Jesus Christ, the Holy Spirit, Virgen de Guadalupe, San Judas Tadeo, San Gabriel, my grandfathers, maternal grandmother, and uncle, who are my guides, inspiration, strength, and reason for my success

and for Dr. Lionsy, whose support and wisdom have helped me through difficult times.

TABLE OF CONTENTS

LIST OF TABLES

LIST OF FIGURES

LIST OF ABBREVIATIONS

AAA	Abdominal Aortic Aneurysm
ADAM	Aneurysm Detection and Management
ADINA	Automatic Dynamic Incremental Non-linear Analysis
AoD	Aortic Dissection
CT	Computed Tomography
FEA	Finite Element Analysis
G & R	Growth and Remodeling
ICA	Intracranial/Cerebral Aneurysm
ICP	Iterative Closest Point
ILT	Intraluminal Thrombus
IRB	Institutional Review Board
MCP-1	Monocyte Chemoattractant Protein-1
MMP	Matrix Metalloproteinase
MPR	Material Property Ratio
MRI	Magnetic Resonance Imaging
MTD	Maximum Transverse Diameter
OHSU	Oregon Health & Science University
P1	Polzer et al., First Material Model
P2	Polzer et al., Second Material Model
ROC	Receiver Operating Characteristic
RV	Raghavan-Vorp Material Model

SP	Segmentation Program/Procedure
TAA	Thoracic Aortic Aneurysm
USPSTF	United States Preventive Services Task Force

LIST OF SYMBOLS

θ	angle in relation to the opening angle ϕ
τ	average shear stress
Ω	body domain in the deformed configuration of the AAA model
$\sigma_{\theta\theta}$	Cauchy circumferential stress
σ_{zz}	Cauchy longitudinal, axial stress
σ_{rr}	Cauchy radial stress
$\boldsymbol{\sigma}$	Cauchy stress tensor
$\sigma_{\theta\theta 0}$	circumferential growth equilibrium stress
$\dot{\lambda}_{g\theta}$	circumferential growth rate
b_θ	circumferential proportionality constant
$\varepsilon_{\theta\theta}$	circumferential strain
$\alpha, \beta, \gamma, \zeta, \eta$	coefficients denoting the measure of stiffness of the AAA wall
$\alpha_{ref}, \beta_{ref}$	coefficients denoting the measure of stiffness of the AAA wall in the reference model
D_1, D_2	coefficients denoting the measure of stiffness of the ILT
c_1, c_2	constants
$\mathbf{F}$	deformation gradient tensor
∇	Del operator
d_i	distance between AAA outer wall surface node and corresponding lumen surface node
σ_{eff}	effective or von Mises stress

W	energy density function
$\mathbf{I_B}$	first invariant of the Left Cauchy-Green deformation tensor **B**
Z	height coordinate of the undeformed configuration
H	hydrostatic pressure
$\mathbf{I}$	identity tensor
ds	infinitesimal contour distance
$\boldsymbol{\varepsilon}$	infinitesimal strain tensor
a	inner radius of the deformed model
A	inner radius of the undeformed, unloaded, and unstressed model & open sector model
a_0	inner radius of the unloaded, closed configuration used in residual stress analysis
$\mathbf{B}$	Left Cauchy-Green deformation tensor
s	length parameter of contour at a time of interest
s'	length parameter of corresponding contour at a later time
$\dot{\lambda}_{gz}$	longitudinal growth rate
ε_{zz}	longitudinal strain
Γ_l	lumen surface of the deformed configuration of the AAA model
n_{L}	node of the lumen surface
dr'	normalized thickness differential
ϕ	opening angle
b	outer radius of the deformed model
B	outer radius of the undeformed, unloaded, and unstressed model &

	open sector model
b_0	outer radius of the unloaded, closed configuration used in residual stress analysis
Γ_o	outer surface of the deformed configuration of the AAA model
v	Poisson ratio
p	pressure
r	radial coordinate of the deformed configuration
R	radial coordinate of the undeformed configuration
u_r	radial displacement
$\dot{\lambda}_{gr}$	radial growth rate
b_r	radial proportionality constant
ε_{rr}	radial strain
$\mathbf{II_B}$	second invariant of the Left Cauchy-Green deformation tensor **B**
τ_0	shear growth equilibrium stress
b_τ	shear proportionality constant
$\sigma_{r\theta}$, σ_{rz}, $\sigma_{\theta z}$	shear stresses
C	stiffness tensor
σ_i	stress of interest (conventional or linear model; Cauchy radial, circumferential, or effective stress)
σ_i^*	stress of interest in the reference model
$\lambda_{\theta\theta}$	stretch ratio in the circumferential direction
λ_{zz}	stretch ratio in the longitudinal direction

λ_{rr}	stretch ratio in the radial direction
$\hat{\boldsymbol{n}}$	unit normal vector
h	wall thickness of the deformed configuration
h_0	wall thickness of the initial configuration of the reference model
E	Young's modulus

ACKNOWLEDGEMENTS

I extend thanks to the following individuals who made this dissertation and graduate training successful.

Dr. Sandra Rugonyi, PhD (S.R.), my mentor

Thesis Advisory and Oral Examination Committee:

Dr. Amir-Farzin Azarbal, MD (A.F.A.)

Dr. George Giraud, MD, PhD (G.G.)

Dr. Mary M. Heinricher, PhD (M.M.H.)

Dr. Monica T. Hinds, PhD (M.T.H.)

Dr. David B. Jacoby, MD (D.B.J.)

Friends and Colleagues:

Dr. Venkat Keshav Chivukula, PhD (V.K.C.)

Johanna Colgrove (J.C.)

Dr. Phong T. Dargon, MD (P.T.D.)

Dr. Rachel Dresbeck, PhD (R.D.)

Dr. Sevan Goenezen, PhD (S.G.)

Dr. Cindy Grimm, PhD (C.G.)

Sharon Kryger (S.K.)

Dr. Ly Phan, PhD (L.P.)

Michelle Vaughan (M.V.)

Dr. Xin Yin, PhD (X.Y.)

Specific contributions are listed below.

AAA FEA Idealized Model Preparation: Jaime E. Zelaya (J.E.Z.), self

AAA FEA Patient Model Preparation Program: S.G. (AAA wall), J.E.Z. (AAA-ILT)

AAA Geometry Extraction from CT scans: J.E.Z.

AAA Geometry Segmentation Software: X.Y. (SP1); M.V., C.G. (SP2)

AAA Patient CT & Data Collection: A.F.A., P.T.D., J.E.Z., S.K.

AAA Patient Database: A.F.A., OHSU Department of Surgery, Division of Vascular Surgery

AAA Programs for Assessing Growth, Computing Stress Distributions using Analytical Solutions, Computing Wall Stress Relative Differences, AAA Geometry Modification, etc.: J.E.Z.

AAA Nodal Correspondence Algorithm: L.P., C.G.

Counseling and Mentorship: S.R., S.G., A.F.A., D.B.J., G.G., M.M.H., M.T.H.

Dissertation Editing: J.E.Z., R.D., J.C., V.K.C., L.P., S.R., A.F.A., D.B.J., G.G., M.M.H., M.T.H.

Dissertation Oversight: S.R., A.F.A., G.G., M.M.H., M.T.H., D.B.J.

Dissertation Writing: J.E.Z.

Figure and Table Preparation: J.E.Z.

Chapter 3 (PLoS ONE Paper):

Analysis and interpretation: J.E.Z., S.G., A.F.A., S.R., G.G.

Concept and design: S.G., A.F.A., S.R.

Contributed reagents/materials/analysis tools: S.G., P.T.D., A.F.A.

Critical revision of the article: J.E.Z., S.R., S.G., A.F.A.

Derivation of Analytical Solution for Non-linear Hyperelastic Tissues: S.G. (main derivation), J.E.Z (derivation of $\sigma_{\theta\theta}$ and σ_{zz}).

Figure and Table Preparation: J.E.Z.

Final approval of the article: J.E.Z., S.G., P.T.D., A.F.A., S.R.

Obtained funding: S.R., J.E.Z.

Overall responsibility: J.E.Z., S.R.

Performed Experiments: J.E.Z., S.G., P.T.D.

Writing the article: J.E.Z., S.R.

The work presented in this dissertation was published in PLoS ONE. The dissertation abstract, third chapter, and Chapter 3 figures/tables were acquired from our published work. The third chapter has been slightly modified from its published form for use in this dissertation. According to the PLoS ONE Open Access Policy and Creative Commons Attribution (CC BY) license, an original work may be reprinted and reused without restriction and for any purpose as long as the original work is properly cited.

Funding:

This work was supported by the NSF DBI-1052688 grant *and a grant from the Oregon Clinical and Translational Research Institute (OCTRI),* i.e., National Center for Advancing Translational Sciences (NCATS) NIH **TL1TR000129.**

ABSTRACT [1]

An abdominal aortic aneurysm (AAA) is a pathological dilation of the abdominal aorta, which carries a high mortality rate if ruptured. The most commonly used surrogate marker of rupture risk in clinical practice is the maximal transverse diameter of the aneurysm. More recent studies suggest that wall stress derived from models of patient-specific aneurysm geometries extracted, for instance, from computed tomography images is a better predictor of rupture risk and an important factor in AAA size progression. However, quantification of wall stress is currently computationally intensive and time-consuming, mainly because AAA walls are modeled with nonlinear mechanical properties. This has limited the potential of computational models in clinical practice. To facilitate computation of wall stresses, we propose to use a linear approach that ensures equilibrium of wall stresses in the aneurysm. This proposed linear model is easy to implement and eliminates the burden of nonlinear computations. To assess the potential of our proposed approach for predicting patient wall stresses, results from both idealized and patient-specific model simulations were compared to those obtained using conventional approaches and to those of a hypothetical, reference abdominal aortic aneurysm model in which wall mechanical properties and the initial unloaded and unstressed configuration were assumed to be known. Our linear approach closely approximated the reference wall stresses for varying model geometries and wall material properties. Our findings suggest that the linear approach could be used as an effective, efficient, and easy-to-use clinical tool to estimate patient-specific wall stresses and ultimately identify AAAs with high rupture risk.

CHAPTER 1: INTRODUCTION

An abdominal aortic aneurysm is a local, abnormal dilation of the abdominal aorta whose maximum transverse diameter (MTD) exceeds 30 mm [2][3][4][5]. Although the pathogenesis and progression of an AAA are not clearly understood, the processes are believed to be influenced by a complex interplay between biological and hemodynamic factors that culminates in a rupture, leading to hemorrhagic shock and death [6][7]. About 80% of the patients with acute ruptured aneurysms who reach a hospital perish, and about 50% of patients who receive emergent surgical repair survive [4][5]. Since survival is low for ruptured AAAs, the most promising practices for improving clinical outcomes are early diagnosis and careful surveillance and management. But early diagnosis is often difficult because the majority of AAAs are asymptomatic until rupture [4][8][9]. AAAs are often detected incidentally during computed tomography (CT) imaging [5][10]. For patients that have been diagnosed with an AAA, the aneurysm is managed by measuring the size of the MTD on ultrasound, CT scan, or magnetic resonance imaging (MRI). AAA rupture risk is known to increase with aneurysm size [11]. The current guidelines recommend surgical repair when the MTD of the AAA reaches 55 mm, or is observed to grow at a rate of greater than 10 mm/year [2].

Use of the MTD for determining AAA rupture risk is concerning because 0-23% of aneurysms smaller than 55 mm have been reported to rupture, whereas 60% of larger AAAs have not ruptured [7][11][12][13][14][15]. Thus, in employing the MTD, clinicians overestimate the stability of smaller aneurysms and expose patients with larger aneurysms to unnecessary surgery. A more sensitive and specific marker for assessing AAA rupture risk is therefore needed. A lack of appropriate rupture risk predictors is the main AAA management problem, and experts from multiple disciplines are working with

physicians to address the issue. The most promising contributions are arising from the field of biomechanics, which has identified wall stress as a better predictor of risk.

Wall stress has been targeted as a predictor for rupture, because, from a mechanical standpoint, AAA rupture occurs when the local stresses on the wall exceed its strength. Thus, assessment of stress distributions throughout the aneurysmal wall could offer important insight about areas more prone to rupture. Compared to the peak transverse diameter, computed wall stress has been reported to better determine which patients were in need of emergent repair [13][16][17][18][19][20].

Wall stress is nevertheless not employed in the clinic because it cannot be directly measured but must be computed using finite element analysis (FEA). Further, current approaches for computing wall stress are time-intensive and difficult. One difficulty in computation is the conventional modeling of AAA tissue as a nonlinear hyperelastic material, i.e., a material in which tissue strain is not proportional to stress (see **Fig. 1**). Strain is a measure of the deformation that a body experiences due to an applied load, compared to the body's original shape. In contrast to nonlinear materials, for a linear material, the stress-strain relationships are proportional, and wall stress computations are therefore simpler and quickly achieved. Although linear computations are more efficient, further research is needed to determine if linear elasticity with small deformations can be used to approximate AAA wall stress. The principal goal of this thesis project is to determine if the modeling of AAA tissues as linear elastic materials with small deformations is an effective, efficient approach for computing patient wall stresses. Improving the efficiency of wall stress computations will help stress-based methods

become promising clinical tools that will better identify patients requiring emergent repair.

The remainder of this chapter will provide further background on what is currently done in the clinic to detect and manage AAAs and on how current strategies are not effective for determining a given patient's rupture risk. Furthermore, the rationale for considering wall stress as a predictor for AAA rupture, which includes an explanation of the role of stress and biological factors in the formation of an AAA, will be provided. The chapter closes with a brief introduction of a few approaches currently used for computing wall stresses and their limitations.

Chapter 2 will discuss the methods employed in this work for computing subject-specific AAA wall stresses. These methods include the acquisition of subject-specific CT scans and relevant medical information, i.e., blood pressure; the extraction of AAA geometries from CT scans in the form of a mesh; and the preparation of AAA meshes and FEA models of aneurysms for the computation of wall stresses.

The heart of the thesis research is found in Chapter 3. To address the thesis objective, we need to determine how well patient wall stresses are predicted by modeling AAAs with linear elastic properties. To perform the analysis, the stresses computed using the linear model need to be compared to a reference wall stress distribution as well as to stresses computed using conventional approaches (see **Fig. 2**) [1]. An ideal reference stress distribution would have been the actual stresses in a patient AAA, but these values cannot be determined because the following are clinically unknown: 1) the patient-specific material properties of the aneurysm; and 2) the initial unloaded AAA configuration. Thus, we generated a hypothetical reference model of an AAA, where we

assumed that we knew the initial unloaded configuration and the tissue properties. We simulated the reference AAA with nonlinear hyperelastic properties described by the Raghavan-Vorp (RV) material model, which is widely used in the field [16][18][21][22][23][24][25][26][27]. The material properties were determined by performing uniaxial tensile testing experiments on AAA tissue samples excised from cadavers or patients undergoing elective repair [28]. Because the reference model material properties and initial configuration were assumed to be known, the computed wall stresses hypothetically served as accurate representations of the stresses in the deformed reference AAA. This deformed, loaded configuration of the reference model represented the CT geometry of the AAA (see **Fig. 2**). The CT geometry was then assumed to be unloaded and unstressed and served as the initial configuration of the conventional and linear models. Assuming an unloaded, unstressed CT geometry is what is typically done in the field before computing wall stresses [23][29][30]. In the conventional model, the AAA was assumed with RV population average material property values and large deformations. The linear model was simulated as a linear material with small deformations. The small displacements of the linear model allowed for the preservation of the CT geometry after blood pressure was applied to the model lumen surface—this was not observed when the conventional approach was used. The wall stresses computed for the linear model were then compared to those of the reference model to assess the potential of the linear model to predict the reference stresses. Wall stress comparisons were also achieved between the conventional and reference models. Reference, conventional, and linear models were developed for idealized representations

of an AAA under different pressures, dimensions, and material properties, as well as for patient-specific AAAs.

Chapter 4 summarizes the general conclusions of the thesis project and presents ideas for future work, which includes a study that evaluates the effectiveness of the linear model for differentiating ruptured AAAs from non-ruptured cases. Chapter 4 also discusses potential applications of the linear model. Examples include using the linear model to 1) elucidate the role that wall stress plays in AAA expansion, which is poorly understood; and 2) predict rupture risk in thoracic aortic aneurysms (TAAs), intracranial/cerebral aneurysms (ICAs), and in thoracic aortic dissections, which are separations of the aortic wall layers caused by blood entering a tear in the thoracic aorta.

Overall, this research attempts to facilitate the consideration of stress-based methods for use in the clinic to assess subject-specific aneurysmal rupture risk and to identify patients in need of emergent repair. If successful, more patient lives will be saved, and fewer patients will undergo unnecessary surgery.

1.1 AAA Epidemiology, Detection, and Management

1.1.1 *AAA Epidemiology*

AAA risk increases with advancing age, and AAAs are more common in white people compared to other races [4][5][31][32][33][34]. Racial differences in AAA prevalence are notable among men, where whites are 2-3 times more likely to suffer from AAA-specific mortality compared to African American men [33]. Low odds ratios of AAA risk were also reported for other races compared to whites, but the findings were

not significant [34]. The racial differences in AAA occurrence and mortality among women are minimal [33][35]. AAAs are most prevalent in white men between the ages of 65 and 83 [5][36]. The prevalence of AAAs in age-equivalent white females is 3.9-6 times less common than in their male counterparts [5][31][32][37]. Even though women constitute a smaller fraction of AAA patients, the risk of rupture and death is much higher than in men, and rupture occurs at smaller aneurysmal sizes [11][32][38][39][40]. A study that assessed the relative importance of AAA size in determining rupture risk in 3,138 men and 907 women reported that the AAA diameter was significantly lower in women (i.e., mean ± SD, 61 ± 14 mm in men vs. 58 ± 13 mm in women, $p < 0.001$), even in the ruptured AAA subgroup (78 ± 19 mm in men vs. 71 ± 21 mm in women, $p < 0.001$) [41][42]. Annually, the incidence of new AAA diagnoses is 3.5 per 1,000 person years [43], and the incidence of rupture is 10.6 per 100,000 person years, with about 7,000-30,000 American deaths [4][32][44].

1.1.2 *AAA Detection*

AAA rupture deaths could be prevented if the aneurysms were diagnosed early, but the majority of AAAs are silent and asymptomatic [45] and are often detected incidentally on CT scans or ultrasound. If ruptured, the AAAs carry a 90% mortality risk [7][14].

Given the high lethality of ruptured AAAs, studies have been conducted to determine if screening for AAAs confers a benefit in reducing AAA mortality risk. One population-based randomized controlled trial evaluated the benefits of ultrasound screening for AAAs in reducing mortality in a cohort of men aged 65-83 years [36].

Ultrasound was selected because of its safety, low cost, and high sensitivity and specificity [46][47]. Screening reduced the overall death rates for men of ages 65 to 75, especially for those with a history of smoking, but not older. A similar population-based ultrasound screening study was conducted, involving a cohort of women [31]. The study reported that ultrasound screening did not result in a reduction in AAA mortality risk in women [48][49]. Following the collective findings, the United States Preventive Services Task Force (USPSTF) recommends ultrasound screening once in men between the ages 65-75 with any history of smoking [31][50] but does not recommend screening women [31].

1.1.3 *AAA Management*

Once an AAA is detected, proper management is indispensable to reduce the risk of rupture and includes pharmacological therapy, life-style modification, observation, surgery, or a combination of these [31][51]. Prior to surgery, the most important element of AAA management is observation. Through observation, clinicians can measure the AAA's maximum transverse diameter (MTD), which is the current clinically accepted marker used for predicting rupture risk and determining intervention [11][17][52][53]. According to Brewster et al., AAAs that are small (e.g., MTD of 30-39 mm), typically have lower rupture risk than intermediate AAAs (MTD of 40-54 mm) and large AAAs (MTDs $\geq$ 55 mm) (about 0% vs. about 0.5-5% vs. 3-50%, respectively) [5][11][54]. The choice of imaging modality used for monitoring an AAA is dependent on the MTD. Because of a lower risk of rupture, small AAAs are generally managed with ultrasound surveillance every 2-3 years [5][31]. The frequency of monitoring increases to every 3-12

months when the aneurysm's MTD grows to 40-55 mm [5][31]. Larger AAAs can be monitored with imaging at a surveillance frequency of 1-6 months, but surgical repair is recommended for AAAs exceeding 55 mm, provided that the patient qualifies for surgery and the surgical risks do not outweigh the benefits [5][55]. For AAAs growing at a rate of 5 mm every 0.5 years regardless of size, a CT scan is recommended to detect possible hemorrhage, since these aneurysms have a high risk for rupturing [5][31]. For symptomatic AAAs, repair is indicated [31][49][56][57][58][59][60]. A summary of the recommendations for AAA management through observation is found in **Table 1**.

If the AAA ruptures, emergent repair is needed [5][49][57][61][62]. Surgical options for AAA patients either consist of endovascular or open surgical repair [5][57][63][64][65]. Although surgical repair of larger aneurysms is indicated due to the increase in rupture risk with size, the question of whether early repair confers a benefit in AAAs smaller than 55 mm remains to be addressed. This is because smaller AAAs have been observed to rupture [7][13], even though their rupture risks are reported as low [11]. To determine the benefits of an early surgical repair compared to ultrasound surveillance in smaller AAAs, the Aneurysm Detection and Management (ADAM) study and the United Kingdom Small Aneurysm Trial performed randomized clinical controlled trials, where older men with AAAs of 40-55 mm were randomly assigned to ultrasound surveillance or early surgical repair [66][67]. Subjects were monitored for a period of 3.5-8 years with death as the primary endpoint [67]. According to the studies, surgical repair of intermediate-sized aneurysms did not seem to confer a long term survival benefit compared to surveillance [66][67]. But a subsequent study of the UK trial, where the follow-up period was extended to 9 years, revealed a survival advantage in men who

received early surgical repair [11]. More studies are needed to determine the benefits of early surgical repair, especially since uncertainty exists as to what AAA size is the best threshold for conducting surgical repair, while ensuring that the surgical risks do not outweigh the benefits of treatment. Because aneurysms smaller than 55 mm have been reported to rupture and AAAs with larger diameters have been observed to not rupture [7][13][68], the use of the maximum transverse diameter as a reliable predictor for rupture is questionable and a better marker is needed.

1.2 Rationale for Consideration of Wall Stress as a Predictor of Risk and the Dual Role of Mechanical and Biological Factors in AAA Development and Progression

1.2.1 *Role of Wall Stress in the Pathogenesis, Progression and Remodeling of an AAA*

Wall stress has been targeted as a predictor of risk because AAA rupture is a mechanical problem, where the forces that are exerted on the wall exceed the wall strength. Additionally, wall stress has been regarded as one of the crucial factors involved in the pathogenesis, growth and remodeling of an AAA [69][70][71][72].

The formation and progression of an AAA are not fully understood but are believed to be the result of a complex interplay between wall stresses and biological processes, e.g., inflammation [6], that affect aneurysmal wall maintenance [73]. The pathogenesis of an AAA is partly thought to arise from the repeated loading imposed on the aorta, which results in the wearing of elastin fibers and sheets in the medial layer of the aorta as one ages [6]. For an aneurysmal tissue, the content of elastin has been found to be significantly lower than in non-aneurysmal tissue [74]. Another histological change

observed in aneurysmal tissue is that the levels of collagen have been found to be both higher and lower compared to normal tissue, with increased collagen breakdown especially noted in ruptured AAAs [71][74][75][76]. An increase in collagen production and loss of elasticity stiffens the AAA wall, resulting in an increase in the blood's pulse wave velocity, a widened pulse pressure and an increase in hemodynamic stress [4][77]. The increased stress contributes to further elastin degeneration and aortic dilation [77].

An AAA's rupture risk increases when the rate of collagen breakdown exceeds that of production [73][78]. An increase in collagen breakdown is thought to result from a pathological increase in cyclic wall stress [72], which increases the circumferential strain on vascular smooth muscle cells. A pathological cyclic strain has been shown to increase levels of periostin, a matricellular protein that promotes the activation of matrix metalloproteinases (MMPs), and monocyte chemoattractant protein-1 (MCP-1) in excised human AAA tissues as well as in mice with induced AAAs [72]. The MMPs breakdown collagen and elastin [71][75][77][79][80], and the increase in elastin degradation products contributes further to the weakening of the AAA wall by attracting mononuclear phagocytes [81]. These and other inflammatory cells, such as B cells, Th-2 CD3+ lymphocytes and mast cells have been shown to infiltrate AAA walls [55][82]. Increased inflammatory cell infiltration is especially noted in aneurysmal tissue juxtaposed to an intraluminal thrombus (ILT), which traps many inflammatory cells [55][83]. Collectively, these cells promote further activation of MMPs [82] and release reactive oxygen species, resulting in further tissue damage, vascular smooth muscle apoptosis, AAA wall weakening [82] and increased rupture risk.

Although the thrombus contributes to the weakening of the wall by hosting a pro-inflammatory environment, the ILT also attenuates the magnitude of wall stresses that are exerted on the wall by the blood [27][84]. Thus, the thrombus appears to have a dual function as an inflammatory reservoir and a protective mechanical cushion [55][85], but there is no consensus as to which role predominates. For this research project, we will focus on the mechanical function of the thrombus.

Walls juxtaposed to the ILT have been observed to be thin [55] suggesting local wall weakening, but the AAA wall also has sites that are thick, measuring up to 4.27 mm, a value 2-3 times as thick as a normal aortic wall [86][87]. The sites of increased thickness could be attributed to sites of calcification or hypertrophy [86][88], for example. Hypertrophic walls would be the normal biological response to increased blood pressure [69][88][89], as the thickening of the wall is thought to help bring the increased wall stresses due to hypertension back down to homeostatic values. Another example of tissue remodeling and maintenance of homeostasis is the circumferential growth of the aortic wall to reduce elevated wall shear. This process has been mathematically modeled by the tissue growth and remodeling theories proposed by Humphrey [69], which will be discussed in Chapter 4. A simplification of these laws is used in an ongoing study that applies the proposed linear model to improve our understanding of wall stress and AAA expansion relationships (see Chapter 4).

1.2.2 *Wall Stress as a Better Predictor of AAA Rupture Risk than the Maximum Transverse Diameter*

In addition to playing an important role in the pathogenesis, progression and remodeling of an AAA, wall stress has been identified as a better predictor of AAA rupture risk compared to the MTD, strengthening the rationale for its consideration as a promising clinical marker to manage AAAs. To evaluate the potential of wall stress as a predictor of AAA rupture risk, several studies employed finite element analysis (FEA) to compute wall stresses, since they cannot be directly measured [13][16][20][27][86][90][91]. In FEA, a set of partial differential equations that establishes equilibrium of forces is numerically solved over the AAA continuum. This is achieved by first dividing the geometry into discrete smaller domains called elements and then simplifying the partial differential equations into algebraic equations involving a finite number of parameters within each element.

A study conducted by Fillinger et al. compared FEA wall stress distributions for ruptured, symptomatic, and elective repaired AAAs. They observed that the peak wall stresses in maximum diameter matched AAAs were significantly higher in ruptured and symptomatic AAAs than in electively repaired cases [16]. In a separate study, Fillinger then compared the effectiveness of the maximum transverse diameter for assessing AAA rupture risk to that of initial peak wall stress in a cohort of 103 patients with asymptomatic AAAs [13]. Within a mean follow-up period of 14 months, 61 patients underwent elective repair and 42 patients received no intervention. Of the patients undergoing elective repair, 22 cases involved ruptured or symptomatic AAAs. A receiver operating characteristic curve (ROC) was generated for both initial peak wall stress and the maximum transverse diameter, which evaluated each parameter's sensitivity (the proportion of aneurysms that have actually ruptured with those correctly identified as

ruptured) while varying specific threshold values for each parameter. The specificity, i.e., the proportion of actual negatives (or non-ruptured events) with those correctly identified as non-ruptured AAAs, was also determined. Wall stress was able to significantly differentiate patients in need of emergent repair better than the diameter, especially at the threshold values where both the sensitivity and specificity were optimized, i.e., 0.44 N/mm^2 for wall stress and 55 mm for diameter. Using the optimal thresholds, Fillinger also performed a Kaplan-Meier analysis evaluating the risk of rupture over time, while analyzing the interaction between wall stress and diameter [13]. Regardless of size, an AAA with low stress had a low risk of rupture, whereas an aneurysm with high wall stress had a higher risk of rupture, suggesting that wall stress is better marker of AAA rupture than the MTD.

Other studies performed by Venkatasubramaniam, Truijers, and Maier also compared the peak wall stress between symptomatic/ruptured AAAs versus asymptomatic aneurysms [18][19][20]. Consistent with the findings of Fillinger et al., the studies found that for AAAs of similar size, the peak wall stress was significantly higher in ruptured AAAs. Additionally, Venkatasubramaniam reported that the site of peak wall stress correlated with the location of rupture [20]. A study performed by Doyle et al. also observed an agreement between the location of peak wall stress and rupture [92]. The collective findings of these studies further corroborate that wall stress is a promising marker for predicting aneurysmal rupture.

1.3 Current Stress-Based Method Limitations and Consideration of the Linear Model as a Promising Solution

Even though wall stress is a better predictor of rupture risk, stress is not yet employed in the clinic because the FEA wall stress computations are quite involved and time-intensive [71][93]. One reason is because the AAA is conventionally modeled as a nonlinear hyperelastic material. FEA solutions involving nonlinear materials are more difficult to converge. Stress-based methods are also not employed in the clinic because conventional methods result in an overestimation of wall stress magnitudes. Conventional approaches assume that the CT AAA geometry is initially unloaded and unstressed when, in fact, the wall is being stressed and distended by the blood. When patient-specific pressure is applied to lumen of the FEA AAA model, the displacements of the AAA become large and the AAA geometry becomes distorted. This distortion leads to an overestimation of the stresses. Uncertainties in patient wall stresses can also result because population average material property values are used in computational models instead of the patient-specific values, since these are unknown.

To encourage consideration of stress-based methods for use in the clinic, we must find ways to simplify and improve wall stress computations. In this dissertation, the linear model is introduced as an easier, efficient method for computing wall stresses without compromising the CT-derived AAA geometry and without the need to know the patient material properties of the AAA at any stage in its formation and progression.

Further information about the research involved in improving the efficiency of AAA wall stress computations using the linear model is found in Chapter 3. The following chapter will describe the methodology employed to prepare an FEA model of a patient's AAA to compute wall stress.

CHAPTER 2: PREPARING A FINITE ELEMENT ANALYSIS MODEL OF A SUBJECT-SPECIFIC ABDOMINAL AORTIC ANEURYSM

The goal of this thesis project is to improve the efficiency of the computations of abdominal aortic aneurysm wall stresses. In order to compute wall stresses for a subject-specific AAA, an FEA model of the aneurysm must be generated, as it will serve as the principal input for the FEA software. The FEA model will contain information about the AAA's geometry and material properties, i.e., measures of tissue stiffness, as well as the boundary conditions that describe the AAA's environment, e.g., the pressures that are applied to the AAA and fixations imposed. The FEA software then uses the input data of the FEA model to numerically solve for wall displacements and wall stresses.

The preparation of the subject-specific FEA model of an AAA requires several steps (see **Fig. 3**), which include i) acquiring computed tomography scans of the subject's AAA as well as subject-specific information, e.g., blood pressure; ii) extracting the AAA and intraluminal thrombus geometries from CT scans using image segmentation algorithms that output geometrical data in the form of surface meshes; iii) organizing mesh nodes to facilitate further processing of the AAA model; and iv) generating an FEA input file that combines the geometry and mechanical property information to prepare the model for FEA computations. A further discussion of these steps is the main focus of this chapter.

2.1 AAA Subject Cohort & Collection of CT AAA Images

The first step involved in the preparation of subject-specific FEA models of an AAA was the collection of subject medical information and CT scans, which were de-identified to protect patient information. The contrast-enhanced spiral CT scans were

obtained as part of a standard of practice to assess AAA rupture risk and were not conducted solely for purposes of this research. Rather, CT images were acquired from an established database of 627 AAA subjects from the Oregon Health & Science University (OHSU) Department of Vascular Surgery. For the primary thesis objective related to improving the efficiency of AAA wall stress computations, the CT scan of Subject A0 was already available to our laboratory (see Chapter 3, Section 2.2D), but we did not have access to the patient's medical information. For an ongoing project concerned with the elucidation of the role that wall stresses play in the expansion of an AAA (see Chapter 4, Section 1), we had access to 87 AAA subjects and their medical records. For this project, a patient needed to have at least three CT scans taken at three different time points, which was the minimum number of time points necessary to evaluate changes in AAA growth rates and wall stress distributions. For a patient, AAA growth is typically assessed by measuring the difference in diameter between two CT scans that were taken at different time points and dividing the difference in diameter by the time interval [94]. Six months was the minimum amount of time that was needed to elapse to determine if an AAA was non-growing [94]. Thus, the primary inclusion criteria were that subjects should have three consecutive CT scans with no surgeries in between, and that the interval of time elapsed between scans should be at least six months. The main exclusion criteria included surgical intervention at any point in the series of three consecutive CT scans; availability of two CT scans or less; and/or scans taken at intervals less than six months. From the cohort of 87 subjects, 41 had two CT scans available and 46 had at least three scans. Of the subjects with three CT scans available, 27 subjects exhibited evidence of surgical intervention, and two subjects had CT scans that were taken at

intervals of less than six months. Of the remaining 17 subjects, eight were also excluded for the following reasons: i) two had CT scans that showed non-aneurysmal infrarenal aortas with no growth; ii) two had infrarenal aortas that were transitioning into becoming small AAAs but these aortas exhibited no growth; iii) two had CT scans that displayed an iliac artery aneurysm rather than an AAA; and iv) two had CT scans whose AAAs were difficult to distinguish from surrounding tissue. Thus, nine subjects were eligible for the study, but only one (Subject A4) was chosen to elucidate the role that wall stress plays in AAA expansion within the time allotted.

The selected patient was an older male with CT scans taken at three time points, at intervals of at least six months. In addition to obtaining CT scan images, the subject's blood pressures and smoking history were acquired from the OHSU electronic health record EPIC. The blood pressure and smoking history were collected because of their crucial role in AAA development, progression, and rupture [55][94][95][96]. The blood pressure data were also collected in order to be used as part of the subject-specific intraluminal pressure boundary condition input needed for the computation of subject AAA wall stresses. We considered blood pressure measurements that were recorded closest to the time when the CT scans were taken (see **Table 2**). When blood pressure information was unavailable, as was the case for Subject A0, a systolic pressure of 0.016 N/mm^2 (120 mmHg) was used. Only information about Subject A4 is summarized in **Table 2**, since medical information for Subject A0 is not available.

Because this retrospective study constituted a minimal risk chart review, subject consent was waived by the OHSU Institutional Review Board (IRB). The study was approved by the OHSU IRB (IRB00007554) [1].

2.2 Extraction of AAA Geometries from CT Scan Images

The second step involved in the preparation of subject-specific FEA models was the extraction of AAA surfaces from CT scan images using two semi-automated, custom-made segmentation algorithms. One program was developed in-house, and the second was created by collaborators at Oregon State University at Corvallis and Washington University in St. Louis, Missouri. The segmentation programs operated independently of each other and were used as alternative ways to extract AAA geometries beginning at the renal-aortic bifurcation and ending at the iliac-aortic bifurcation (see **Fig. 4**). These algorithms acquired two surfaces for each AAA from the CT scans: 1) the lumen surface, which is the interface between the blood and the AAA wall and/or intraluminal thrombus (ILT); and 2) the outer wall of the AAA. The segmentation algorithms could not be used to acquire both the inner and outer AAA wall surfaces because the AAA wall thickness was difficult to delineate due to the inherent limitations of the CT scan resolution. Thus, if one wall surface was segmented, the other was obtained by offsetting the distribution of nodes of the segmented wall surface by a certain distance. This method and both segmentation processes are described below.

Our custom-made segmentation procedure (SP1) allows the user to manually trace the first contour around the contrast-enhanced AAA lumen on the CT scan image of interest. Subsequent contours are then automatically obtained along the AAA midline (see **Fig. 4**), and around the contrasted lumen. The program then allows for the examination and manual correction of erroneous contours. After the raw contours are

inspected, smoothing algorithms are implemented in order to reduce surface-extraction noise. Finally, contours are "stacked" in order to generate the 3-D lumen geometry in the form of a surface mesh, where the nodes of the mesh are organized into cross-sectional rings. The lumen surface mesh for Subject A0 was obtained using SP1. Because the AAA of Subject A0 did not have a thrombus, the lumen mesh also represented the inner wall surface of the AAA. To obtain the outer wall surface mesh for Subject A0, a custom-made MATLAB (vR2010b, Math Works, Inc., Natick, MA) program was written to take the lumen surface mesh nodes as input and uniformly displace each node radially outward a distance of 1.5 mm. This distance is the median wall thickness measured from a population of AAA tissue specimens excised from cadavers or patients undergoing elective repair [86]. The geometry of Subject A0 was used to address the primary thesis objective, which is to determine if the linear model can be used to compute patient wall stresses in an efficient manner (see Chapter 3).

For the ongoing AAA expansion study (see Chapter 4, Section 1), our collaborators' segmentation program (SP2) was used to extract AAA surfaces from CT scans (see **Fig. 3**) taken at three time points. SP2 allows the user to trace transverse and longitudinal cross-sectional contours around the AAA lumen or outer wall and allows the user to edit and smooth the contours before the next tracing. Moreover, the user has the opportunity to choose the 3-D orientation of the cross-sections where the contours will be outlined, allowing for a more controlled tracing—this is in contrast to SP1, where the tracing of contours is strictly confined to planes that are transverse to the midline of the AAA's body. Further, the mesh can be generated and smoothed in SP2 as the contours are being outlined. The ability to trace, edit, and smooth contours and orient the cross-

sectional plane for tracing (while creating the surface mesh) provides the user with greater control for producing AAA surface meshes. Because SP2 offers better control for segmentation than SP1and has an easy-to-use graphic user interface, the outer wall and lumen surfaces of the AAA at three time points were acquired for Subject A4 using only this segmentation approach. The mesh for Subject A0, however, was not segmented using SP2 because this algorithm was not available earlier in the study when the subject mesh was extracted and used for the computation of wall stresses.

Unlike the case of Subject A0, the AAA of Subject A4 has an ILT. Thus, the lumen surface is not representative of the inner wall. To obtain the inner wall surface, the segmented outer wall and lumen meshes were first parameterized before proceeding, since the meshes obtained from SP2 were unstructured. Further details about how the mesh "organization" was achieved are described in Section 2.3 below. Briefly, a custom-made algorithm was written to arrange the unstructured mesh into 80 "stacked" rings of nodes. Each ring was set to have 80 nodes, resulting in a total of 6,400 nodes for each mesh. The program also ensured that the nodes between surfaces, such as those of the lumen and outer wall at different time points, were corresponding. Once the outer and lumen meshes were parameterized, the outer surface was used as input for another custom-made MATLAB program that uniformly displaced each outer node 1.5 mm radially inward. The resulting distribution of displaced points defined the inner surface of the AAA wall. The MATLAB program additionally computed the distance d_i between an outer wall surface node and its corresponding counterpart lumen surface node (n_L) to check whether d_i was less than or equal to 1.5 mm. A distance of less than 1.5 mm suggested that n_L was closer to the outer wall node than was the corresponding inner wall

node. This implies that the lumen surface locally protruded into the inner wall surface, which results in geometrical distortion if uncorrected.

To avoid geometrical distortion in areas where $d_i \leq 1.5$ mm, the lumen and inner wall nodes were adjusted. More specifically, n_L was displaced 0.5 mm radially inward and away from the AAA wall, whereas, the inner wall node was displaced 0.1 mm radially outward toward its corresponding outer wall node. The adjustment of points also helped to circumvent the challenge of modeling an AAA with a patchy thrombus. The movement of lumen nodes allowed for the creation of a thin layer of thrombus where $d_i \leq$ 1.5 mm, ensuring that the thrombus covered the inner wall surface continuously, which greatly facilitated the creation of the FEA model. A thin layer of an ILT was used so that wall stresses in the area do not become greatly attenuated, as greater attenuation in stress magnitude was expected if the ILT thickness was large [85]. After adjusting specific nodes and running the programming pipeline, we generated three surfaces for each AAA, i.e., the outer and inner wall and lumen surfaces that specified the geometry of the wall and ILT (see **Fig. 5**).

2.3 Parameterization of Mesh Nodes

Since SP2 yields unstructured surface meshes with scattered nodes, a custom-made program was written to not only to "organize" the surface nodes into "stacked" rings [97], but also to arrange the nodes for the purpose of establishing nodal correspondence between surfaces at different time points. Determining the point-by-point correspondence between surfaces becomes indispensable for assessing differences in

geometrical structure and local expansion rates. To obtain the correspondence between AAA surfaces, the program first aligns the surfaces using the Iterative Closest Point (ICP) method [98][99]. Implementation of ICP results in the minimization of the differences in position between the surfaces. This is necessary because of the way CT scans were setup and taken. After surface alignment is achieved, the ends of the surfaces being compared are cut using parallel cutting planes, resulting in surfaces with ends cut at the same angle. Subsequently, the program determines a consistent parameterization that minimizes the change in relative geodesic distance between any two points on the surface. Thus, the parameterization serves as an initial correspondence. A refinement of the initial correspondence is then performed using a strain relaxation technique. This technique first computes the strain in deforming one surface at one time point to the surface at a later time and subsequently modifies the initial correspondence so that changes in strain are minimized throughout the surface. The final correspondence is represented as parameterized meshes with corresponding nodes for all AAA surfaces being compared.

2.4 Preparation of the FEA Input File for Computation of Wall Stress in FEA Software

After parameterizing the surface meshes, the geometrical data were used to generate the finite element meshes. These meshes are used by the FEA software ADINA (v 8.8.3-9.0.1, ADINA R & D, Inc., Watertown, MA) to compute wall stresses. To create the finite element meshes, 2 custom-made MATLAB scripts were written. One program

yielded an FEA input file modeling an AAA without a thrombus, whereas the second program prepared an FEA input file modeling an aneurysm that contained an ILT. Both input files use the surface meshes to define the geometrical lines, surfaces, and volumes that compose the FEA tissue bodies. Once the volumes and surfaces are defined, the FEA mesh grid is created by dividing the tissues into 27/4 3-D hexahedral elements. The 27/4 elements are hybrid elements composed of 27 displacement degrees of freedom and 4 pressure degrees of freedom, and these elements satisfy the inf-sup condition [1][100]. The use of hybrid elements is beneficial when modeling materials that are incompressible (i.e., materials whose volumes do not change with an applied load) or nearly-incompressible, as the mixed elements ensure numerical stability during computations (see Chapter 3, Section 2.2) [1]. In this project, the AAA wall and ILT tissues were modeled as almost incompressible materials. For the linear model, the near incompressibility of the tissues was modeled by setting the Poisson's ratio v to a value of 0.4999 (see Chapter 3, Section 2.1A), and the FEA elements were modeled as linear elastic solid structures with arbitrary, yet high, Young's moduli E, which are measures of stiffness. Large E magnitudes were chosen to ensure that the geometrical integrity of the AAA was preserved upon the application of pressures. Unless otherwise indicated, the Young's moduli of the wall and thrombus were set to $E_{wall} = 8.4 \times 10^9$ N/mm^2 and $E_{ILT} = 1.25 \times 10^9$ N/mm^2, respectively (see Chapter 3, Sections 2.1A and 2.2C). The subject-specific average blood pressure was applied to the lumen surface of Subject A4's AAA, whereas the normal systolic blood pressure was used for Subject A0. No pressure was applied on the outer surface in both patient models. The ends of the AAA wall and AAA-ILT models were fixed in the longitudinal direction in order to simulate the tethering of

the aneurysm to the rest of the aorta. Two points at one end of the AAA wall were also fixed to avoid rigid body motion. Once the boundary conditions, linear material properties, and geometries were defined, the FEA models were used to compute wall stresses.

Fig. 3 summarizes the approach employed in this project for computing subject-specific AAA wall stresses in FEA. Methods similar to the ones presented in this chapter were implemented for computing FEA wall stresses in idealized 2-D axisymmetric models of an AAA. These approaches are explained in further detail in Chapter 3 and are important for investigating how wall stress computational efficiency can be improved.

CHAPTER 3: IMPROVING THE EFFICIENCY OF ABDOMINAL AORTIC ANEURYSM WALL STRESS COMPUTATIONS [1]

Jaime E. Zelaya[a], Sevan Goenezen[b], Phong T. Dargon[c], Amir-Farzin Azarbal[c], and Sandra Rugonyi[a]

[a]Department of Biomedical Engineering, Oregon Health & Science University, Portland, OR 97239, USA

[b]Department of Mechanical Engineering, Texas A & M University, College Station, TX 77843, USA

[c]Department of Surgery, Division of Vascular Surgery, Oregon Health & Science University, Portland, OR 97239, USA

Received December 2, 2013; Accepted June 5, 2014; Published July 9, 2014

Complete Address:

3303 SW Bond Avenue

Mail Code: CH13B

Portland, Oregon 97239

Tel: 503-418-9310

Fax: 503-418-9311

rugonyis@ohsu.edu

3.1 Introduction

The AAA maximum transverse diameter (MTD) is an accepted clinical marker for assessing the risk of rupture, and surgical repair is indicated for an AAA with an MTD $\geq$ 55 mm or an AAA growing at 10mm/year. In employing the MTD, clinicians overestimate the stability of smaller aneurysms, and larger, stable AAAs can be subject to unnecessary surgery. A better marker of rupture is thus needed.

Wall stress has been found to be a better, more promising predictor of rupture risk than MTD [13][16][18][19][20][92]. This is not only because tissues tear apart when wall stress exceeds a threshold stress for rupture, which depends on the tissue strength, but also because peak wall stresses are found to be significantly higher in ruptured AAAs than in non-ruptured, size-matched AAAs [20]. Further, the site of peak wall stress correlates with the location of rupture [20][92]. Additionally, wall stress is thought to play an important role in AAA tissue growth and remodeling (G&R). Recent theories of G&R [101][102] postulate that vascular tissues grow and remodel so that homeostatic wall stresses are conserved. According to these theories, an increase in wall stress will result in tissue growth and remodeling that lowers wall stress to homeostatic levels; likewise, an increase in wall shear stress will result in an increase in vascular diameter that will lower shear stresses to homeostatic values. These G&R mechanisms are postulated to act during AAA expansion, explaining the possible relationship between wall stress and AAA progression. Thus, wall stress has been the subject of extensive AAA biomechanical research [22] and is typically obtained using finite element analysis (FEA) [27][86][90][91].

To compute wall stress, average or systolic intraluminal pressures are conventionally applied to image-derived, patient-specific geometries that are assumed to be unloaded and unstressed [103][104]. In these models, the AAA walls are assumed to be nonlinear hyperelastic with mechanical properties measured from cadaver tissues or tissues from patients undergoing elective repair [22][28][105][106]. Incorrectly assuming that imaged geometries are unloaded, however, implies that application of intraluminal pressures to the walls will result in overly distorted AAA geometries, typically with overestimated wall stress distributions [23][29][106][107]. To resolve this problem, algorithms have been developed for approximating the tissue unloaded configuration from available loaded CT scan or magnetic resonance imaging (MRI) geometries [23][29][104][108]. Applying intraluminal pressures to these computed unloaded geometries results in wall deformations that closely approximate the original loaded AAA geometry and more accurately predict wall stress. However, these promising methods are difficult to implement and are computationally intensive [104]. This is because computation of the undeformed unloaded configuration involves the solution of an inverse nonlinear problem. In fact, given the nonlinear properties of AAA walls, even calculation of wall stresses from a known unloaded, unstressed configuration is involved and requires extensive computations. Even when using methods to recover the unloaded geometry, limitations of current models include: residual stresses, which are characteristic of vascular tissues, are neglected; spatial changes in aneurysmal tissue properties along and across the wall are neglected; and "true" boundary conditions, including the effects of internal and external structures (thrombus and external organs), are unknown and frequently neglected or approximated. For AAA wall stresses to

become a useful clinical indicator and be applicable in a clinical environment, a more efficient and robust methodology is needed for estimating wall stresses from patient-specific geometries.

In this study, we propose modeling AAAs using FEA linear models as a means of obtaining equilibrium stresses in a more robust and computationally efficient way. Because linear models assume infinitesimally small displacements and strains, the approach preserves the integrity of the imaged geometry, and the application of intraluminal pressures achieves equilibrium of forces and wall stresses directly in the patient-specific geometry. We assess the effectiveness of our approach using idealized models and patient-specific models of AAAs. We also explore the effect of employing different nonlinear wall material properties and residual stresses on wall stress computations in idealized models and compare results with those obtained from linear models.

3.2 Methods

3.2.1 *Problem Formulation and Equations Employed*

To determine the relative accuracy of the linear approach to compute AAA wall stresses, we employed three models: a reference model, a conventional model, and our proposed linear model (see **Fig. 2**). The reference model (**Fig. 2A**) was used as a reference for wall stresses (see below for a more detailed description of the model). In the reference model, initial conditions and tissue properties are assumed to be known. The conventional model (**Fig. 2B**) represents the most commonly used approach to computing

wall stress, in which the patient deformed configuration is used as an unloaded, unstressed initial configuration and walls are assumed to have nonlinear, hyperelastic material properties. The linear model (**Fig. 2C**) also uses the patient deformed configuration as an unloaded, unstressed initial configuration, but solution of the model does not change the wall geometry, and equilibrium stresses are obtained in the patient geometry. Wall stresses obtained using the linear and conventional models were compared to stresses obtained using the reference model. Comparisons were performed first using idealized models, such as straight tubular models representing the arterial wall and idealized curved axisymmetric models of the AAA. Comparisons were then extended to a subject-specific AAA geometry. For the tubular models, we further explored the effects of using different reported nonlinear tissue mechanical properties and the effects of residual stresses on wall stress. We then compared wall stresses obtained with nonlinear models to those obtained using the linear model approach.

3.2.1A Model Formulation

For all models considered, we solved the equations of equilibrium

$$\nabla \cdot \boldsymbol{\sigma} = 0 \quad \text{in } \Omega \tag{1}$$

with boundary conditions

$$\boldsymbol{\sigma} \cdot \boldsymbol{n} = -p\boldsymbol{n} \quad \text{on } \Gamma_l, \qquad \boldsymbol{\sigma} \cdot \boldsymbol{n} = 0 \quad \text{on } \Gamma_o \tag{2}$$

where $\boldsymbol{\sigma}$ is the Cauchy stress tensor; p is the intraluminal blood pressure and was chosen here as the systolic pressure (0.016 N/mm^2 = 120 mmHg) unless otherwise stated; $\hat{\boldsymbol{n}}$ is a unit vector normal to the wall surface; Ω is the body domain in the deformed configuration; and Γ_l and Γ_o refer to the lumen and outer surfaces of the deformed

configurations of the AAA models, respectively. Note that the choice of using systolic pressure is arbitrary and does not affect the results presented, since the hypothetical reference models are also assumed to be subjected to systolic pressure.

The reference and conventional models assumed nonlinear, hyperelastic wall material properties. Specifically, AAA walls were assumed to be almost incompressible, homogeneous, and isotropic with an energy density function W of the form [28][106]

$$W = \alpha\left(\mathbf{I_B} - 3\right) + \beta\left(\mathbf{I_B} - 3\right)^2 + \gamma\left(\mathbf{I_B} - 3\right)^3, \tag{3}$$

where α, β and γ are coefficients that denote the properties of the tissue; $\mathbf{I_B}$ is the first invariant of the Left Cauchy-Green tensor $\mathbf{B}$ ($\mathbf{I_B}$ = tr$\mathbf{B}$) with $\mathbf{B} = \mathbf{F}\mathbf{F}^T$; and $\mathbf{F}$ is the deformation gradient tensor. The constitutive relations corresponding to the nonlinear material represented in **Eq. 3** are described by

$$\boldsymbol{\sigma} = -H\mathbf{I} + 2\frac{\partial W}{\partial \mathbf{I_B}}\mathbf{B}, \tag{4}$$

where H is the hydrostatic pressure and $\mathbf{I}$ is the identity tensor.

The values of coefficients in **Eq. 3** were determined from human tissue samples subjected to tensile tests. Material properties of AAA tissues have been measured in different studies with varying degrees of accuracy [28][106][109]. One of the pioneering studies, by Raghavan and Vorp [28], assumed that W (**Eq. 3**) had two terms ($\gamma = 0$) and fitted stress-strain results from uniaxial tissue tensile tests to find the coefficients α and β for each tissue sample. While the study found that the coefficients vary from sample to sample, it provided a population average, which is frequently used in the AAA literature to represent the material properties of AAA tissues. More recently, Polzer et al. [106] measured AAA patient tissue samples using biaxial tensile tests and fitted the resulting stress-strain curves to an energy-density function similar to that of **Eq. 3** but consisting of

5 terms, i.e., $W = \alpha(\mathbf{I_B} - 3) + \beta(\mathbf{I_B} - 3)^2 + \gamma(\mathbf{I_B} - 3)^3 + \zeta(\mathbf{I_B} - 3)^4 + \eta(\mathbf{I_B} - 3)^5$, where ζ and η are also coefficients that denote the properties of the tissue. The study found that even though W was assumed to be isotropic, it approximated the mechanical behavior of the tissue well. The study also found striking variations in mechanical properties among sampled tissues. Here, for comparison, we used mechanical properties obtained in the Raghavan-Vorp and Polzer studies (see **Table 3**, $\zeta = \eta = 0$ for the two patient-specific tissue material properties selected from Polzer et al.). We extensively employed the population average mechanical properties found by Raghavan and Vorp (RV in **Table 3**) [28], as these properties are widely used. To assess the effects of patient-specific tissue mechanical properties, which are not known in clinical practice, we varied the values of α and β ($\gamma = 0$) and also used coefficients obtained by Polzer et al. from two different patient-tissue samples (P1 and P2; see **Table 3**) in the reference models.

In the linear model, the wall was assumed to be an almost incompressible, linear elastic material, characterized by an arbitrary, albeit high, Young's modulus E, which ensures infinitesimal deformations without compromising wall stress values. Linear constitutive relations were given by

$$\boldsymbol{\sigma} = \mathbf{C}\boldsymbol{\varepsilon}, \tag{5}$$

where $\mathbf{C}$ is the stiffness tensor, which, for an isotropic material, depends on E and the Poisson's ratio v, and $\boldsymbol{\varepsilon}$ is the infinitesimal strain tensor. Unless otherwise stated, we used $E = 8.4\text{x}10^9$ N/mm^2 and $v = 0.4999$ in computations using the linear model.

Differences among the reference, conventional, and linear models were in the choice of material properties and initial configurations (see **Fig. 2**). In all models, the initial configuration was assumed to be unloaded and unstressed. For the reference

model, the initial configuration was chosen arbitrarily and represented the unstressed and unloaded configuration of the tissue that was assumed to be known in our models (but which is unknown in clinical practice). For the conventional and linear models, however, the initial configuration was taken as the deformed configuration of the reference model. This choice of initial configuration intended to simulate the use of the loaded geometry obtained from CT scans or other imaging techniques as an unstressed, unloaded configuration, both in the conventional and linear approaches. The reference model, conversely, simulates the loading of tissues from the unknown unstressed configuration, and thus represents a more accurate model of wall stress.

Once the stress distributions were computed for all models, the wall stresses obtained from the conventional and linear models were compared to the stresses from the reference model in order to determine the degree to which conventional and linear approaches approximated reference stresses. The analysis was performed on both idealized and patient-specific models of AAAs, which are described further below. For idealized thick-wall tubular AAA models, analytical expressions exist for linear models and were derived in what follows for the hyperelastic tissue models.

3.2.1B Analytical Expressions for an Axisymmetric Thick-Wall Tube under Internal Pressure

Consider an axisymmetric thick-wall tube as a simple representation of a blood vessel (see **Fig. 6**). Initially, the vessel is assumed to be undeformed, unloaded and unstressed with an inner radius A and outer radius B. In addition, the vessel is assumed to be constrained at both ends in the longitudinal direction, and a uniform internal pressure

p is applied on the luminal surface. Application of the internal pressure results in a deformed geometry with inner and outer radii *a* and *b*, respectively.

Employing cylindrical coordinates, the equilibrium equation (**Eq. 1**) for this case reduces to

$$\frac{\partial \sigma_{rr}}{\partial r} + \frac{\sigma_{rr} - \sigma_{\theta\theta}}{r} = 0, \tag{6}$$

where r is the radius of the deformed configuration and σ_{rr} and $\sigma_{\theta\theta}$ are the Cauchy radial and circumferential stresses, respectively [102].

The boundary conditions for the problem (**Eq. 2**) become

$$\sigma_{rr}\left(r = a\right) = -p, \tag{7}$$

$$\sigma_{rr}\left(r = b\right) = 0. \tag{8}$$

3.2.1B.i *Analytical Solutions for Nonlinear Hyperelastic Tissue Model*

We assume the wall properties to be incompressible and nonlinear hyperelastic with a parabolic strain energy density function *W* as proposed by Raghavan et al. [28], see **Eq. 3** (with $\gamma = 0$) and constitutive equations given by **Eq. 4**.

If $\lambda_{\theta\theta}$, λ_{rr}, and λ_{zz} represent the stretch ratios in the circumferential, radial, and longitudinal directions, respectively, then for a tube under internal pressure,

$$\lambda_{\theta\theta} = \frac{r}{R},\ \lambda_{rr} = \frac{\partial r}{\partial R},\ \lambda_{zz} = 1. \tag{9}$$

where *r* and R are the radii of the deformed and initial (unstressed) configurations, respectively (see **Fig. 6**).

Thus, for the thick-wall tube model considered here, **F** and **B** are

$$\mathbf{F}=\begin{pmatrix}\lambda_{\theta\theta} & 0 & 0\\ 0 & \lambda_{rr} & 0\\ 0 & 0 & \lambda_{zz}\end{pmatrix},\quad \mathbf{B}=\mathbf{F}\mathbf{F}^{\mathbf{T}}=\begin{pmatrix}\lambda_{\theta\theta}{}^{2} & 0 & 0\\ 0 & \lambda_{rr}{}^{2} & 0\\ 0 & 0 & \lambda_{zz}{}^{2}\end{pmatrix} \tag{10}$$

$$\text{and } \boldsymbol{\sigma}=\begin{pmatrix}\sigma_{\theta\theta} & 0 & 0\\ 0 & \sigma_{rr} & 0\\ 0 & 0 & \sigma_{zz}\end{pmatrix}=2\mathbf{B}\left(\alpha+2\beta\left(\mathbf{I}_{\mathbf{B}}-3\right)\right)-H\mathbf{I}, \tag{11}$$

where σ_{zz} is the Cauchy longitudinal stress.

Replacing into **Eq. 6** results in

$$\frac{\partial\sigma_{rr}}{\partial r}=\frac{1}{r}\left[2\left(\lambda_{\theta\theta}^{2}-\lambda_{rr}^{2}\right)\left(\alpha+2\beta\left(\lambda_{\theta\theta}^{2}+\lambda_{rr}^{2}-2\right)\right)\right]. \tag{12}$$

Further, for an incompressible material [102],

$$\lambda_{rr}\lambda_{\theta\theta}\lambda_{zz}=1, \tag{13}$$

and, therefore, using **Eqs. 9** and **13** and solving for r,

$$\frac{r}{R}\frac{\partial r}{\partial R}=1, \tag{14}$$

$$r=\sqrt{R^{2}+b^{2}-B^{2}}, \tag{15}$$

$$\lambda_{\theta\theta}=\frac{r}{\sqrt{B^{2}-b^{2}+r^{2}}},\ \ \lambda_{rr}=\frac{1}{\lambda_{\theta\theta}}. \tag{16}$$

Using **Eqs. 8**, **12** and **16** and solving for σ_{rr} then yields

$$\begin{aligned}\sigma_{rr}\left(r\right)=&\left(2\beta-\alpha\right)\ln\left(\frac{B^{2}}{B^{2}-b^{2}+r^{2}}\right)+\alpha\left(B^{2}-b^{2}\right)\left(\frac{1}{r^{2}}-\frac{1}{b^{2}}\right)+2\left(\alpha-2\beta\right)\ln\left(\frac{b}{r}\right)\\&+4\beta\left[\frac{b^{2}-B^{2}}{2B^{2}}-\frac{b^{2}-B^{2}}{2\left(B^{2}-b^{2}+r^{2}\right)}+\frac{\left(B^{2}-b^{2}\right)^{2}}{4}\left(\frac{1}{r^{4}}-\frac{1}{b^{4}}\right)\right],\end{aligned} \tag{17}$$

and using **Eq. 7**,

$$-p=(2\beta-\alpha)\ln\left(\frac{B^2}{B^2-b^2+a^2}\right)+\alpha\left(B^2-b^2\right)\left(\frac{1}{a^2}-\frac{1}{b^2}\right)+2(\alpha-2\beta)\ln\left(\frac{b}{a}\right)$$
$$+4\beta\left[\frac{b^2-B^2}{2B^2}-\frac{b^2-B^2}{2\left(B^2-b^2+a^2\right)}+\frac{(B^2-b^2)^2}{4}\left(\frac{1}{a^4}-\frac{1}{b^4}\right)\right]. \tag{18}$$

In order to solve **Eq. 18** for *a* and *b*, an additional equation is needed. Since the cross-sectional areas of the undeformed and deformed configurations are equal due to incompressibility,

$$\pi\left(b^2-a^2\right)=\pi\left(B^2-A^2\right), \quad \text{or} \quad a^2=b^2-B^2+A^2. \tag{19}$$

By substituting the equation for *a* in **Eq. 19** into **Eq. 18** and numerically solving for *b* (given α, β, *A* and *B*), the values for *b* and *a* that satisfy the boundary conditions (**Eqs. 7** and **8**) can be obtained.

Once *a* and *b* are computed, **Eqs. 6** and **17** are used to obtain an expression for the circumferential stress,

$$\sigma_{\theta\theta}(r)=\frac{-2(2\beta-\alpha)r^2}{\left(B^2-b^2+r^2\right)}+\frac{4\beta\left(b^2-B^2\right)r^2}{\left(B^2-b^2+r^2\right)^2}-\frac{\alpha\left(B^2-b^2\right)}{r^2}+\beta\left(B^2-b^2\right)^2\left[\frac{-3}{r^4}-\frac{1}{b^4}\right]$$
$$-2(\alpha-2\beta)+(2\beta-\alpha)\ln\left(\frac{B^2}{B^2-b^2+r^2}\right)-\frac{\alpha\left(B^2-b^2\right)}{b^2}+2(\alpha-2\beta)\ln\left(\frac{b}{r}\right) \tag{20}$$
$$+\frac{2\beta\left(b^2-B^2\right)}{B^2}-\frac{2\beta\left(b^2-B^2\right)}{B^2-b^2+r^2}.$$

To solve for σ_{zz}, we first find an equation for *H* using **Eq. 11**,

$$H=2\alpha\lambda_{rr}^2+4\beta\lambda_{rr}^2\left(\lambda_{\theta\theta}^2+\lambda_{rr}^2-2\right)-\sigma_{rr}. \tag{21}$$

Substituting **Eq. 21** into the expression for σ_{zz} from **Eq. 11** then yields,

$$\sigma_{zz} = 2\alpha + 4\beta\left(\lambda_{\theta\theta}^2 + \lambda_{rr}^2 - 2\right) - 2\alpha\lambda_{rr}^2 - 4\beta\lambda_{rr}^2\left(\lambda_{\theta\theta}^2 + \lambda_{rr}^2 - 2\right) + \sigma_{rr}. \tag{22}$$

Thus, the analytical solutions for wall stresses in a tubular model when tissue properties are assumed to be nonlinear hyperelastic (**Eq. 3** with $\gamma = 0$) are given by **Eqs. 17**, **20** and **22**, once the deformed internal and external tube radii *a* and *b* are calculated using **Eqs. 18** and **19**.

3.2.1B.ii. *Analytical Solutions for the Linear Tissue Model*

Analytical solutions for the case of a thick-wall tube under internal pressure with linear wall properties under small deformations can be found elsewhere (e.g. [110]). For completeness we included the equations together with some of the steps required in the derivation of equations. The constitutive relations for a linear elastic material, assuming infinitesimally small displacements in polar coordinates, are [110]

$$\begin{aligned} &\sigma_{rr} = \frac{E}{(1+\nu)(1-2\nu)}\left[\nu\varepsilon_{\theta\theta} + (1-\nu)\varepsilon_{rr}\right],\ \sigma_{\theta\theta} = \frac{E}{(1+\nu)(1-2\nu)}\left[\nu\varepsilon_{rr} + (1-\nu)\varepsilon_{\theta\theta}\right], \\ &\sigma_{zz} = \nu(\sigma_{rr} + \sigma_{\theta\theta}), \end{aligned} \tag{23}$$

where E is the Young's modulus and ν is the Poisson ratio, and ε_{rr} and $\varepsilon_{\theta\theta}$ are the radial and circumferential strains, respectively, with $\varepsilon_{zz} = 0$.

For a linear axisymmetric tube with internal pressure, the strain-displacement relations in polar coordinates are

$$\varepsilon_{rr} = \frac{\partial u_r}{\partial r}, \quad \varepsilon_{\theta\theta} = \frac{u_r}{r}, \tag{24}$$

where u_r is the radial displacement.

Substituting **Eqs. 23** and **24** into **Eq. 6** results in the following differential equation:

$$\frac{E(1-\nu)}{(1+\nu)(1-2\nu)}\left[\frac{\partial^2 u_r}{\partial r^2}+\frac{1}{r}\frac{\partial u_r}{\partial r}-\frac{u_r}{r^2}\right]=0. \quad (25)$$

The solution of **Eq. 25** is

$$u_r = c_1 r + c_2 \frac{1}{r}, \quad (26)$$

where c_1 and c_2 are constants. Using the boundary conditions (**Eqs. 7** and **8**), wall stresses are obtained:

$$\sigma_{rr}(r)=\frac{-pa^2b^2}{\left(a^2-b^2\right)}\left[\frac{1}{b^2}-\frac{1}{r^2}\right], \quad \sigma_{\theta\theta}(r)=\frac{-pa^2b^2}{\left(a^2-b^2\right)}\left[\frac{1}{b^2}+\frac{1}{r^2}\right], \quad \sigma_{zz}=\frac{-2\nu pa^2}{\left(a^2-b^2\right)}. \quad (27)$$

Note that, due to the assumption of small displacements, while displacements are computed, the geometry is assumed to remain unchanged (so that $a = A$, $b = B$, and $r = R$ independent of p). Thus, stresses depend on p but not E.

3.2.1C Effective Stress

The effective or von Mises stress is a measure of local maximum stresses that takes into account the contribution of normal stresses in addition to shear stresses and is extensively used to report stresses in the AAA literature [23][25][27]. However, it is worth mentioning that other measures of stress or perhaps stretch might be more relevant in determining AAA risks of expansion and of rupture [22]. Because of their wide use, however, we chose to report effective stresses, and for idealized AAA geometries, circumferential and radial stresses were also considered. Note further that we are not employing effective stresses as a rupture criterion, but only as a convenient way of reporting wall stresses. In cylindrical coordinates the effective stress is calculated as follows:

$$\sigma_{eff} = \sqrt{\frac{\left(\sigma_{rr} - \sigma_{\theta\theta}\right)^2 + \left(\sigma_{rr} - \sigma_{zz}\right)^2 + \left(\sigma_{\theta\theta} - \sigma_{zz}\right)^2 + 6\left(\sigma_{r\theta}^2 + \sigma_{rz}^2 + \sigma_{\theta z}^2\right)}{2}}, \qquad (28)$$

where $\sigma_{r\theta}$, σ_{rz}, and $\sigma_{\theta z}$ are shear stresses.

3.2.2 *Models of AAA*

The specific geometrical models of AAA considered and strategies employed to solve for the model wall stresses are described below.

3.2.2A Axisymmetric Thick-Wall Tubular Model of AAA

The arterial wall was first modeled as an axisymmetric, thick-wall, straight circular tube with applied internal pressure and no longitudinal strain. To determine how geometry affects stress distributions, wall stresses were computed from the analytical solutions using different initial configurations (i.e. initial tube dimensions, see **Fig. 6**). These initial configuration geometries were employed in the reference model, and the resulting deformed configuration of the reference model was used as the initial unloaded configuration in the conventional and linear models (see **Fig. 2**). Additionally, an array of material property values was tested to assess the effect of tissue mechanical properties on stress distributions. To simulate the clinical situation in which wall tissue properties are not known, we allowed the values of α and β to vary in the reference model ($\gamma = 0$), while using RV population average values in the conventional model and a constant elasticity ($E = 8.4\text{x}10^9$ N/mm^2) in the linear model. Wall stresses from the linear and conventional models were then compared to corresponding reference stresses.

We also studied the effect of using different AAA tissue properties (RV, P1, and P2, see **Table 3**) on wall stresses. Since analytical expressions were not available for all material properties, we employed FEA implemented in ADINA to solve for wall stresses in an idealized 2-D axisymmetric tubular model. To discretize the 2-D geometry, we used optimal 9/3 axisymmetric elements, which are quadrilateral mixed displacement/pressure based elements (with 9 displacement degrees of freedom and 3 pressure degrees of freedom) that satisfy the inf-sup condition, ensuring numerical stability when solving problems involving incompressible or almost incompressible media such as the AAA wall tissue [100]. In our models, we used six elements spanning the thickness of the wall. Simulations were performed such that the deformed configuration of the hyperelastic models, used here as reference models, was the same regardless of the specific nonlinear material property employed. This deformed configuration, further, was used as the initial unloaded geometry for the linear model. Wall stresses obtained from the reference models were then compared to stresses from the linear model.

For the nonlinear FEA models presented here and throughout the study, the convergence criterion for equilibrium iterations was specified by energy. The convergence ratio for out-of-balance energy was set to a tolerance value of 0.001. The nonlinear iteration scheme used was the full Newton method, and the maximum number of iterations implemented for every time step was set to 15. Convergence was achieved for non-linear and linear models using 15 to 60 time steps and 1 time step, respectively.

We further explored the effect of residual stresses on wall stress distributions. Residual stresses are the stresses that remain on a vascular wall after loads imposed on the tissue have been removed. They manifest in blood vessels as a shrinkage in the axial

length when vessel segments are cut longitudinally (axial stresses) and as an opening of the unloaded circular cross-section, characterized by an opening angle [111], when vessel segments are cut radially (circumferential stresses). To model circumferential residual stresses in tubular models of AAA, we started from a 2-D open sector in the initial configuration (see **Fig. 7A**). The dimensions of the sector were determined so that the closed unloaded configuration was the same, independent of opening angle. The open sector was modeled as a plane strain 2-D problem in ADINA, and symmetry was considered by modeling half of the sector (see **Fig. 7B**). The open sector was then closed by imposing a displacement in the direction of closure on one end of the sector. Note that this way of modeling residual stresses cannot be implemented in patient-specific models of the AAA. Once the 2-D segment was closed, an internal pressure (p = 0.016 N/mm^2) was imposed to obtain the distribution of wall stresses. The obtained deformed configuration served as the initial, unloaded, unstressed geometry of the linear model, and wall stresses obtained with the linear model and nonlinear models with varying residual stresses were then compared. Different hyperelastic material properties (RV, P1 and P2; see **Table 3**) were employed to determine the effect of tissue mechanical properties on residual and loaded wall stresses. The geometry was discretized using mixed 9/3 elements, and convergence of results was achieved using 180 elements, with 3 elements spanning the wall thickness.

3.2.2B Idealized AAA Models with Non-Uniform Wall Thickness

We implemented idealized geometrical models of AAAs with non-uniform wall thickness to explore the effect of varying thickness on wall stress computations. To this

end, we started using a thick-wall tubular model of the AAA with no residual stresses, in which wall thickness varied longitudinally. We also simulated a model in which the wall thickness varied circumferentially, assuming plane strain conditions. Analytical solutions were not available for these cases; therefore, the analysis was performed using FEA in ADINA. Mixed 9/3 elements were used to discretize the geometries. RV material properties were used here for the reference and conventional models. Reference, conventional, and linear models were simulated with the described non-uniform wall thickness. Wall stresses were then compared to establish the accuracy of the linear model in accounting for changes in wall thickness.

3.2.2C Idealized Curved Axisymmetric Model of AAA

To assess the effect of wall curvature on the stresses, the arterial wall was modeled as a curved axisymmetric structure. The outer wall radius *B* of the 2-D axisymmetric initial configuration was specified by the following equation:

$$B = 7.5\cos(\frac{\pi Z}{65}) + 17.5, \qquad Z \in [-65, 65], \tag{29}$$

where *Z* is the height, and *B* and *Z* are in mm. The height was chosen to be 130 mm [112]. The maximum diameter was 50 mm, and the wall thickness was 1.5 mm, the reported median thickness [28][86]. The model was constrained at both ends in the longitudinal direction but was allowed to move and deform freely in the radial direction. The analysis was performed using FEA in ADINA, with the AAA wall discretized using 9/3 mixed elements.

For these models, we further incorporated an intraluminal thrombus (ILT) in our FEA simulations and compared results with and without the thrombus. When the ILT was modeled, the lumen radius, L, was specified by,

$$L = 1.25\cos(\frac{\pi Z}{65}) + 8.75, \qquad Z \in [-65, 65], \tag{30}$$

and the ends of the thrombus were fixed in the longitudinal direction only. The thrombus was also discretized using mixed 9/3 elements.

Like the AAA wall, the thrombus was treated as a nonlinear, homogeneous, isotropic, incompressible material but with the following energy-density function:

$$W = D_1\left(\mathbf{II_B} - 3\right) + D_2\left(\mathbf{II_B} - 3\right)^2, \tag{31}$$

where D_1 and D_2 are coefficients [84], and $\mathbf{II_B}$ is the second invariant of the Left Cauchy-Green deformation tensor $\mathbf{B}$ ($\mathbf{II_B} = 0.5[(\mathrm{tr}\mathbf{B})^2 - \mathrm{tr}(\mathbf{B})^2]$). The ranges of measured values for D_1 and D_2 (95^{th} percentile confidence intervals) obtained from patients undergoing elective repair were as follows: D_1 = 0.0199-0.036 N/mm^2 and D_2 = 0.0216-0.0356 N/mm^2 [84]. In general, the thrombus is more compliant than the tissue wall. The stiffness ratio between the wall and the ILT, which we refer to as the material property ratio (MPR), was computed from the nonlinear models using the ratio of the wall coefficient α (**Eq. 3**) and the intraluminal thrombus coefficient D_1 (**Eq. 31**), i.e., (α/D_1). Because the MPR determines differences in stresses between the wall and ILT, the linear models that included a thrombus were implemented assuming an MPR between the elastic moduli E of the wall and ILT. MPR was first set at 6.7, which is the ratio of the population average values of the wall and ILT, i.e., α = 0.174 N/mm^2/D_1 = 0.026 N/mm^2. In order to determine how implementation of different MPRs affected the distribution of

stresses, we varied MPR in our computations and compared computed wall stresses. The AAA wall material properties were modeled using the energy-density function W proposed by Raghavan and Vorp [28], **Eq. 3** with $\gamma = 0$. Varying MPRs were obtained by changing the coefficient of the thrombus D_1 and the coefficient α for the wall. Values of MPR considered were 4, 6.7, and 10.25. An MPR of 4 was achieved by modeling a weak wall stiffness ($\alpha = 0.144$ N/mm^2, $\beta = 1.152$ N/mm^2) and relatively stiff thrombus ($D_1 = 0.036$ N/mm^2, $D_2 = 0.0356$ N/mm^2). Conversely, an MPR of 10.25 was achieved by modeling a relatively stiff wall ($\alpha = 0.204$ N/mm^2, $\beta = 2.61$ N/mm^2) and weak thrombus ($D_1 = 0.0199$ N/mm^2, $D_2 = 0.0216$ N/mm^2) [28][84]. For the linear model, the wall elasticity modulus was set at a value of $E = 8.4\text{x}10^9$ N/mm^2, and different MPR values were generated by varying the elasticity modulus of the thrombus. For the models excluding and including the ILT, convergence was achieved with a total of 390 and 1,690 elements, respectively, with 3 and 10 elements spanning the thickness of the wall and thrombus, respectively.

3.2.2D Subject-Specific Model of AAA

To assess the effect of AAA geometry on wall stress distributions and the degree to which the conventional and linear models correctly capture these distributions, a patient-specific model was implemented. The initial configuration of the patient-specific AAA had no ILT and was extracted from contrast-enhanced spiral CT scan images of a de-identified patient (Subject A0, see Chapter 2). Information about of the extraction procedure of the AAA geometry and preparation of the patient-specific AAA FEA model is found in Chapter 2.

The acquired patient AAA outer wall geometry was used as the unloaded configuration of the reference model. The deformed configuration obtained from the reference model, assuming RV material properties, was subsequently employed as the unloaded configuration for the conventional and linear models. Convergence of results was achieved using 4,800 elements.

3.2.2E Wall Stress Comparisons

Wall stresses obtained from the conventional and linear models were compared to stresses obtained from reference models. Point-by-point differences in stresses were computed as follows:

$$\frac{\left|\sigma_i - \sigma_i^*\right|}{\left|\sigma_i^*\right|}, \tag{32}$$

where σ_i is the stress of interest (conventional or linear model; circumferential, radial or effective stress) and σ^*_i is the corresponding stress in the reference model. **Eq. 32** was also used to calculate differences in maximum effective stresses with respect to those in the reference model. For models solved using FEA, stress differences with respect to the reference model were plotted for the whole model and over the wall thickness. These analyses allowed for an objective comparison of wall stress.

To facilitate comparisons of solutions over a range of tissue mechanical properties (characterized by **Eq. 3** with α and β; $\gamma = 0$), differences in stress were integrated over the normalized thickness and normalized to the reference stress integral,

$$\frac{\left(\int_0^1 \left|\sigma_i - \sigma_i^*\right| dr'\right)}{\int_0^1 \left|\sigma_i^*\right| dr'}, \tag{33}$$

where *dr'* is the normalized thickness differential. For convenience, this calculation was employed only for the axisymmetric tubular models using analytical solutions of stresses.

3. 3 Results

3.3.1 *Convergence of Linear Model to Equilibrium Stresses*

To ensure that the linear model with applied internal pressures achieved the same equilibrium stresses independent of the Young's modulus *E* employed, a convergence study was first performed. Analytically, for the axisymmetric tubular model, wall stresses depended on the radius and wall thickness of the initial, undeformed configuration and the applied internal pressure. Furthermore, wall stresses depended on wall material properties in the case of hyperelastic tissues (see **Eqs. 17**, **20** and **22**) but were independent of wall mechanical properties when tissues were assumed to be linear and elastic with infinitesimally small deformations and strains (see **Eqs. 27**). As expected, when the linear axisymmetric models were implemented using FEA (assuming small displacements and strains), wall stresses did not vary significantly (<0.1%) as *E* was increased from 1 to 10^{10} N/mm^2. Similarly, wall stresses did not vary significantly with varying values of *E* (<0.2%) in linear idealized and patient-specific models of an AAA. Estimation of equilibrium stresses using the linear model was therefore effectively independent of the *E* employed. We chose an arbitrary high Young's modulus (*E* = 8.4×10^9 N/mm^2) to use in our linear models. In applying this choice of elasticity modulus,

the wall displacements computed for the idealized and patient-specific AAA models were negligible (< 1.3×10^{-9} mm).

3.3.2 *Axisymmetric Tubular Model of an AAA with Parabolic Energy-Density Function*

Wall stress versus normalized wall thickness plots were initially generated for the axisymmetric tubular model to determine how the wall stresses of the linear and conventional models compared to those of the reference model (see **Fig. 8**). Here, conventional and reference models used the RV material properties (see **Table 3**). Compared to the radial (σ_{rr}) and axial stresses (σ_{zz}), the circumferential stresses ($\sigma_{\theta\theta}$) had larger magnitude values, contributing the greatest weight to the calculation of effective stress (see **Eq. 28**). Values of $\sigma_{\theta\theta}$ computed using the linear model were closer to those obtained from the reference model than values obtained using the conventional model. A similar finding was observed for the effective stress. On the other hand, σ_{rr} was almost the same throughout the wall thickness for all models, representing the effect of the pressure boundary conditions on radial stresses.

For a thick-wall tubular model under equilibrium, the following condition is satisfied,

$$h\int_0^1 \sigma_{\theta\theta} dr' = p\,a, \tag{34}$$

where h and a are the wall thickness and lumen radius of the deformed configuration, respectively; dr' is the normalized thickness differential; and p the applied internal pressure (see **Fig. 6**). The integral of $\sigma_{\theta\theta}$ over the thickness (left hand side of **Eq. 34**), was about 0.24 N/mm for both the linear and reference models. This was expected since the deformed wall configuration was practically identical for both models, and the boundary

conditions were the same. The integral, however, was larger for the conventional model (0.26 N/mm), reflecting the additional radial expansion of the wall under the conventional approach.

To assess how closely the linear and conventional approaches approximated reference stresses under different conditions, computations were performed for a range of α and β values ($\gamma = 0$) and different initial geometries (see **Fig. 9**). To effectively compare and visualize stress differences (with respect to reference stresses) as a function of the parameters α and β in the reference model, we used **Eq. 33** so that each case (linear, conventional) was represented by one value, which we chose to report as a percent stress difference. We found that, irrespective of the tissue properties used in the reference model, stresses obtained using the linear model were closer to the stresses in the reference model than were the stresses obtained using the conventional model (see **Fig. 9**). Differences with respect to reference stresses decreased for both the linear and conventional models as α increased. Increasing β, however, had only a small effect on stress differences. Increasing the model external radius B while keeping a constant wall thickness h_0 resulted in increased stress differences between the conventional and reference models and decreased differences between linear and reference models (compare **Figs. 9A**, **9C** and **9E**; and **9B**, **9D** and **9F**). Both B and h_0 correspond to the initial configuration of the reference model. Increasing h_0 while keeping B constant resulted in decreased stress differences between the conventional and reference models but an increased difference between the linear and reference models (compare **Figs. 9A** and **9B**; **9C** and **9D**; **9E** and **9F**). In general, however, the linear model approximated reference stresses better than the conventional model.

To determine how well the maximum effective stress is approximated by the linear and conventional approaches, we examined our previous results (**Fig. 9**) but reported differences in maximum effective stress (see **Fig. 10**). Maximum stresses were generally overestimated in the conventional model and underestimated in the linear model (see **Fig. 8**) when tissue properties for the reference model were within physiological range. We found that in most cases, the linear model approximated the maximum stress better than the conventional model within the physiological range of α and β, and the difference gap between linear and conventional models increased with increasing diameter and decreased with increasing thickness.

Increasing the applied internal pressure in the models from 0.016 N/mm^2 to 0.027 N/mm^2 (120 mmHg to 200 mmHg) increased the magnitude of the differences in wall stresses for the conventional model but not for the linear model (see **Figs. 11** and **12**). After increasing internal pressure, the linear model provided the better approximation of maximum effective stresses within the physiological range of tissue mechanical properties.

3.3.3 *Idealized AAA Models with Non-Uniform Wall Thickness*

To explore whether the linear model could be used to effectively study the effect of varying wall thickness, wall stresses were computed on idealized models of non-uniform wall thickness (see **Fig. 13**). RV material properties were used for the reference and conventional models. While the wall stresses obtained from the reference, conventional and linear models were similar, the stresses obtained using the linear model

were closer approximations of the reference stresses. The linear approach could therefore be used for estimating wall stresses and studying the effects of wall thickness.

3.3.4 *Idealized Curved and Subject-Specific AAA Models*

To determine how the wall stresses of the linear and conventional models compared to the wall stresses from the reference model when curvature was considered, we used an idealized axisymmetric model of an AAA in which the walls were curved and an internal pressure was applied to the inner wall (see **Fig. 14A**). RV tissue mechanical properties were used for the reference and conventional models. Effective wall stresses computed using the reference, conventional or linear models were similar, with larger stresses found in the wall region with greater curvature. Plots of wall stresses across the wall thickness and differences in effective stresses with respect to the reference configuration computed using **Eq. 32** further revealed that the linear model approximated the reference stresses better than the conventional model.

We then incorporated an intraluminal thrombus (ILT) to the idealized AAA model to assess its effect on wall stress and determine the degree to which the linear and conventional approaches approximate the reference stresses in the presence of the ILT (see **Fig. 14B**). To this end, we used average values of material properties for both the wall (RV properties) and thrombus in the reference and conventional models, and we used the average MPR for the linear model. We found that effective stresses that were computed using the reference model were better approximated by the linear model than by the conventional model. We then varied the model MPRs (in the reference, conventional and linear models). Values of MPR considered were 4, 6.7 (average), and

10.25. The stresses of the linear model were found to be closer to those of the reference stresses for all MPRs considered (see **Fig. 15**). We also observed that as the MPR of the reference configuration is varied, wall stresses considerably change.

To assess the effect of complex curvature and asymmetrical geometry on wall stresses, we considered a patient-specific (Subject A0) geometrical AAA model with applied internal pressure (see **Fig. 14C**). We made the assumption that the patient AAA geometry obtained from CT scan images corresponded to the unloaded configuration; therefore, we used this geometry as the initial configuration in the reference model. Conventional and linear models used the deformed configuration obtained from the reference model (after applying an internal pressure) as their initial configuration. While stress distributions looked similar for the linear, conventional and reference models, local effective stress plots across the wall thickness (from selected regions) showed that, in general, linear stresses better approximated the reference stresses. Computed differences in stress with respect to the reference stress values (using **Eq. 32**) at the inner and outer surfaces, where differences in stress were expected to be larger, further revealed that stresses from the linear model, compared to those of the conventional model, were closer to the reference stresses (see **Figs. 14C** and **16**).

3.3.5 *Axisymmetric Tubular Model of an AAA with Varying Tissue Properties and Residual Stresses*

To determine how the choice of tissue mechanical properties affects wall stresses, we simulated the axisymmetric tubular model using different nonlinear tissue properties (RV, P1 and P2; see **Table 3**). For these models, the initial, unloaded configuration

varied slightly, such that the deformed configuration was the same for all nonlinear models, while the linear model employed this deformed configuration as its initial geometry. Two cases were considered in which the external diameters and thicknesses of the deformed configuration were: 1) 35.5 mm and 1.25 mm, respectively; and ii) 73.9 mm and 1.21 mm, respectively. The applied internal pressure (0.016 N/mm^2) was the same for the two cases. We found that the wall stresses computed using the nonlinear models (RV, P1 and P2) varied significantly and were different from those computed using the linear model (see **Fig. 17**). As expected, however, the integral of the circumferential stresses over the deformed wall thickness, left hand side of **Eq. 34**, was the same for all models (since the deformed configuration was the same), indicating that equilibrium of stresses was obtained.

Next, we considered the effect of residual stresses (see **Fig. 7**) on computed wall stresses. We considered cases with different material properties and different initial opening angles. We varied the angle θ in the initial unstressed configuration, ensuring that the closed configuration (unloaded configuration with residual stresses) was the same for all cases. In the closed configuration, the outer radius b_0 was 30 mm, while the wall thickness was 1.5 mm. An internal pressure (p = 0.016 N/mm^2) was then applied to the closed configuration, and the loaded, deformed configuration was obtained. For comparison, the linear approach was applied to the deformed configuration of the case with no residual stresses ($\theta = 0°$). We found that, as expected, increasing the opening angle increased the magnitude of residual stresses (see **Fig. 18**, left panels). Residual stresses were negative in the inner portion of the wall and positive in the outer portion of it, with magnitudes that depended on both the opening angle and wall material properties.

Loading the closed geometries with an internal pressure resulted in wall stresses that were progressively smaller in magnitude with increasing opening angle (see **Fig. 18**, right panels). As a consequence, the gradient of stresses across the wall decreased with increasing θ until a flat wall stress profile across the wall thickness was obtained. Increasing the opening angle beyond this point resulted in a change in the sign of the wall stress gradient (inner wall had lower stress than the outer wall). The opening angle at which a flat wall stress profile across the wall thickness was achieved strongly depended on the wall material properties considered. Computations performed using the linear model showed a relatively flat stress profile across the wall thickness (see **Fig. 18**, right panels) that was representative of nonlinear models that accounted for residual stresses. These results serve as a way of elucidating possible effects of residual stresses on AAA tissue stresses, even though the residual stresses cannot currently be computed on patient-specific models.

3.4 Discussion

Wall stress computations of vascular tissues and, in particular, of AAA tissues are difficult to achieve. This is because tissue mechanical properties are nonlinear and anisotropic and could vary spatially; cardiovascular loads generate large tissue deformations; and patient-specific geometries can be intricate while proper boundary conditions can be difficult to estimate. When stresses are computed using numerical techniques, such as FEA, nonlinearities introduce convergence problems, in which the solution does not converge to equilibrium (i.e., equilibrium of forces is not achieved).

These difficulties force researchers to seek solutions by loading the tissues in small increments. These steps, however, introduce computational and model-preparation challenges that make achievement of solutions extremely difficult for non-experts and tedious for experts. Moreover, wall stresses are typically computed assuming that the loaded geometries obtained from CT scans, MRI scans, or ultrasound images are unstressed and unloaded [103][104]. Application of internal pressures to these geometries results in large, artificial deformations and stress overestimation [23][29], which are shown in this study. While methodologies to find the initial unloaded and unstressed configuration have been proposed [23], they are difficult to implement [104]. Moreover, current methodologies do not account for residual stresses, unknown spatial changes in material properties, or the effects of external organs on AAA tissues. Thus, computations of wall stress are extremely time-consuming and might not yet be accurate given that patient-specific tissue mechanical properties, residual stresses and outside boundary conditions are not known.

To facilitate the computation of wall stresses, we propose using linear models of AAAs. Our linear models assume not only linear wall material properties, but also infinitesimally small displacements and strains. Thus, the linear models can compute equilibrium wall stresses while preserving the loaded patient-specific geometry. The simplicity of the approach allows computations to be achieved quickly, without nonlinear iterations or small incremental load steps and without the need to know the tissue mechanical properties. We found that the proposed linear approach not only offers the benefits of computational efficiency and simplicity, but also approximates reference stresses better than conventional models in various AAA geometries. Additionally,

computations using the linear model provided a desirable and physiologically relevant flat wall stress profile over the wall thickness.

3.4.1 *Limitations*

Our linear, conventional, and reference models involved several simplifying assumptions. These assumptions included the following: i) tissue mechanical properties used were isotropic and uniform; and ii) residual stresses were generally neglected, although we included an analysis of residual stresses for idealized tubular models. These simplifications, nevertheless, are typically used in models of AAA [22][103][113], and therefore our study is relevant in elucidating uncertainties introduced by these assumptions.

AAA walls are best characterized as nonlinear anisotropic tissues [15][22][105][109][114][115]. Like our study, many studies of AAA, however, have been performed assuming isotropic and uniform nonlinear mechanical properties for wall tissues [22][27][106][113][116][117]. This is because anisotropic material properties, including the anisotropy directions, are unknown for a specific patient; are more difficult to implement than the hyperelastic isotropic material properties typically assumed; and are more prone to model convergence issues. Likewise, heterogeneities in AAA tissue properties are also not known and cannot currently be measured on patients. Similar to the conventional modeling approach with isotropic material properties, use of anisotropic and even heterogeneous material properties generates artificial model distortions. Large uncertainties are nevertheless introduced by the lack of precise knowledge of the patient-specific tissue material properties. In a recent study [106], biaxial tensile test results from

anisotropic AAA tissues obtained from patients were fitted to an isotropic energy-density function with relative good correlation among tensile test data and function values. Like our study, this previous study showed that the specific choice of tissue mechanical properties employed has a large effect on wall stress, including wall stress gradients across the wall thickness. The study concluded that tissue material properties are important, and that residual stresses, which decrease stress gradients across the wall, might be needed to more accurately estimate wall stresses. Further, other studies [106][118][119][120] also acknowledged that, physiologically, wall stress is likely to be nearly uniformly distributed in blood vessel walls, with residual stresses helping to achieve a more uniform stress distribution. Because equilibrium of forces is satisfied for the linear models in the intact patient geometrical configuration, and stress gradients across the wall thickness obtained using linear models of AAA are minimal, the linear approach holds promise as an effective, computationally efficient method for estimating wall stresses in patient-specific AAAs.

Even though circumferential residual stresses and longitudinal loads are present in blood vessels [118], we generally assumed the unloaded configurations to be unstressed, as done conventionally [103][113]. We also assumed that external organs do not affect AAA wall stress. We explored, however, the effect of residual stresses on loaded tissue wall stresses. In an idealized straight tube model, residual stresses result in a more uniform circumferential stress distribution than the case with no residual stresses (see **Fig. 18**). A more uniform stress distribution is postulated to optimize smooth muscle performance [120] and thus it is assumed to be a more physiological scenario. This is because a uniform stress distribution also implies uniform strains (elongation) of smooth

muscle cells across the wall thickness. Smooth muscle contraction efficiency is optimized when individual cells share the same strains and contract together at the same time. Residual stresses (and residual strains) therefore help to bring smooth muscle cells across the wall to a similar strain under loading conditions, which results in a more uniform mechanical environment that improves contractility [119]. AAA walls, however, have expanded and weakened through extensive remodeling and might hold only little residual stresses and/or longitudinal stresses. This is supported by the clinical observation that AAA tissue collapses when the aneurysm is unloaded and pathology studies that demonstrate a paucity of smooth muscle cells in the wall of AAAs compared to normal aorta. Nevertheless, accurate estimations of patient-specific wall stresses might be elusive in light of large differences in wall stresses obtained using different tissue material properties from actual AAA tissue samples. Thus, even in the absence of residual stresses, the linear approach may remain effective in approximating wall stresses in AAA tissues, regardless of the limitations in our approach.

Another limitation of the linear model is its inability to capture AAA deformations throughout the cardiac cycle, which may be useful to assess wall stiffness and, perhaps, tissue mechanical changes and tissue degradation. Typically, the change in diameter of a normal aorta near the renal-aortic bifurcation throughout the cardiac cycle is about 2 mm [121]. Although AAA tissue has been reported to have less distensibility than a normal aorta due to a loss of tissue elasticity, an increase in collagen deposition, and a possible mechanical cushioning effect from the thrombus [74][122], AAA deformations may be significant. The linear model, however, may be used together with gated imaging modalities, e.g., electrocardiography gated CT scans or MRI scans, which

allow image reconstruction at specific phases of the cardiac cycle. Wall stresses specific to AAA geometries at different desired phases, e.g. end-systole and end-diastole, could then be obtained, and wall stresses can subsequently be related to the extent of deformation measured between AAA geometries. This information may be helpful in the assessment of aneurysmal tissue degradation and thus in assessments of rupture and expansion risks.

3.4.2 *Advantages of the Linear Model*

The proposed linear model applied to AAA tissues generally yielded good approximations of wall stresses with relatively small stress gradients across the wall thickness. The wall stresses obtained with the linear model were frequently closer to reference stresses than the stresses obtained using a conventional approach. Further, the linear model captured the physiologically relevant situation of small stress gradients across the wall thickness that is a consequence of residual stresses. Because the linear model achieved equilibrium of stresses on the patient-specific geometry directly, boundary conditions (the intraluminal pressure applied to the inner AAA wall) were exactly satisfied on the deformed patient-specific geometry. This results in a reduction of artifacts due to geometrical distortions of the AAA geometry beyond those of patient tissue deformations that frequently occur when conventional approaches are used. Even when approaches that first compute the unloaded configuration are employed, in which equilibrium and boundary conditions are also satisfied directly on the patient-specific geometry, the linear approach yields wall stresses with a relatively flat stress profile

across the wall. Further, these advantages are achieved in a computationally efficient way, with a relatively easy and straight-forward implementation.

Incorporation of thickness variability in models of AAA has been shown to result in significant differences in wall stress compared to models with a uniform thickness [87]. This is an important consideration because tissue thickness is typically not uniform in patients [87]. The use of uniform thickness models, however, comes from limitations in imaging technologies, from which determination of wall thickness variations is difficult. With the improvement of imaging technologies, however, it is easy to envision that wall-thickness variations would soon be incorporated into wall segmentation algorithms from images [87][123]. The linear model could therefore be used for reliably studying the effects of wall thickness.

Advantages of the linear approach make it a promising tool for further AAA wall stress investigations and implementation in clinical practice. The linear model does not require the computation of an initial configuration; does not artificially distort the imaged, loaded geometry; and can approximate wall stresses when wall tissue properties are unknown. Further, the linear models achieve relatively small wall stress gradients across the wall thickness, which might be physiologically relevant. The linear model has the additional advantage over the conventional model (and even over models that compute the unloaded configuration) of being much faster and easier to implement, with wall stress solutions being obtained directly without the need of nonlinear iterations or time-consuming load steps. The linear approach, thus, is a robust and computationally efficient tool in computing wall stresses for patient-specific AAA studies.

3.4.3 *Effect of Thrombus in the Calculation of Wall Stresses*

Consideration of an intraluminal thrombus (ILT) in the AAA models could be important since it decreases the magnitude of the wall stresses [85][124]. The linear model approximated reference wall stresses very well (< 5% difference) when the wall-ILT MPR were the same for the reference and linear models (see **Fig. 15**). This indicates that when the patient-specific wall-ILT property ratios are known, the linear approach is highly effective at estimating wall stresses. In a more clinical relevant scenario, determining the patient-specific wall-ILT MPR is not currently feasible. To circumvent this problem, we employed a mean MPR, obtained from mean patient tissue and ILT mechanical property measurements. Other groups that used conventional approaches or approaches that compute the unloaded configuration also had to rely on average tissue and ILT material properties (not only MPR). To assess uncertainties in using average properties, we employed a mean MPR value of 6.7 for the linear and conventional models, while allowing the MPR of the reference model to vary. We observed that wall stress differences between the linear and reference models vary significantly (from 3.7% to 66%, the latest for the most extreme case of MPR = 4 in the reference model). This is, however, an intrinsic difficulty that all models face (conventional approaches yielded differences in wall stresses with respect to reference stresses that ranged from 6.3% to 111.2%), since patient-specific material properties are unknown. Thus, care will need to be exercised in the computation of wall stresses from models with thrombi to make sure that wall estimations and associated risk calculations are conservative.

3.4.4 *Effect of Boundary Conditions in the Calculation of Wall Stresses*

Typically, continuum mechanics equations (**Eqs. 1** and **2**) establish equilibrium of forces in the deformed configuration. This implies that boundary conditions are applied to the final, deformed configuration. As presented before, this choice also implies that, in a cylindrical model, equilibrium in the reference and linear models will yield the same value for the integral of $\sigma_{\theta\theta}$ over the wall thickness (see **Eq. 34**), ensuring that linear estimates of wall stresses are similar to reference wall stresses. The conventional nonlinear models, however, yield a different equilibrium integral because application of internal pressure produces a deformation beyond that of the imaged equilibrium configuration. Application of internal pressure boundary conditions with respect to the undeformed configuration, rather than the deformed configuration, in the conventional approach could yield stresses that are closer to those obtained using the reference model. In fact, when applying internal pressures to the undeformed configuration, the magnitude of Cauchy stresses $\sigma_{\theta\theta}$ and σ_{rr} were closer to reference stresses, than those obtained when the internal pressure was applied to the deformed configuration (see **Figs. 19 and 20**). Conventional and linear models then yielded similar estimations of wall stress. The linear model, however, not only provides and alternative way of computing AAA wall stresses, but also has the advantages of easy implementation, solution efficiency, and independence of tissue mechanical properties.

3.4.5 *Potential Clinical Applications*

While wall stress could provide better estimation of AAA rupture risk and expansion than the maximal aneurysm diameter [13][20][113], current difficulties in the computation of patient-specific wall stresses, rupture risk, and AAA size progression still

remain. These difficulties include uncertainties in the tissue material properties and tissue strength; computation of the unloaded configuration (including residual stresses); unknown boundary conditions (including the effect of external organs and the ILT); and the nonlinearity of the models, which increase the complexity of the computations involved. While patient-specific AAA loaded geometries can be imaged and segmented for use in FEA computation of wall stresses, these models do not account for the patient-specific tissue mechanical properties, which are unknown and challenging to obtain without tissue dissection. To circumvent these problems, researchers have been using average values of AAA tissue material properties and average tissue strengths obtained from cadaver studies or tissues obtained from patients undergoing elective repair. Thus, while stresses are calculated on patient-specific geometries and perhaps patient-specific blood pressures, the remaining assumptions in the model are not patient-specific. The use of hyperelastic tissue material properties in the AAA models, in addition, makes the FEA solution difficult to achieve and time-consuming. Therefore, while several promising studies relating AAA wall stresses, AAA size progression, and rupture risk have been conducted in the research arena, these models have not been widely translated into clinical practice.

Improving the accuracy and efficiency of wall stress computations is a key step for assessing an AAA patient's risk of rupture and for improving our understanding of how wall stresses relate to AAA progression. We have shown that the use of different tissue material properties and tissue opening angles can lead to drastic changes in computed wall stresses and wall stress gradients across the wall thickness (**Figs. 17** and **18**). Furthermore, wall stresses depend on the mechanical properties of the intraluminal

thrombus and interaction with external organs, which are also typically unknown. The collective uncertainties introduced by unknown patient-specific tissue material properties, degree of residual stresses, and degree of tissue degradation and strength indicate that computation of truly patient-specific AAA wall stresses might be elusive. The proposed linear model provides a relatively simple methodology to estimate wall stresses, which is not only computationally efficient, but that also ensures satisfaction of wall stress equilibrium directly in the patient-specific AAA geometry. Further, the linear model does not require knowledge of tissue mechanical properties, and yields a physiologically relevant wall stress profile across the wall thickness.

Implementation of the linear model will tremendously facilitate automation of the computational process to obtain patient-specific AAA wall stresses. This can translate into the computation of patient-specific wall stresses in a much shorter time. Improving the accuracy and speed for wall stress computations are indispensable for identifying patients who are at higher risk for AAA rupture or expansion to the renal arteries or iliac bifurcation and require emergent repair. Previous studies have shown that wall stress better discriminates rupture and expansion risks than maximal AAA diameter. Studies are undergoing to determine the extent to which wall stresses determined from the linear model can indeed be used in predicting patient-specific outcomes. The proposed linear model has shown so far to be a promising clinical tool for possibly predicting AAA rupture and expansion risk. With the computation of wall stress enormously simplified by using the linear approach, studies of rupture and expansion risk can be more easily performed and extended and prediction of patient outcomes more readily obtained.

CHAPTER 4: SUMMARY, CONCLUSIONS, AND ONGOING/FUTURE WORK

The study presented in this dissertation set out to explore a more efficient method for computing patient-specific AAA wall stresses, which have been shown to be better predictors of rupture risk than the currently used maximum transverse diameter [13][16][17][18][19][20]. The need for this research is indisputable because stress-based methods are currently far from being usable as clinical tools for the assessment of AAA rupture risk. This is because stress-based methods are time-intensive and difficult. The difficulty of these methods is partly attributed to the modeling of AAA tissues as nonlinear materials. Adding to the difficulty in computation is the lack of knowledge of patient-specific AAA tissue properties, which cannot be determined without tissue excision. Thus, the material properties that are often employed are population average values rather than patient-specific. Current methods also rely on the assumption that the CT AAA geometry is initially unloaded and unstressed. When pressure is applied to the lumen of the nonlinear AAA model, artificial distortions and overestimated wall stresses result. Efforts to minimize these geometrical distortions require the computation of an initial unloaded, unstressed configuration of an AAA, which involves the use of complex inverse mathematical algorithms.

One way to circumvent many of the presented problems is to model the AAA as a linear elastic material with small displacements and strains. Computations involving the use of linear elastic materials can be achieved much more quickly and easily than nonlinear models. Knowing the benefits that are conferred by the linear model, the study sought to answer the following vital question: can patient-specific wall stresses be computed more efficiently by characterizing AAA tissues as linear elastic materials? The

answer to this question depended on whether the linear model could predict patient wall stresses with good approximation.

In Chapter 3, the linear model was shown to closely approximate reference stresses compared to the conventional model for patient-specific AAA models, as well as idealized models of an AAA. Moreover, the stresses computed using the linear model closely approximated the stress distributions of diverse nonlinear material property models that accounted for the presence of residual stresses. These stress distributions were relatively uniform across the wall thickness and represented a relevant physiological state where the mechanical strain of smooth muscle cells across the wall was equalized to optimize contractility. More importantly, the linear model closely approximated the reference stresses without knowledge of patient-specific AAA tissue properties, which are typically unknown in clinic. These findings suggest that the linear model confers the benefit of computing patient-specific wall stresses in an efficient manner. This achievement is the first step needed to consider stress-based methods for use in the clinic to determine patient-specific AAA rupture risks.

The linear model may be a promising clinical tool for assessing AAA rupture risk, but its applicability is not restricted to this use. The easy-to-use characteristic of the linear model makes it an exceptional tool for research. In fact, the linear model is currently used in an ongoing research project to elucidate the role that wall stress plays in AAA progression. The project attempts to determine if the tissue growth and remodeling laws (see Section 4.1.1) are reasonable descriptors of AAA growth in response to the imposed stresses. If the tissue growth laws are applicable, they may be useful for predicting the extent of AAA expansion and rupture risk.

The remainder of this chapter will briefly introduce current work that employs the linear model and a simplified use of the tissue growth laws to study wall stress and AAA expansion relationships. Additionally, we introduce an idea for a study that aims to evaluate the linear model's ability to differentiate wall stress distributions in not only ruptured and non-ruptured AAAs, but also other cardiovascular diseases, such as TAAs, aortic dissections, and intracranial aneurysms. This particular study is needed for further assessing the linear model's utility as a clinical tool for predicting rupture risk in AAAs and other vascular diseases.

4.1 Elucidating Wall Stress-AAA Expansion Relationships

4.1.1 *Tissue Growth & Remodeling Theory Laws*

Although wall stress is involved in the progression of an AAA [69] (see Chapter 1, Section 2), this relationship remains poorly understood, and efforts to elucidate the relationship have been discouraging. This is because AAA growth has been reported to be discontinuous with periods of growth and non-growth, making the task of predicting future aneurysmal expansion quite difficult [94]. One study, however, showed a positive correlation between AAA expansion and the peak wall stress at the shoulder of the AAA, i.e., the point where the surface changes from positive to negative curvature and vice versa [113]. Another study reported that lower wall stresses were associated with lower AAA growth rate [125]. These findings attest to the possibility that a relationship between wall stress and AAA growth can be found and further elucidated to assess how wall stress distributions can be applied to predict AAA growth.

In our ongoing study, we set out to determine if the relationship between wall stress and aneurysmal expansion can be described by the tissue growth and remodeling laws [102], which are based on the concepts of homeostasis and equilibrium [69][102]. The forces in a mature aorta wall are in equilibrium with the hemodynamic forces, and homeostasis is maintained. If the forces applied to the aortic wall become chronically disrupted, homeostatic wall stresses are no longer conserved. In order to restore homeostasis, the aorta will remodel or grow. For example, in the case of an abnormal increase in blood flow, the aorta will grow in diameter in order to reduce wall shear [126][127]. The tissue growth and remodeling process in response to stress is expressed mathematically as follows for a small cross-sectional segment of aortic tissue [102]:

$$\dot{\lambda}_{gr} = b_r \left(\sigma_{\theta\theta} - \sigma_{\theta\theta 0} \right), \tag{35}$$

where **Eq. 35** is representative of the rate of tissue growth in the radial direction $\dot{\lambda}_{gr}$; b_r is a radial proportionality constant; $\sigma_{\theta\theta}$ is the Cauchy circumferential stress component and $\sigma_{\theta\theta 0}$ is the circumferential growth equilibrium stress;

$$\dot{\lambda}_{g\theta} = b_\theta \left(\sigma_{\theta\theta} - \sigma_{\theta\theta 0} \right) + b_\tau \left(\tau - \tau_0 \right), \tag{36}$$

where **Eq. 36** describes the rate of circumferential growth $\dot{\lambda}_{g\theta}$; b_θ and b_τ are circumferential and shear proportionality constants, respectively; and τ and τ_0 are the average shear stress on the endothelium due to blood flow [102] and shear growth equilibrium stress, respectively; and

$$\dot{\lambda}_{gz} = 0, \tag{37}$$

where $\dot{\lambda}_{gz}$ is the longitudinal growth rate. Although AAA growth in the longitudinal direction in response to wall stress could be notable, in this ongoing study, the rate of growth is assumed to be zero [102]. This is done to facilitate our initial analysis of how wall stresses affect growth in the circumferential direction.

4.1.2 *Simplified Use of a Tissue Growth and Remodeling Law*

In order to determine if the tissue growth laws are reasonable descriptors of AAA progression, we are first exploring the relationship between circumferential wall stress and circumferential growth. To facilitate investigation of this relationship, we simplified the growth and remodeling law described in **Eq. 36** by omitting the shear and the circumferential equilibrium stress terms. In excluding these terms, we intended to limit the number of variables involved and assess if aneurysmal growth could be reasonably predicted by only knowing the circumferential stress distributions. Once this relationship is understood, the shear stress and equilibrium stress terms can be sequentially introduced in future studies to better understand how each term further affects AAA growth. The simplified form of **Eq. 36** is

$$\dot{\lambda}_{g\theta} = b_{\theta}\sigma_{\theta\theta}. \tag{38}$$

Eqs. 36 and **38** describe circumferential growth in an infinitesimal sector of AAA tissue. To account for growth around the AAA cross-section, a contour integral must be computed

$$\oint \dot{\lambda}_{g\theta}\, ds = \oint b_\theta \sigma_{\theta\theta}(s)\, ds\,, \tag{39}$$

where the circumferential growth term is

$$\lambda_{g\theta} = \frac{\partial s'}{\partial s}\,, \tag{40}$$

and *s* and *s*' are the length parameters of corresponding contours at the time of interest and at a future time, respectively, and *ds* is the infinitesimal distance. **Eq. 39** simplifies to

$$\frac{P - P^*}{\Delta t} = b_\theta \oint \sigma_{\theta\theta}(s)\, ds\,, \tag{41}$$

where *P** is the perimeter of an AAA cross-section contour (in mm) at the time of interest, and *P* is the perimeter of the corresponding cross-section contour at a future time, respectively; and Δt represents the elapsed time (in years) between the two time points.

An assessment of localized (cross-sectional) growth provides crucial information about how the AAA expands in response to the local wall stress distribution. If this form of evaluation is applied to an AAA that is divided into multiple cross-sections, then an overall assessment of growth can be achieved, improving our understanding of wall stress and AAA expansion relationships. Current methods offer limited knowledge about this important relationship because a partial evaluation of aneurysmal growth is typically reported, which only involves the measurement of changes in the diameter length at a few specific locations over time [94][113][125][128].

4.1.3 *Potential Significance*

If a good correlation is found between the local wall stress distributions and AAA growth as described in **Eq. 41**, then the coefficient b_θ can be calculated and used as a patient-specific parameter to predict growth for the AAA at a future time point. This predictive power can be invaluable in determining which areas of the AAA are more prone to growth and are at greatest risk for rupture.

4.1.4 *Computing Cross-Sectional Growth and Wall Stresses*

To preliminarily assess the wall stress-AAA growth relationship described by **Eq. 41**, the AAA from Subject A4 introduced in Chapter 2 was used. Three CT scans of Subject A4's infrarenal AAA were acquired at three different times, which were the minimum number of time points necessary to evaluate changes in AAA growth rates and wall stress distributions. The AAA geometries were each segmented from acquired CT scans using a collaborator's segmentation program (SP2) and were subsequently organized into cross-sectional rings using the approach explained in Chapter 2, Section 3. To facilitate the evaluation of growth throughout the AAA, a MATLAB program was written to calculate the rate of growth for every cross-section using the left hand expression in **Eq. 41**—the program was also written compute the wall stress contour integrals for each cross-section. As part of a preliminary analysis, growth was assessed between the AAAs at the first two time points.

Once the growth rates were calculated, the AAA wall stresses were computed at the first time point using the linear model and the approaches established in Chapter 2. The AAA was modeled with an ILT using 27/4 hexahedral elements for both the wall and ILT. Convergence of wall stress results was achieved using 9,600 wall elements and

19,200 ILT elements, respectively, with 3 and 5 elements spanning the thicknesses of the wall and thrombus, respectively. In order to determine if the amount of attenuation in the magnitude of wall stress due to the thrombus matches with expectation, the effective wall stresses of the AAA-ILT model were compared to those of the same AAA modeled in the absence of an ILT. In this study, assessing differences in effective stress was more convenient than for differences in circumferential stress. The thrombus-free AAA was simulated with 9,600 27/4 hexahedral elements, with 3 elements spanning the thickness. Relative differences in effective stress were computed using **Eq. 32**.

4.1.5 *Preliminary Results*

When the effective stress distributions of the patient AAA modeled without a thrombus were compared to those of the same AAA with an ILT, we observed that inclusion of a thrombus greatly attenuated the wall stress magnitudes. In fact, in regions where the average circumferential ILT thickness was 1-1.8 mm, the effective stresses were attenuated by 0.4-59%. We were surprised to see a large attenuation in wall stress magnitude in areas where the thrombus was relatively thin because these results conflicted with those of a previous study. In our initial study, we compared wall stresses between axisymmetric idealized curved models of an AAA that excluded and included an ILT with a uniform thickness of 1 mm. We found that wall stresses in the AAA-ILT model were attenuated by 10.5-14.7% (see **Fig. 21**). Thus, we were not expecting to observe large reductions in wall stress magnitudes in areas juxtaposed to a thin thrombus for the patient-specific model. Future efforts will be devoted to understanding why large wall stress attenuations were observed and whether these attenuations are accurate.

Despite the presented difficulty, we have developed methods that include implementation of a simplified tissue growth and remodeling law to assess growth throughout the AAA rather than at specific locations. Moreover, the proposed methods exploit the benefits of the linear model to compute wall stresses efficiently. Our approach is promising because it facilitates the study of wall stress and AAA expansion relationships, which may allow us to identify 1) ways to predict aneurysmal growth from a distribution of wall stresses and 2) AAAs that are at greatest risk for rupture.

4.2 To Rupture or Not to Rupture? That is the Linear Model's Question

Our understanding of wall stress-AAA expansion relationships and AAA rupture risk assessment would also greatly improve if the linear model can be evaluated in its potential to differentiate AAAs that are likely to rupture from those that are more stable. In Chapter 3, the linear model was shown to predict the reference wall stresses with good approximation, irrespective of the material properties, geometries, and pressures used, suggesting that the linear model has great potential for yielding good estimates of the wall stress distributions in a patient-specific AAA. Thus, we propose that the linear model can effectively distinguish wall stress distributions between AAAs that have ruptured from those that have not. More specifically, we believe that wall stresses computed using the linear model for ruptured AAAs will more likely be higher than for non-ruptured AAAs. This is because wall stresses have been shown to be typically higher in ruptured aneurysms [13][18][19][20]. It is worth mentioning that an evaluation of AAA rupture should also account for wall strength distributions [17][18][129]; however,

because the non-invasive determination of patient-specific wall strength is infeasible (due to the need for tissue excision), performing a study that analyzes how wall stress alone is able to predict AAAs that rupture is an appropriate, important first step.

The analysis can be also be extended to differentiating ruptured and non-ruptured cases in thoracic aortic aneurysms (TAAs), intracranial/cerebral aneurysms (ICAs), and aortic dissection (AoD) of TAAs, i.e., separations of the aortic wall layers caused by blood entering a tear in the thoracic aorta. Wall stress is thought to play an important role in the formation, progression and rupture of AoDs, TAAs, and ICAs [130][131][132][133][134][135][136][137][138][139][140][141][142][143][144]. For instance, wall stress distributions have been shown to coincide with the site of AoD formation [133]; peak wall stress was shown to be strongly correlated with TAA expansion rate [135]; and models relating peak wall stress and strength have great promise for predicting rupture risk in diagnosed ICAs [145]. Further research is needed to assess the relationship between wall stresses and rupture risk for each disease as well as between wall stress and the risk of formation of AoDs in TAAs, because size has not been a good predictor of both types of risk [133][137][146][147]. To assess these relationships, a future study can be conducted where the linear model is 1) used to compute the wall stress distributions for patients suffering from TAAs, AoDs, and ICAs; and 2) then evaluated in its effectiveness to differentiate wall stress distributions between ruptured versus non-ruptured cases for each disease, as well as stresses in TAAs with and without AoDs. These analyses will be important for also assessing the linear model's broader clinical utility.

The design of the future study will be similar to that of a retrospective cohort study, where patients have developed the outcome of interest but the investigations "jump back" in time, identify an exposure of interest, and follow patients prospectively until they manifest the outcome. This is done to study the relationship between exposure and the outcome. In the case of AAAs, TAAs and ICAs, the outcomes of interest are not only symptomatic/ruptured aneurysms but also expansion requiring repair. Another outcome of interest for AAAs is extension to the juxtarenal aorta. For AoDs, the clinically relevant endpoint is rupture. In all cases, the "exposures" will include wall stress patterns (e.g., peak wall stress and mean wall stress) that were computed using the linear model. For each disease, an ROC curve can be generated using the wall stress patterns as predictors for each clinically relevant endpoint. For example, in the case of size-matched AAAs where peak stress will be evaluated as a predictor of rupture risk, an ROC curve will be generated to assess the effectiveness of peak wall stress in discriminating ruptured and non-ruptured cases as threshold values of stress are varied. A Youden's J statistic will be applied to select the threshold value of peak wall stress that optimizes the sensitivity and specificity. Using the optimal discriminant value, the number of patients correctly predicted as ruptured and non-ruptured will be recorded, and statistical significance between the two groups will be evaluated using a paired *t* test. The analysis outlined in this example can be repeated for other diseases and for each clinically relevant endpoint. One difficulty that may be encountered in these studies is having a low number of patients because the clinically relevant endpoint is unusual or rare, e.g., juxtarenal expansion of the AAA and AoD/TAA rupture [148][149]. To increase statistical power in these cases, the juxtarenal expansion of the AAA can be pooled with growing AAAs

requiring repair, and patients suffering from ruptured aortic dissections can be pooled with patients that have ruptured TAAs. Collectively, the analyses that will be conducted for future project can help verify the ability of the linear model to discern AAAs, TAAs, ICAs and AoDs that are likely to grow and/or rupture, strengthening the model's utility as a clinical tool.

Because of its simplicity, the linear model offers an efficient way to compute patient-specific wall stresses. This robust model is granting stress-based methods an opportunity to be considered as clinical tools rather than solely in research. The introduction of the linear model is the start of a promising research direction that may culminate in the eventual replacement of the maximum transverse diameter as the marker of choice for evaluating rupture risk and/or growth in AAAs, TAAs, ICAs and AoDs. If this proves to be the case, more patient lives will be saved, and fewer patients will undergo unnecessary surgery.

REFERENCES

1. Zelaya JE, Goenezen S, Dargon PT, Azarbal A-F, Rugonyi S (2014) Improving the efficiency of abdominal aortic aneurysm wall stress computations. PLoS ONE 9: 1-18.
2. Martufi G, Di Martino ES, Amon CH, Muluk SC, Finol EA (2009) Three-dimensional geometrical characterization of abdominal aortic aneurysms: Image-based wall thickness distribution. J. Biomech. Eng. 131: 610151-6101511.
3. McGloughlin TM, Doyle BJ (2010) New approaches to abdominal aortic aneurysm rupture risk assessment: Engineering insights with clinical gain. Arterioscl. Thromb. Vasc. Biol. 30: 1687-1694.
4. Nordon IM, Hinchliffe RJ, Loftus IM, Thompson MM (2011) Pathophysiology and epidemiology of abdominal aortic aneurysms. Nat. Rev. Cardiol. 8: 92-102.
5. Silverstein MD, Pitts SR, Chaikof EL, Ballard DJ (2005) Abdominal aortic aneurysm (AAA): cost-effectiveness of screening, surveillance of intermediate-sized AAA, and management of symptomatic AAA. Proc. (Bayl. Univ. Med. Cent.) 18: 345-367.
6. Lasheras JC (2007) The Biomechanics of Arterial Aneurysms. Annu. Rev. Fluid. Mech. 39: 293-319.
7. Vorp DA, Vande Geest JP (2005) Biomechanical determinants of abdominal aortic aneurysm rupture. Arterioscl. Thromb. Vasc. Biol. 25: 1558-1566.
8. Cornuz J, Sidoti Pinto C, Tevaearai H, Egger M (2004) Risk factors for asymptomatic abdominal aortic aneurysm: systematic review and meta-analysis of population-based screening studies. Eur. J. Public Health 14: 343-349.

9. Weston JP (1995) Chiropractic management of abdominal aortic aneurysm: a case report. The Journal of the C. C. A. 39: 75-79.

10. Siegel CL, Cohan RH (1994) CT of abdominal aortic aneurysms. A. J. R. Am. J. Roentgenol. 163: 17-29.

11. Brewster DC, Cronenwett JL, Hallett JW, Jr., Johnston KW, Krupski WC, et al. (2003) Guidelines for the treatment of abdominal aortic aneurysms. Report of a subcommittee of the Joint Council of the American Association for Vascular Surgery and Society for Vascular Surgery. J. Vasc. Surg. 37: 1106-1117.

12. Darling RC, Messina CR, Brewster DC, Ottinger LW (1977) Autopsy study of unoperated abdominal aortic aneurysms. The case for early resection. Circulation 56: II161-164.

13. Fillinger MF, Marra SP, Raghavan ML, Kennedy FE (2003) Prediction of rupture risk in abdominal aortic aneurysm during observation: Wall stress versus diameter. J. Vasc. Surg. 37: 724-732.

14. Nicholls SC, Gardner JB, Meissner MH, Johansen HK (1998) Rupture in small abdominal aortic aneurysms. J. Vasc. Surg. 28: 884-888.

15. Vorp DA (2007) Biomechanics of abdominal aortic aneurysm. J. Biomech. 40: 1887-1902.

16. Fillinger MF, Raghavan ML, Marra SP, Cronenwett JL, Kennedy FE (2002) In vivo analysis of mechanical wall stress and abdominal aortic aneurysm rupture risk. J. Vasc. Surg. 36: 589-597.

17. Kleinstreuer C, Li Z (2006) Analysis and computer program for rupture-risk prediction of abdominal aortic aneurysms. Biomed. Eng. Online 5: 19.

18. Maier A, Gee MW, Reeps C, Pongratz J, Eckstein HH, et al. (2010) A comparison of diameter, wall stress, and rupture potential index for abdominal aortic aneurysm rupture risk prediction. Ann. Biomed. Eng. 38: 3124-3134.

19. Truijers M, Pol JA, Schultzekool LJ, van Sterkenburg SM, Fillinger MF, et al. (2007) Wall stress analysis in small asymptomatic, symptomatic and ruptured abdominal aortic aneurysms. Eur. J. Vasc. Endovasc. Surg. 33: 401-407.

20. Venkatasubramaniam AK, Fagan MJ, Mehta T, Mylankal KJ, Ray B, et al. (2004) A comparative study of aortic wall stress using finite element analysis for ruptured and non-ruptured abdominal aortic aneurysms. Eur. J. Vasc. Endovasc. Surg. 28: 168-176.

21. Gasser TC, Auer M, Labruto F, Swedenborg J, Roy J (2010) Biomechanical rupture risk assessment of abdominal aortic aneurysms: model complexity versus predictability of finite element simulations. Eur. J. Vasc. Endovasc. Surg. 40: 176-185.

22. Humphrey JD, Holzapfel GA (2012) Mechanics, mechanobiology, and modeling of human abdominal aorta and aneurysms. J. Biomech. 45: 805-814.

23. Lu J, Zhou X, Raghavan ML (2007) Inverse elastostatic stress analysis in pre-deformed biological structures: Demonstration using abdominal aortic aneurysms. J. Biomech. 40: 693-696.

24. Raghavan ML, Vorp DA, Federle MP, Makaroun MS, Webster MW (2000) Wall stress distribution on three-dimensionally reconstructed models of human abdominal aortic aneurysm. J. Vasc. Surg. 31: 760-769.

25. Scotti CM, Jimenez J, Muluk SC, Finol EA (2008) Wall stress and flow dynamics in abdominal aortic aneurysms: Finite element analysis vs. fluid-structure interaction. Comput. Methods Biomech. Biomed. Engin. 11: 301-322.

26. Speelman L, Bohra A, Bosboom EM, Schurink GW, van de Vosse FN, et al. (2007) Effects of wall calcifications in patient-specific wall stress analyses of abdominal aortic aneurysms. J. Biomech. Eng. 129: 105-109.

27. Wang DH, Makaroun MS, Webster MW, Vorp DA (2002) Effect of intraluminal thrombus on wall stress in patient-specific models of abdominal aortic aneurysm. J. Vasc. Surg. 36: 598-604.

28. Raghavan ML, Vorp DA (2000) Toward a biomechanical tool to evaluate rupture potential of abdominal aortic aneurysm: Identification of a finite strain constitutive model and evaluation of its applicability. J. Biomech. 33: 475-482.

29. de Putter S, Wolters BJ, Rutten MC, Breeuwer M, Gerritsen FA, et al. (2007) Patient-specific initial wall stress in abdominal aortic aneurysms with a backward incremental method. J. Biomech. 40: 1081-1090.

30. Gee MW, Reeps C, Eckstein HH, Wall WA (2009) Prestressing in finite deformation abdominal aortic aneurysm simulation. J. Biomech. 42: 1732-1739.

31. Aggarwal S, Qamar A, Sharma V, Sharma A (2011) Abdominal aortic aneurysm: a comprehensive review. Exp. Clin. Cardiol. 16: 11-15.

32. DeRubertis BG, Trocciola SM, Ryer EJ, Pieracci FM, McKinsey JF, et al. (2007) Abdominal aortic aneurysm in women: prevalence, risk factors, and implications for screening. J. Vasc. Surg. 46: 630-635.

33. Blanchard JF (1999) Epidemiology of abdominal aortic aneurysms. Epidemiol. Rev. 21: 207-221.

34. Lederle FA, Johnson GR, Wilson SE, Chute EP, Hye RJ, et al. (2000) The aneurysm detection and management study screening program: validation cohort and final results. Aneurysm Detection and Management Veterans Affairs Cooperative Study Investigators. Arch. Intern. Med. 160: 1425-1430.

35. Johnson G, Jr., Avery A, McDougal EG, Burnham SJ, Keagy BA (1985) Aneurysms of the abdominal aorta. Incidence in blacks and whites in North Carolina. Arch. Surg. 120: 1138-1140.

36. Norman PE, Jamrozik K, Lawrence-Brown MM, Le MT, Spencer CA, et al. (2004) Population based randomised controlled trial on impact of screening on mortality from abdominal aortic aneurysm. B. M. J. 329: 1259.

37. Wilmink AB, Quick CR (1998) Epidemiology and potential for prevention of abdominal aortic aneurysm. Br. J. Surg. 85: 155-162.

38. Norman PE, Powell JT (2007) Abdominal aortic aneurysm: the prognosis in women is worse than in men. Circulation 115: 2865-2869.

39. Larsson E, Labruto F, Gasser TC, Swedenborg J, Hultgren R (2011) Analysis of aortic wall stress and rupture risk in patients with abdominal aortic aneurysm with a gender perspective. J. Vasc. Surg. 54: 295-299.

40. Thompson SG, Brown LC, Sweeting MJ, Bown MJ, Kim LG, et al. (2013) Systematic review and meta-analysis of the growth and rupture rates of small abdominal aortic aneurysms: implications for surveillance intervals and their cost-effectiveness. Health Technol. Assess. 17: 1-118.

41. Lo RC, Bensley RP, Hamdan AD, Wyers M, Adams JE, et al. (2013) Gender differences in abdominal aortic aneurysm presentation, repair, and mortality in the Vascular Study Group of New England. J. Vasc. Surg. 57: 1261-1268, 1268 e1261-1265.

42. Lo RC, Lu B, Fokkema MT, Conrad M, Patel VI, et al. (2014) Relative importance of aneurysm diameter and body size for predicting abdominal aortic aneurysm rupture in men and women. J. Vasc. Surg. 59: 1209-1216.

43. Wilmink AB, Hubbard CS, Day NE, Quick CR (2001) The incidence of small abdominal aortic aneurysms and the change in normal infrarenal aortic diameter: implications for screening. Eur. J. Vasc. Endovasc. Surg. 21: 165-170.

44. Acosta S, Ogren M, Bengtsson H, Bergqvist D, Lindblad B, et al. (2006) Increasing incidence of ruptured abdominal aortic aneurysm: a population-based study. J. Vasc. Surg. 44: 237-243.

45. de Boer NJ, Knaap SFC, de Zoete A (2009) Clinical detection of abdominal aortic aneurysm in a 74-year-old man in chiropractic practice. J. Chiropr. Med. 9: 38-41.

46. Costantino TG, Bruno EC, Handly N, Dean AJ (2005) Accuracy of emergency medicine ultrasound in the evaluation of abdominal aortic aneurysm. J. Emerg. Med. 29: 455-460.

47. Lindholt JS, Vammen S, Juul S, Henneberg EW, Fasting H (1999) The validity of ultrasonographic scanning as screening method for abdominal aortic aneurysm. Eur. J. Vasc. Endovasc. Surg. 17: 472-475.

48. Scott RA, Wilson NM, Ashton HA, Kay DN (1995) Influence of screening on the incidence of ruptured abdominal aortic aneurysm: 5-year results of a randomized controlled study. Br. J. Surg. 82: 1066-1070.

49. Moll FL, Powell JT, Fraedrich G, Verzini F, Haulon S, et al. (2011) Management of abdominal aortic aneurysms clinical practice guidelines of the European society for vascular surgery. Eur. J. Vasc. Endovasc. Surg. 41 Suppl 1: S1-S58.

50. Crow P, Shaw E, Earnshaw JJ, Poskitt KR, Whyman MR, et al. (2001) A single normal ultrasonographic scan at age 65 years rules out significant aneurysm disease for life in men. Br. J. Surg. 88: 941-944.

51. Wilmink TB, Quick CR, Day NE (1999) The association between cigarette smoking and abdominal aortic aneurysms. J. Vasc. Surg. 30: 1099-1105.

52. Johansson G, Nydahl S, Olofsson P, Swedenborg J (1990) Survival in patients with abdominal aortic aneurysms. Comparison between operative and nonoperative management. Eur. J. Vasc. Surg. 4: 497-502.

53. Swedenborg J (2008) Abdominal aortic aneurysm in the interval 5.0-5.5 cm, art or evidence? Scand. J. Surg. 97: 128-130.

54. Peppelenbosch N, Buth J, Harris PL, van Marrewijk C, Fransen G, et al. (2004) Diameter of abdominal aortic aneurysm and outcome of endovascular aneurysm repair: does size matter? A report from EUROSTAR. J. Vasc. Surg. 39: 288-297.

55. Vega de Ceniga M, Gomez R, Estallo L, de la Fuente N, Viviens B, et al. (2008) Analysis of Expansion Patterns in 4-4.9 cm abdominal aortic aneurysms. Ann. Vasc. Surg. 22: 37-44.

56. Tambyraja AL, Raza Z, Stuart WP, Murie JA, Chalmers RTA (2004) Does immediate operation for symptomatic non-ruptured abdominal aortic aneurysm compromise outcome? Eur. J. Vasc. Endovasc. Surg. 28: 543-546.

57. Yilmaz N, Peppelenbosch N, Cuypers PW, Tielbeek AV, Duijm LE, et al. (2002) Emergency treatment of symptomatic or ruptured abdominal aortic aneurysms: the role of endovascular repair. J. Endovasc. Ther. 9: 449-457.

58. Giles KA, Hamdan AD, Pomposelli FB, Wyers MC, Dahlberg SE, et al. (2009) Population-based outcomes following endovascular and open repair of ruptured abdominal aortic aneurysms. J. Endovasc. Ther. 16: 554-564.

59. Giles KA, Pomposelli FB, Hamdan AD, Wyers MC, Schermerhorn ML (2009) Comparison of open and endovascular repair of ruptured abdominal aortic aneurysms from the ACS-NSQIP 2005-07. J. Endovasc. Ther. 16: 365-372.

60. Holt PJ, Karthikesalingam A, Poloniecki JD, Hinchliffe RJ, Loftus IM, et al. (2010) Propensity scored analysis of outcomes after ruptured abdominal aortic aneurysm. Br. J. Surg. 97: 496-503.

61. Gloviczki P, Pairolero PC, Mucha P, Jr., Farnell MB, Hallett JW, Jr., et al. (1992) Ruptured abdominal aortic aneurysms: repair should not be denied. J. Vasc. Surg. 15: 851-857; discussion 857-859.

62. Ernst CB (1993) Abdominal aortic aneurysm. N. Engl. J. Med. 328: 1167-1172.

63. United Kingdom ETI, Greenhalgh RM, Brown LC, Powell JT, Thompson SG, et al. (2010) Endovascular versus open repair of abdominal aortic aneurysm. N. Engl. J. Med. 362: 1863-1871.

64. Veith FJ, Gargiulo NJ (2007) Endovascular aortic repair should be the gold standard for ruptured AAAs, and all vascular surgeons should be prepared to perform them. Perspect. Vasc. Surg. Endovasc. Ther. 19: 275-282.

65. Winterborn RJ, Amin I, Lyratzopoulos G, Walker N, Varty K, et al. (2009) Preferences for endovascular (EVAR) or open surgical repair among patients with abdominal aortic aneurysms under surveillance. J. Vasc. Surg. 49: 576-581 e573.

66. Lederle FA, Wilson SE, Johnson GR, Reinke DB, Littooy FN, et al. (2002) Immediate repair compared with surveillance of small abdominal aortic aneurysms. N. Engl. J. Med. 346: 1437-1444.

67. Powell JT, Blair S, Brady AR, Brown LC, Browse N, et al. (1998) Mortality results for randomised controlled trial of early elective surgery or ultrasonographic surveillence for small abdominal aortic aneurysms. Lancet 352: 1649-1655.

68. Limet R, Sakalihassan N, Albert A (1991) Determination of the expansion rate and incidence of rupture of abdominal aortic aneurysms. J. Vasc. Surg. 14: 540-548.

69. Taber LA (1998) A model for aortic growth based on fluid shear and fiber stresses. J. Biomech. Eng. 120: 348-354.

70. Ailawadi G, Eliason JL, Upchurch GR, Jr. (2003) Current concepts in the pathogenesis of abdominal aortic aneurysm. J. Vasc. Surg. 38: 584-588.

71. Hope TA, Hope MD (2011) Improved risk assessment for abdominal aortic aneurysm rupture: off-the-wall imaging. J. Am. Coll. Cardiol. 58: 2531-2532.

72. Yamashita O, Yoshimura K, Nagasawa A, Ueda K, Morikage N, et al. (2013) Periostin links mechanical strain to inflammation in abdominal aortic aneurysm. PLoS One 8: e79753.

73. Bonow RO, Mann DL, Zipes DP, Libby P (2012) Braunwald's Heart Disease: A Textbook of Cardiovascular Medicine, Single Volume. Elsevier.

74. He CM, Roach MR (1994) The composition and mechanical properties of abdominal aortic aneurysms. J. Vasc. Surg. 20: 6-13.

75. Carmo M, Colombo L, Bruno A, Corsi FR, Roncoroni L, et al. (2002) Alteration of elastin, collagen and their cross-links in abdominal aortic aneurysms. Eur. J. Vasc. Endovasc. Surg. 23: 543-549.

76. Lindeman JH, Ashcroft BA, Beenakker JW, van Es M, Koekkoek NB, et al. (2010) Distinct defects in collagen microarchitecture underlie vessel-wall failure in advanced abdominal aneurysms and aneurysms in Marfan syndrome. Proc. Natl. Acad. Sci. U. S. A. 107: 862-865.

77. Keen RR, Dorbin PB (2000) Development of Aneurysms. Georgetown, Texas: Landes Bioscience.

78. Wilson WR, Anderton M, Schwalbe EC, Jones JL, Furness PN, et al. (2006) Matrix metalloproteinase-8 and -9 are increased at the site of abdominal aortic aneurysm rupture. Circulation 113: 438-445.

79. Abdul-Hussien H, Soekhoe RG, Weber E, von der Thusen JH, Kleemann R, et al. (2007) Collagen degradation in the abdominal aneurysm: a conspiracy of matrix metalloproteinase and cysteine collagenases. Am. J. Pathol. 170: 809-817.

80. Sakalihasan N, Delvenne P, Nusgens BV, Limet R, Lapiere CM (1996) Activated forms of MMP2 and MMP9 in abdominal aortic aneurysms. J. Vasc. Surg. 24: 127-133.

81. Hance KA, Tataria M, Ziporin SJ, Lee JK, Thompson RW (2002) Monocyte chemotactic activity in human abdominal aortic aneurysms: role of elastin degradation peptides and the 67-kD cell surface elastin receptor. J. Vasc. Surg. 35: 254-261.

82. Miyake T, Morishita R (2009) Pharmacological treatment of abdominal aortic aneurysm. Cardiovasc. Res. 83: 436-443.

83. Sagan A, Mrowiecki W, Mikolajczyk TP, Urbanski K, Siedlinski M, et al. (2012) Local inflammation is associated with aortic thrombus formation in abdominal aortic aneurysms. Relationship to clinical risk factors. Thromb. Haemost. 108: 812-823.

84. Di Martino ES, Vorp DA (2003) Effect of variation in intraluminal thrombus constitutive properties on abdominal aortic aneurysm wall stress. Ann. Biomed. Eng. 31: 804-809.

85. Speelman L, Schurink GW, Bosboom EM, Buth J, Breeuwer M, et al. (2010) The mechanical role of thrombus on the growth rate of an abdominal aortic aneurysm. J. Vasc. Surg. 51: 19-26.

86. Raghavan ML, Kratzberg J, Castro de Tolosa EM, Hanaoka MM, Walker P, et al. (2006) Regional distribution of wall thickness and failure properties of human abdominal aortic aneurysm. J. Biomech. 39: 3010-3016.

87. Raut SS, Jana A, de Oliveira V, Muluk SC, Finol EA (2013) The importance of patient-specific regionally varying wall thickness in abdominal aortic aneurysm biomechanics. J. Biomech. Eng. 135: 810101-8101010.

88. Malayeri AA, Natori S, Bahrami H, Bertoni AG, Kronmal R, et al. (2008) Relation of aortic wall thickness and distensibility to cardiovascular risk factors (from the Multi-Ethnic Study of Atherosclerosis [MESA]). Am. J. Cardiol. 102: 491-496.

89. Matsumoto T, Hayashi K (1994) Mechanical and dimensional adaptation of rat aorta to hypertension. J. Biomech. Eng. 116: 278-283.

90. Stringfellow MM, Lawrence PF, Stringfellow RG (1987) The influence of aorta-aneurysm geometry upon stress in the aneurysm wall. J. Surg. Res. 42: 425-433.

91. Thubrikar MJ, Al-Soudi J, Robicsek F (2001) Wall stress studies of abdominal aortic aneurysm in a clinical model. Ann. Vasc. Surg. 15: 355-366.

92. Doyle BJ, McGloughlin TM, Miller K, Powell JT, Norman PE (2014) Regions of high wall stress can predict the future location of rupture of abdominal aortic aneurysm. Cardiovasc. Intervent. Radiol. 37: 815-818.

93. Doyle BJ, Callanan A, McGloughlin TM (2007) A comparison of modelling techniques for computing wall stress in abdominal aortic aneurysms. Biomed. Eng. Online 6: 38.

94. Kurvers H, Veith FJ, Lipsitz EC, Ohki T, Gargiulo NJ, et al. (2004) Discontinuous, staccato growth of abdominal aortic aneurysms. J. Am. Coll. Surg. 199: 709-715.

95. Brown LC, Powell JT (1999) Risk factors for aneurysm rupture in patients kept under ultrasound surveillance. UK Small Aneurysm Trial Participants. Ann. Surg. 230: 289-296; discussion 296-287.

96. Powell JT, Brown LC, Trial UKSA (2001) The natural history of abdominal aortic aneurysms and their risk of rupture. Adv. Surg. 35: 173-185.

97. Phan L, Knutsen AK, Bayly PV, Rugonyi S, Grimm C (2011) Refining shape correspondence for similar objects using strain. Eurographics Workshop on 3D Object Retrieval 17-24.

98. Besl PJ, McKay ND (1992) A method for registration of 3-D shapes. IEEE T. Pattern Anal. 14: 239-256.

99. Brown BJ, Rusinkiewicz S (2007) Global non-rigid alignment of 3-D scans. ACM T. Graphic 26: 1-9.

100. Bathe K-J (1996) Finite Element Procedures. Upper Saddle River: Prentice Hall. 291-295.

101. Rodriguez EK, Hoger A, McCulloch AD (1994) Stress-dependent finite growth in soft elastic tissues. J. Biomech. 27: 455-467.

102. Taber LA, Humphrey JD (2001) Stress-modulated growth, residual stress, and vascular heterogeneity. J. Biomech. Eng. 123: 528-535.

103. Gee MW, Forster C, Wall WA (2010) A computational strategy for prestressing patient-specific biomechanical problems under finite deformation. Int. J. Numer. Meth. Biomed. Eng. 26: 52-72.

104. Speelman L, Bosboom EM, Schurink GW, Buth J, Breeuwer M, et al. (2009) Initial stress and nonlinear material behavior in patient-specific AAA wall stress analysis. J. Biomech. 42: 1713-1719.

105. Rodriguez JF, Ruiz C, Doblare M, Holzapfel GA (2008) Mechanical stresses in abdominal aortic aneurysms: Influence of diameter, asymmetry, and material anisotropy. J. Biomech. Eng. 130: 210231-2102310.

106. Polzer S, Gasser TC, Bursa J, Staffa R, Vlachovsky R, et al. (2013) Importance of material model in wall stress prediction in abdominal aortic aneurysms. Med. Eng. Phys. 35: 1282-1289.

107. Roy D, Kauffmann C, Delorme S, Lerouge S, Cloutier G, et al. (2012) A literature review of the numerical analysis of abdominal aortic aneurysms treated with endovascular stent grafts. Comput. Math. Methods Med. 2012: 1-16.

108. Raghavan ML, Ma B, Fillinger MF (2006) Non-invasive determination of zero-pressure geometry of arterial aneurysms. Ann. Biomed. Eng. 34: 1414-1419.

109. Vande Geest JP, Sacks MS, Vorp DA (2006) The effects of aneurysm on the biaxial mechanical behavior of human abdominal aorta. J. Biomech. 39: 1324-1334.

110. Bauchau OA, Carig JI (2009) Structural Analysis: With Applications to Aerospace Structures. New York, London: Springer Science Business Media. 117-122.

111. Holzapfel GA, Gasser TC, Ogden RW (2000) A new constitutive framework for arterial wall mechanics and a comparative study of material models. J. Elasticity 61: 1-48.

112. Atar E, Belenky A, Hadad M, Ranany E, Baytner S, et al. (2006) MR angiography for abdominal and thoracic aortic aneurysms: Assessment before endovascular repair in patients with impaired renal function. Am. J. Roentgenol. 186: 386-393.

113. Li ZY, Sadat U, U-King-Im J, Tang TY, Bowden DJ, et al. (2010) Association between aneurysm shoulder stress and abdominal aortic aneurysm expansion: A longitudinal follow-up study. Circulation 122: 1815-1822.

114. Di Achille P, Celi S, Di Puccio F, Forte P (2011) Anisotropic AAA: Computational comparison between four and two fiber family material models. J. Biomech. 44: 2418-2426.

115. Tong J, Cohnert T, Regitnig P, Holzapfel GA (2011) Effects of age on elastic properties of the intraluminal thrombus and the thrombus-covered wall in abdominal aortic aneurysms: biaxial extension behaviour and material modelling. Eur. J. Vasc. Endovasc. Surg. 42: 207-219.

116. Kaazempur-Mofrad MR, Younis HF, Patel S, Isasi A, Chung C, et al. (2003) Cyclic strain in human carotid bifurcation and its potential correlation to atherogenesis: Idealized and anatomically-realistic models. J. Eng. Math. 47: 299-314.

117. Younis HF, Kaazempur-Mofrad MR, Chan RC, Isasi AG, Hinton DP, et al. (2004) Hemodynamics and wall mechanics in human carotid bifurcation and its consequences for atherogenesis: investigation of inter-individual variation. Biomech. Model Mechanobiol. 3: 17-32.

118. Fung YC (1991) What are the residual stresses doing in our blood vessels? Ann. Biomed. Eng. 19: 237-249.

119. Rachev A (2003) Remodeling of arteries in response to changes in their mechanical environment. In: Holzapfel GA, Ogden RW, editors. Biomechanics of soft tissue in cardiovascular systems. New York: Springer. p. 265.

120. Rachev A, Greenwald SE (2003) Residual strains in conduit arteries. J. Biomech. 36: 661-670.

121. Teutelink A, Muhs BE, Vincken KL, Bartels LW, Cornelissen SA, et al. (2007) Use of dynamic computed tomography to evaluate pre- and postoperative aortic changes in AAA patients undergoing endovascular aneurysm repair. J. Endovasc. Ther. 14: 44-49.

122. Molacek J, Baxa J, Houdek K, Treska V, Ferda J (2011) Assessment of abdominal aortic aneurysm wall distensibility with electrocardiography-gated computed tomography. Ann. Vasc. Surg. 25: 1036-1042.

123. Shum J, DiMartino ES, Goldhamme A, Goldman DH, Acker LC, et al. (2010) Semiautomatic vessel wall detection and quantification of wall thickness in computed tomography images of human abdominal aortic aneurysms. Med. Phys. 37: 638-648.

124. Mower WR, Quinones WJ, Gambhir SS (1997) Effect of intraluminal thrombus on abdominal aortic aneurysm wall stress. J. Vasc. Surg. 26: 602-608.

125. Speelman L, Hellenthal FA, Pulinx B, Bosboom EMH, Breeuwer M, et al. (2010) The influence of wall stress on AAA growth and biomarkers. Eur. J. Vasc. Endovasc. Surg. 39: 410-416.

126. Giddens DP, Zarins CK, Glagov S (1990) Response of Arteries to Near-Wall Fluid Dynamic Behavior. Appl. Mech. Rev. 43: S98-S102.

127. Khanafer KM, Bull JL, Upchurch GR, Jr., Berguer R (2007) Turbulence significantly increases pressure and fluid shear stress in an aortic aneurysm model under resting and exercise flow conditions. Ann. Vasc. Surg. 21: 67-74.

128. Brady AR, Thompson SG, Fowkes FG, Greenhalgh RM, Powell JT, et al. (2004) Abdominal aortic aneurysm expansion: risk factors and time intervals for surveillance. Circulation 110: 16-21.

129. Vande Geest JP, Di Martino ES, Bohra A, Makaroun MS, Vorp DA (2006) A biomechanics-based rupture potential index for abdominal aortic aneurysm risk assessment: Demonstrative application. Ann. N. Y. Acad. Sci. 1085: 11-21.

130. Cebral JR, Castro MA, Burgess JE, Pergolizzi RS, Sheridan MJ, et al. (2005) Characterization of cerebral aneurysms for assessing risk of rupture by using patient-specific computational hemodynamics models. A.J.N.R. Am. J. Neuroradiol. 26: 2550-2559.

131. Celi S, Berti S (2014) Three-dimensional sensitivity assessment of thoracic aortic aneurysm wall stress: a probabilistic finite-element study. Eur. J. Cardiothorac. Surg. 45: 467-475.

132. Erbel R, Eggebrecht H (2006) Aortic dimensions and the risk of dissection. Heart 92: 137-142.

133. Nathan DP, Xu C, Gorman JH, 3rd, Fairman RM, Bavaria JE, et al. (2011) Pathogenesis of acute aortic dissection: a finite element stress analysis. Ann. Thorac. Surg. 91: 458-463.

134. Pasta S, Rinaudo A, Luca A, Pilato M, Scardulla C, et al. (2013) Difference in hemodynamic and wall stress of ascending thoracic aortic aneurysms with bicuspid and tricuspid aortic valve. J. Biomech. 46: 1729-1738.

135. Shang EK, Nathan DP, Sprinkle SR, Vigmostad SC, Fairman RM, et al. (2013) Peak wall stress predicts expansion rate in descending thoracic aortic aneurysms. Ann. Thorac. Surg. 95: 593-598.

136. Shojima M, Oshima M, Takagi K, Torii R, Hayakawa M, et al. (2004) Magnitude and role of wall shear stress on cerebral aneurysm: computational fluid dynamic study of 20 middle cerebral artery aneurysms. Stroke 35: 2500-2505.

137. Zhou X, Raghavan ML, Harbaugh RE, Lu J (2010) Patient-specific wall stress analysis in cerebral aneurysms using inverse shell model. Ann. Biomed. Eng. 38: 478-489.

138. Humphrey JD, Canham PB (2000) Structure, mechanical properties, and mechanics of intracranial saccular aneurysms. J. Elast. 61: 49-81.

139. Kyriacou SK, Humphrey JD (1996) Influence of size, shape and properties on the mechanics of axisymmetric saccular aneurysms. J. Biomech. 29: 1015-1022.

140. Ma B, Harbaugh RE, Raghavan ML (2004) Three-dimensional geometrical characterization of cerebral aneurysms. Ann. Biomed. Eng. 32: 264-273.

141. Ma B, Lu J, Harbaugh RE, Raghavan ML (2007) Nonlinear anisotropic stress analysis of anatomically realistic cerebral aneurysms. J. Biomech. Eng. 129: 88-96.

142. Seshaiyer P, Hsu FPK, Shah AD, Kyriacou SK, Humphrey JD (2001) Multiaxial mechanical behavior of human saccular aneurysms. Comput. Methods Biomed. Eng. 4: 281-289.

143. Shah AD, Harris JL, Kyriacou SK, Humphrey JD (1998) Further roles of geometry and properties in the mechanics of saccular aneurysms. Comput. Methods Biomech. Biomed. Engin. 1: 109-121.

144. Shah AD, Humphrey JD (1999) Finite strain elastodynamics of intracranial saccular aneurysms. J. Biomech. 32: 593-599.

145. Kroon M (2011) Simulation of Cerebral Aneurysm Growth and Prediction of Evolving Rupture Risk. Modelling and Simulation in Engineering 2011: 1-10.

146. Korja M, Lehto H, Juvela S (2014) Lifelong rupture risk of intracranial aneurysms depends on risk factors: a prospective Finnish cohort study. Stroke 45: 1958-1963.

147. Pape LA, Tsai TT, Isselbacher EM, Oh JK, O'Gara P T, et al. (2007) Aortic diameter >or = 5.5 cm is not a good predictor of type A aortic dissection: observations from the International Registry of Acute Aortic Dissection (IRAD). Circulation 116: 1120-1127.

148. Kubota H, Endo H, Noma M, Tsuchiya H, Yoshimoto A, et al. (2013) Airway obstruction by a retropharyngeal hematoma secondary to thoracic aortic aneurysm rupture. J. Cardiothorac. Surg. 8: 232.

149. Hebballi R, Swanevelder J (2009) Diagnosis and management of aortic dissection. C.E.A.C.C.P. 9: 14-18.

150. Raghavan ML, Webster MW, Vorp DA (1996) Ex vivo biomechanical behavior of abdominal aortic aneurysm: assessment using a new mathematical model. Ann. Biomed. Eng. 24: 573-582.

TABLES

AAA Classification	Size of maximum transverse diameter (MTD) (mm)	Monitoring Frequency (years)	Recommended Management Strategy	Reference
Small	30≤MTD<40	2-3	ultrasound surveillance	[5]
Intermediate	40≤MTD<55	0.25-1	surveillance with ultrasound, CT, or MRI	[5][31]
Large	MTD≥55	0.083-0.5	surgery, surveillance with CT	[5][31]
Symptomatic/AAAs growing at 5 mm per 0.5 years	Any	-	surgery, CT	[5][31]

Table 1. AAA management strategies based on observation and measurement of the maximum transverse diameter.

Variable	Subject A4 (83 year old male)		
	t_1	t_2	t_3
Timing (years)	0	1.57	3.05
Systolic pressure mmHg, (N/mm^2)	130 (0.0173)	140 (0.0187)	122 (0.0163)
Diastolic pressure mmHg, (N/mm^2)	90 (0.0120)	80 (0.0107)	76 (0.0101)
Average pressure mmHg, (N/mm^2)	103.33 (0.0138)	100 (0.0133)	91.33 (0.0122)
Maximum diameter mm	56.5	61.4	65.8
Notes	former smoker; hypertension; blood pressure information was acquired at t_1+0.16 yrs.	blood pressure information was acquired at t_2+0.58 yrs.	stent repair seen on CT scan three months after t_3; blood pressure information was acquired at t_3+0.16 yrs.

Table 2. CT scan timing, blood pressure and medical information for Subject A4.

The de-identified, contrast-enhanced spiral CT images used in this study were acquired by the OHSU Department of Vascular Surgery as a standard of care rather than solely for research. The times when the second and third CT scans were obtained were evaluated with respect to that of the first CT scan. Blood pressure information was collected and needed to compute wall stresses. Because the blood pressure data were not necessarily available at the same time when the CT scans were acquired, we selected pressures that were recorded at a time closest to when CT scanning occurred.

Material Model	α (N/mm^2)	β (N/mm^2)	γ (N/mm^2)	Reference
Raghavan-Vorp (RV)	0.174	1.881	0	[28]
Polzer et al. sample (P1)	0.0145	0	2.259	[106]
Polzer et al. sample (P2)	0.022	1.461	1.0	[106]

Table 3. Coefficients of AAA tissue material properties (see Eq. 3). For the RV model, only the population average values are shown, whereas patient-specific material properties are displayed for P1 and P2. The material properties were obtained from the literature and determined from tensile testing experiments performed on tissues excised from cadavers and patients undergoing elective repair.

FIGURES

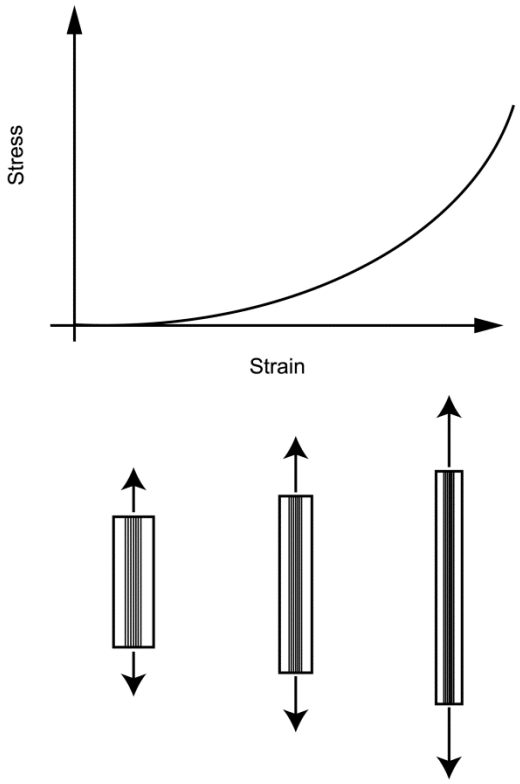

Figure 1. Schematic showing the stress-strain relationship of a nonlinear material subject to loading. The idea used for the creation of this figure comes from Raghavan et al. [150].

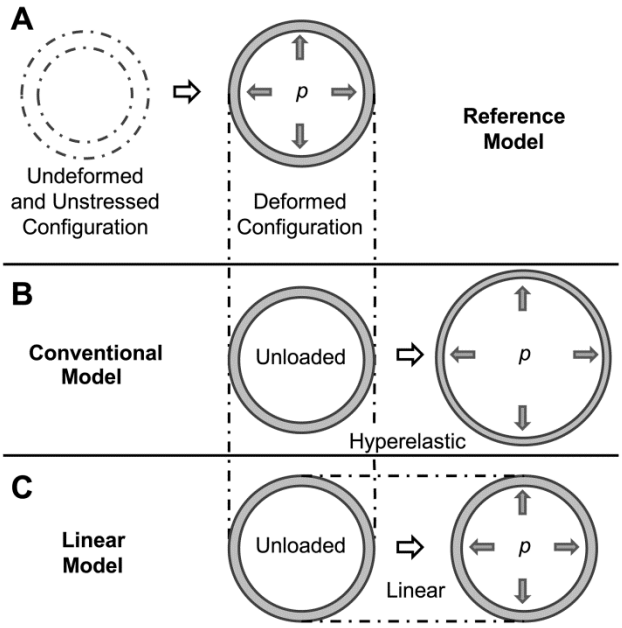

Figure 2. Schematic showing the AAA models employed. In all models, an internal pressure is applied to an initially unloaded, undeformed configuration. Differences between models are in the choice of the wall material properties and initial configuration employed. (A) Reference model: the walls are characterized by hyperelastic nonlinear material properties; the initial configuration, which is assumed to be known, represents the clinically unknown unloaded and unstressed wall configuration, and the deformed (loaded) configuration represents the deformed geometry that is imaged from the patient. (B) Conventional model: the walls are assumed to have hyperelastic nonlinear properties; the initial configuration is chosen as the deformed configuration obtained from the reference model (but this configuration is assumed to be unloaded and unstressed). After application of an internal pressure in the conventional model, the initial configuration further deforms into a loaded configuration. (C) Linear model: the walls are assumed to have linear elastic properties, with infinitesimally small deformations and strains; the initial configuration is chosen as the deformed configuration obtained from the reference

model (as in the conventional model). Because of the assumptions made in the linear model, the initial configuration barely deforms, preserving the geometrical characteristics of imaged patient geometries. Obtained from [1].

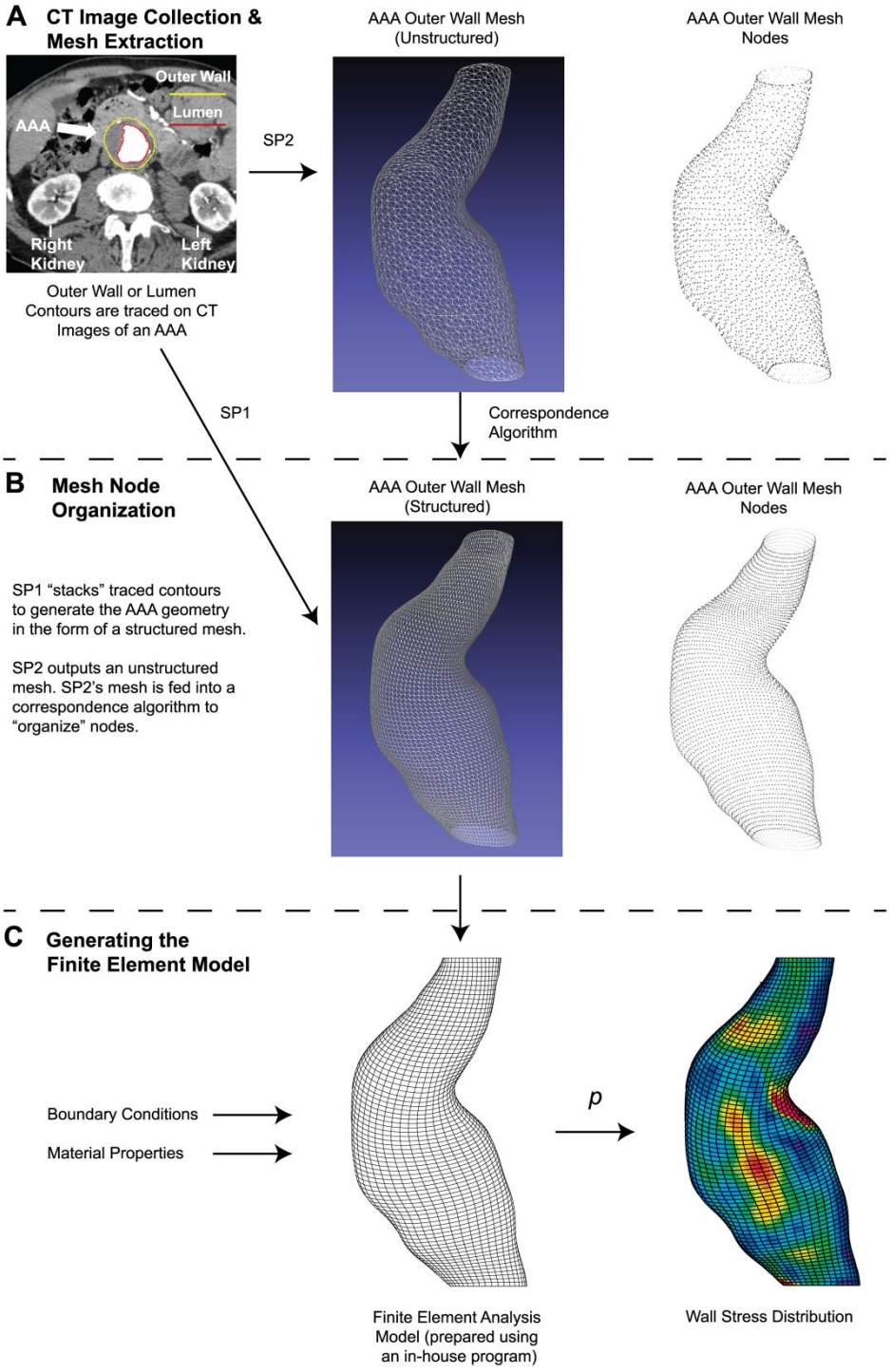

Figure 3. Summary of the methods employed to generate a finite element model of a subject-specific AAA. The finite element analysis (FEA) model of an AAA is needed for

the computation of wall stress. (A) The preparation of the FEA model involves the collection of CT images and the extraction of the AAA wall and lumen surfaces from the CT scan images. Note that for simplicity, only the outer wall surface of the AAA at one time point is displayed in the figure. Two segmentation programs (SPs) were employed to achieve the surface extractions in two different ways. SP1 is a relatively more automated program than SP2 and provides less control in choosing the orientation of the planes for contour tracing. SP1 extracts the contours and reduces extraction noise before "stacking" the contours to generate the AAA surface geometry in the form of a mesh. SP2 allows for a more controlled tracing of the contours and outputs an unstructured mesh. (B) For convenience and to use the meshes for analysis, the nodes were "organized" into cross-sectional rings. SP1 achieves this step as part of its algorithm. SP2, on the other hand, does not. Thus, a point correspondence algorithm is applied to the SP2-derived meshes (outer wall and lumen surfaces) to parameterize the surface meshes. (C) After the meshes are parameterized, they are ready to be used as input for an in-house program that produces an FEA input file for ADINA, the FEA software. The input file uses the structured surface meshes to generate the FEA AAA body, which is then defined with specific tissue properties (measures of stiffness). The boundary conditions, i.e., fixations and intraluminal pressures, are also specified in the input file. Once this information is provided, the FEA model is then used to compute wall stresses.

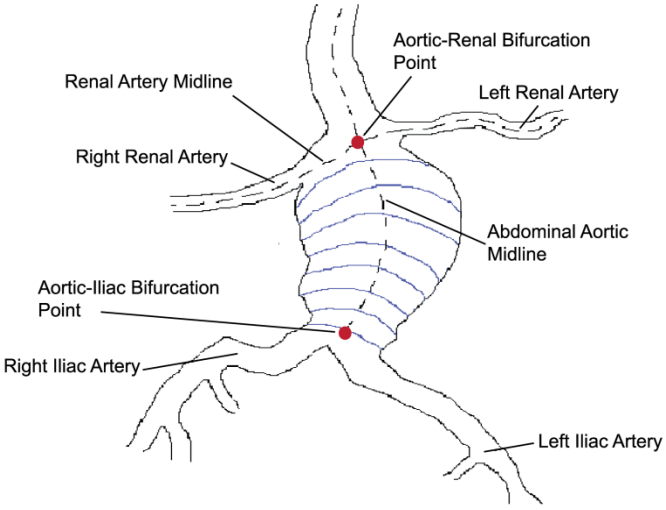

Figure 4. Schematic of an abdominal aortic aneurysm. CT scans are traced beginning from the aortic-renal bifurcation point and end in the aortic-iliac bifurcation point. The AAA midline is shown as a dashed line between the bifurcation points. The blue lines in the figure represent the contours or "rings" of the different AAA cross-sections that compose the aneurysm's mesh.

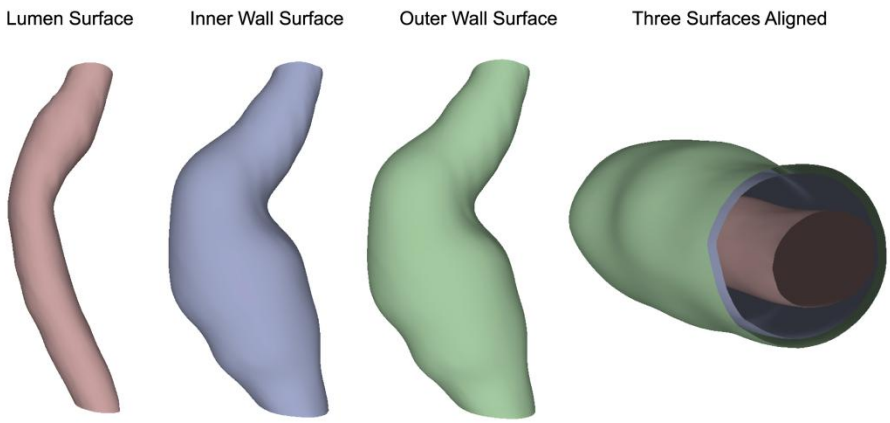

Figure 5. Lumen and wall surface meshes of Subject A4. The lumen and inner and outer wall surfaces were extracted from the CT scan images for Subject A4 using SP2 at three times, but only the surfaces for one time point are shown. All three surfaces are needed to generate the finite element mesh for the computation of wall stresses. On the left, a patient-left view of the three surfaces is presented. On the right, the three surfaces are aligned, anteriorly rotated by 90 degrees, and shown from the aortic-iliac bifurcation's perspective, looking toward the rostrum. The area between the outer and inner wall surfaces represents the AAA wall, whereas the area between the lumen and inner wall surfaces represents the thrombus.

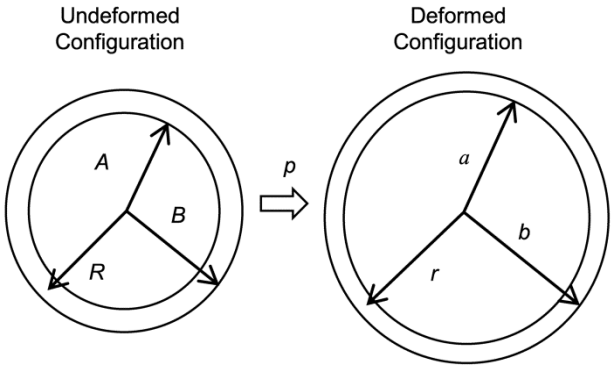

Figure 6. Thick-wall cylindrical model with applied internal pressure used for the derivation of analytical solutions. The undeformed configuration is assumed to be unstressed and unloaded; the deformed configuration is obtained after applying an internal pressure *p*. *A*, *B* and *R* represent the internal wall radius, external wall radius and radial coordinate, respectively, in the undeformed configuration; *a*, *b*, and *r*, represent the internal wall radius, external wall radius and radial coordinate, respectively, in the deformed configuration. Obtained from [1].

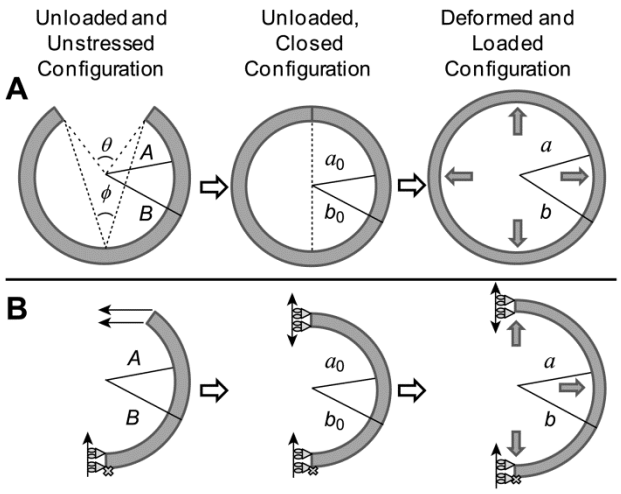

Figure 7. Modeling of residual stresses in a tubular vessel. (A) Schematics of the physical tissue configurations: an initial unloaded, unstressed and undeformed circular section (with radii *A* and *B*) is closed, which generates residual stresses in the unloaded configuration. This closed configuration (with radii a_0 and b_0) is loaded to generate the final deformed and loaded configuration (radii *a* and *b*) that represents arterial tissues under load. The open sector schematics also show the definition of the opening angle ϕ in relation to the angle θ. (B) Schematics of the FEA model implemented to compute residual stresses and their effects on the loaded configuration. We first modeled an unstressed, unloaded and undeformed open sector. We then imposed a horizontal displacement on the open end of the sector to close the segment and generate residual stresses. The closed sector was then loaded with an internal pressure to compute the loaded configuration and resulting wall stresses. Obtained from [1].

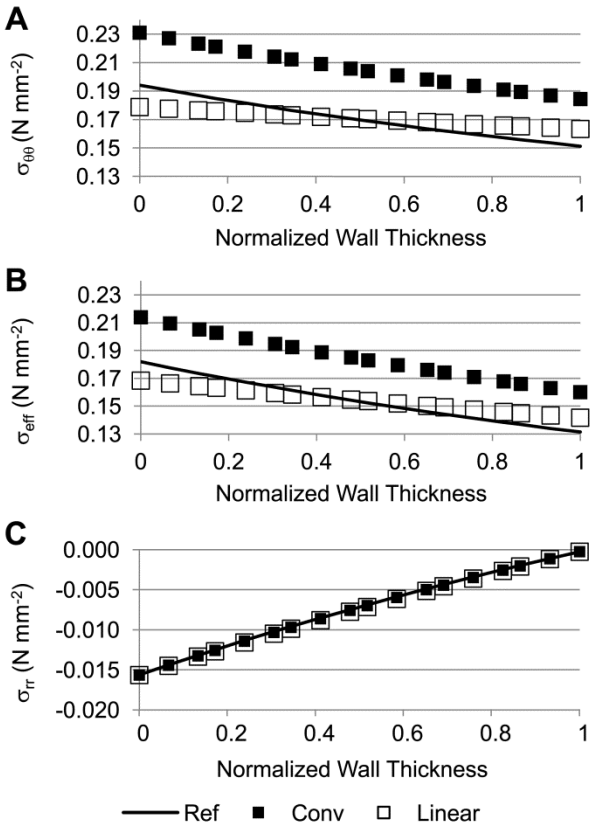

Figure 8. Stress comparisons among the reference, conventional, and linear models of an axisymmetric thick-wall tubular geometry. (A) Circumferential wall stress; (B) effective wall stress; and (C) radial wall stress distributions are plotted across the normalized wall thickness. For the reference model, the inner and outer radii in the deformed configuration were 14.8 mm and 16.1 mm, respectively; for the conventional model, the inner and outer radii in the deformed configuration were 16.27 mm and 17.53 mm, respectively; applied internal pressure, p = 0.016 N/mm^2 (120 mmHg); RV material properties were used for both the reference and conventional models. Obtained from [1].

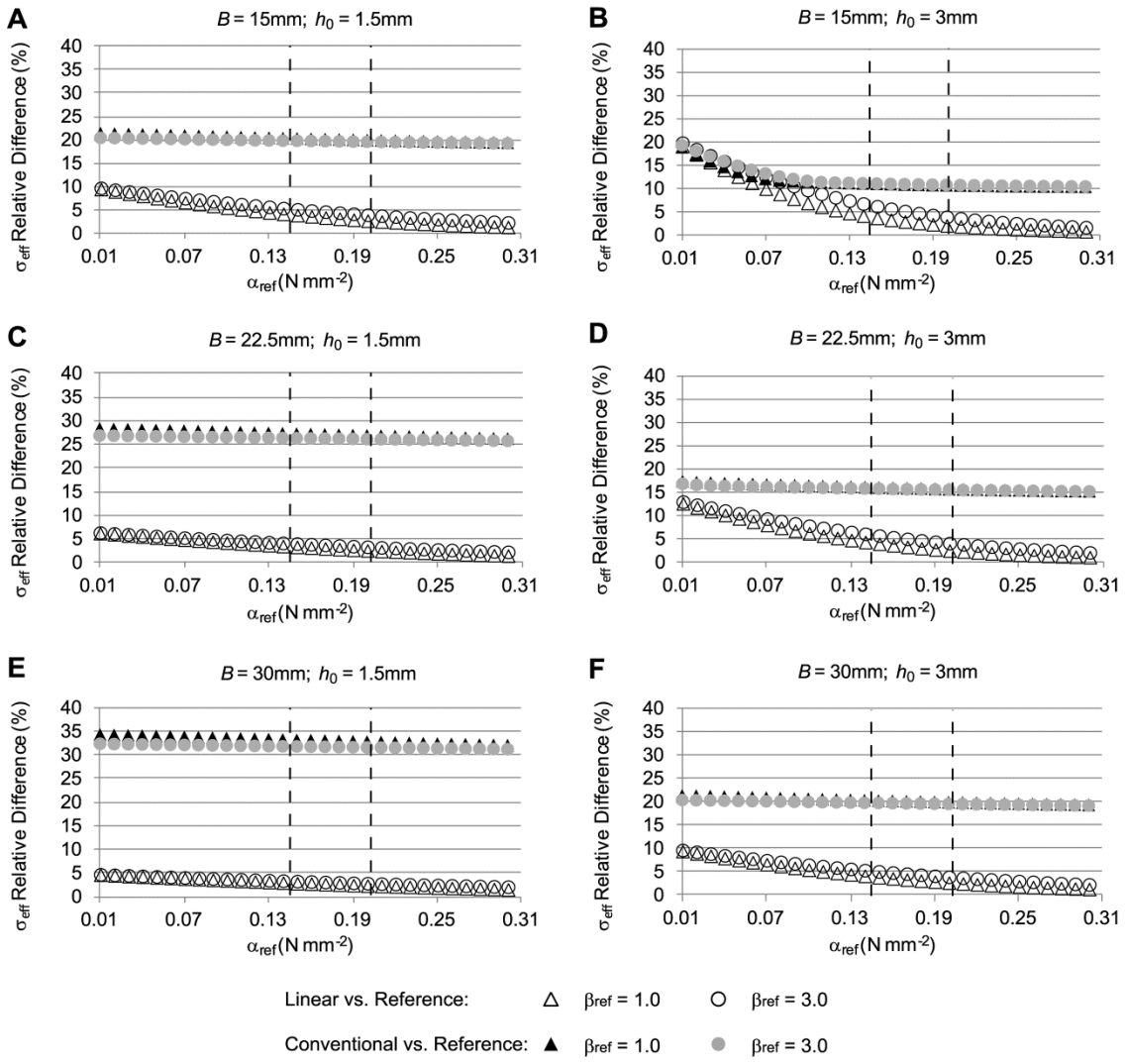

Figure 9. Relative differences in effective wall stress distributions for the case of a tubular arterial model (using an internal pressure of 120 mmHg). The figure shows differences of effective wall stress distributions obtained from the conventional and linear models, with respect to the stress distributions from the reference model, computed using **Eq. 33**. To simulate the clinical situation where the material properties of the AAA are unknown, the material constants α and β ($\gamma = 0$) were varied in the reference model (α_{ref} and β_{ref} reported values), whereas population average α and β ($\alpha = 0.174$ N/mm^2, $\beta = 1.881$ N/mm^2; RV material properties) were used in the conventional model, and constant

elasticity ($E = 8.4\text{x}10^9$ N/mm^2) was used in the linear model. Further, the initial geometry was varied to represent different aneurysm sizes and wall thicknesses. In all cases, applied internal pressure was 0.016 N/mm^2 (120 mmHg). Reported geometrical model external radius B and wall thickness h_0 correspond to the initial configuration of the reference model. The dashed lines indicate the physiological range of the material property values for α_{ref}. Obtained from [1].

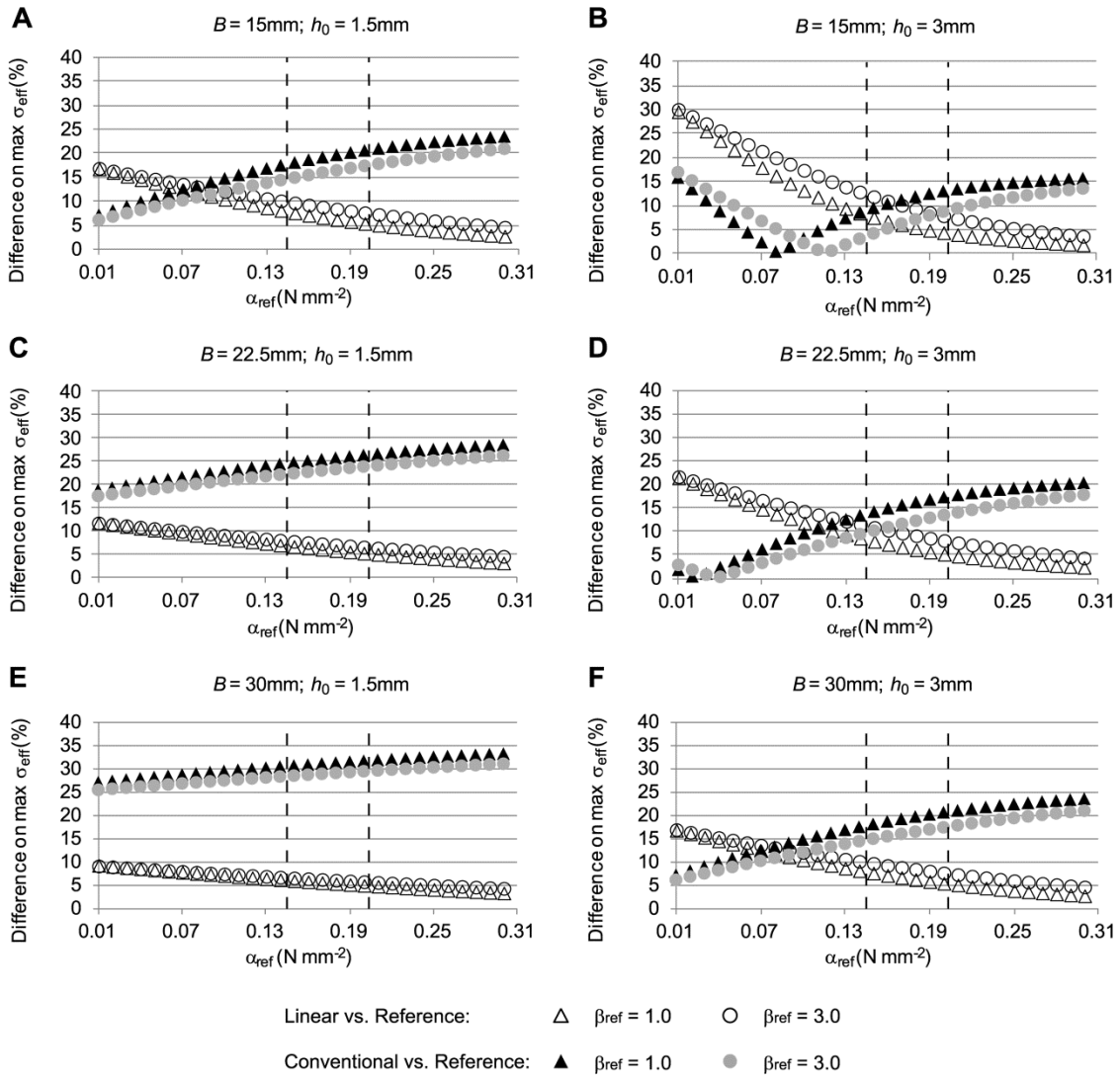

Figure 10. Relative differences in maximum effective wall stress distributions for a tubular arterial model (using an internal pressure of 120 mmHg). Models simulated are the same as for **Fig. 9**, but differences in maximal wall stresses with respect to reference stresses, computed using **Eq. 32**, are reported instead. The reported material coefficients α_{ref} and β_{ref} correspond to those of the reference model. RV material properties (α = 0.174 N/mm^2, β =1.881 N/mm^2) were used in the conventional model, and a constant elasticity (E = 8.4x10^9 N/mm^2) was used in the linear model. Applied internal pressure was 0.016 N/mm^2 (120 mmHg). The initial geometry was varied to represent

different aneurysm sizes and wall thicknesses. The dashed lines indicate the physiological range of the material property values for $\alpha_{ref.}$ Obtained from [1].

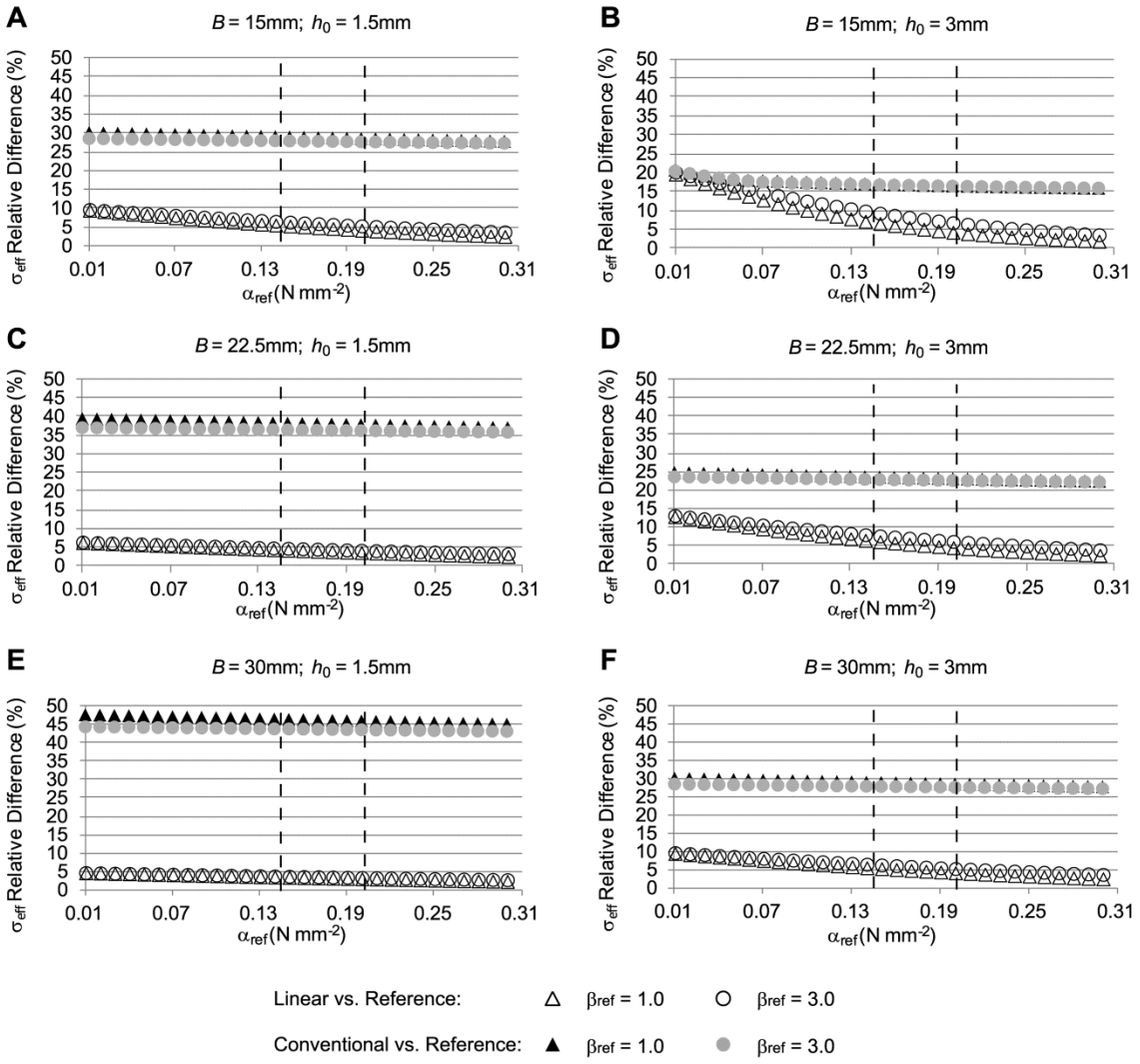

Figure 11. Relative differences in effective wall stress distributions for the case of a tubular arterial model (using an internal pressure of 200 mmHg). Similar to **Fig. 9**, differences of effective wall stress distributions obtained from the conventional and linear models, with respect to the stress distributions from the reference model are shown, but the applied internal pressure was increased to 0.027 N/mm^2 (200 mmHg). Material constants α_{ref} and β_{ref} reported corresponded to those of the reference model. RV material properties (α = 0.174 N/mm^2, β =1.881 N/mm^2) were used in the conventional model, and constant elasticity (E = 8.4x10^9 N/mm^2) was used in the linear model. The figure shows

results obtained when the initial geometry was varied in the reference model. The dashed lines indicate the physiological range of the material property values for α_{ref}. Obtained from [1].

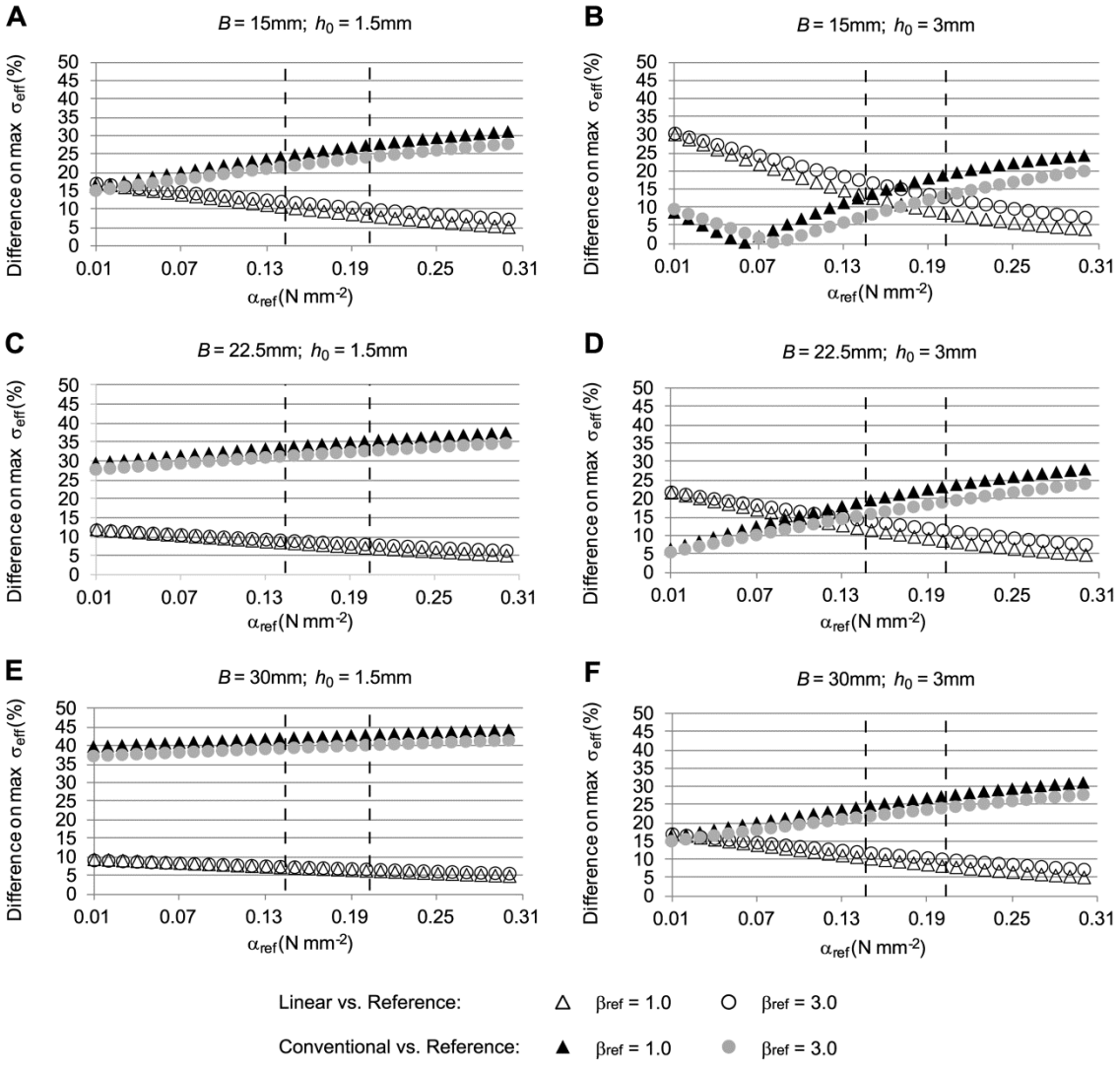

Figure 12. Relative differences in maximum effective wall stress distributions for a tubular arterial model (using an internal pressure of 200 mmHg). Models simulated are the same as for **Fig. 11**, with an applied internal pressure p = 0.027 N/mm^2 (200 mmHg), but the differences in maximal wall stresses (with respect to reference wall stresses) are reported instead. Material constants α_{ref} and β_{ref} reported correspond to those of the reference model. RV material properties (α = 0.174 N/mm^2, β =1.881 N/mm^2) were used in the conventional model, and constant elasticity (E = 8.4x10^9 N/mm^2) was used in the linear model. The figure shows results obtained when the initial geometry was varied

in the reference model. The dashed lines indicate the physiological range of the material property values for α_{ref}. Obtained from [1].

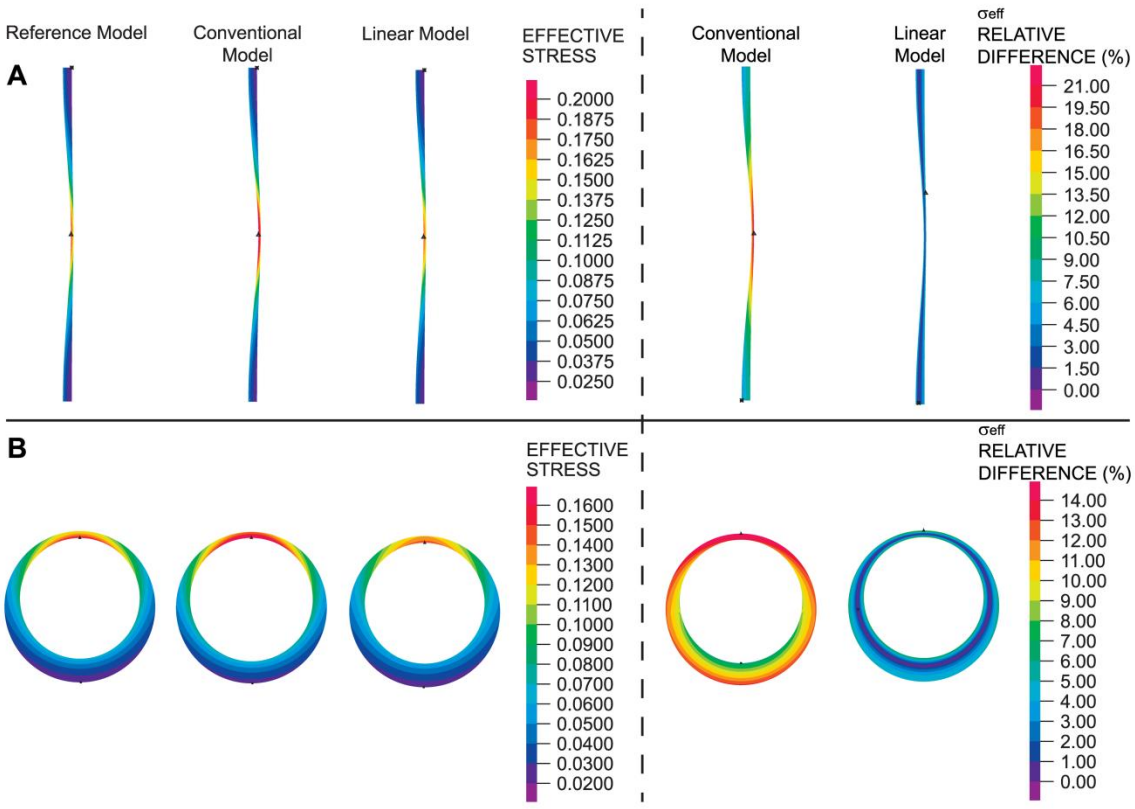

Figure 13. Effect of variable wall thickness on wall stress distributions. (A) Axisymmetric model with longitudinally-varying wall thickness. (B) Plane strain model with circumferentially-varying wall thickness. In all cases, an internal pressure of 0.016 N/mm^2 (120 mmHg) was applied. For both geometries considered, effective wall stresses (in units of N/mm^2) are shown as computed using reference, conventional and linear models (left). Differences in the effective wall stress with respect to reference wall stresses for the linear and conventional approaches are also shown (right). Obtained from [1].

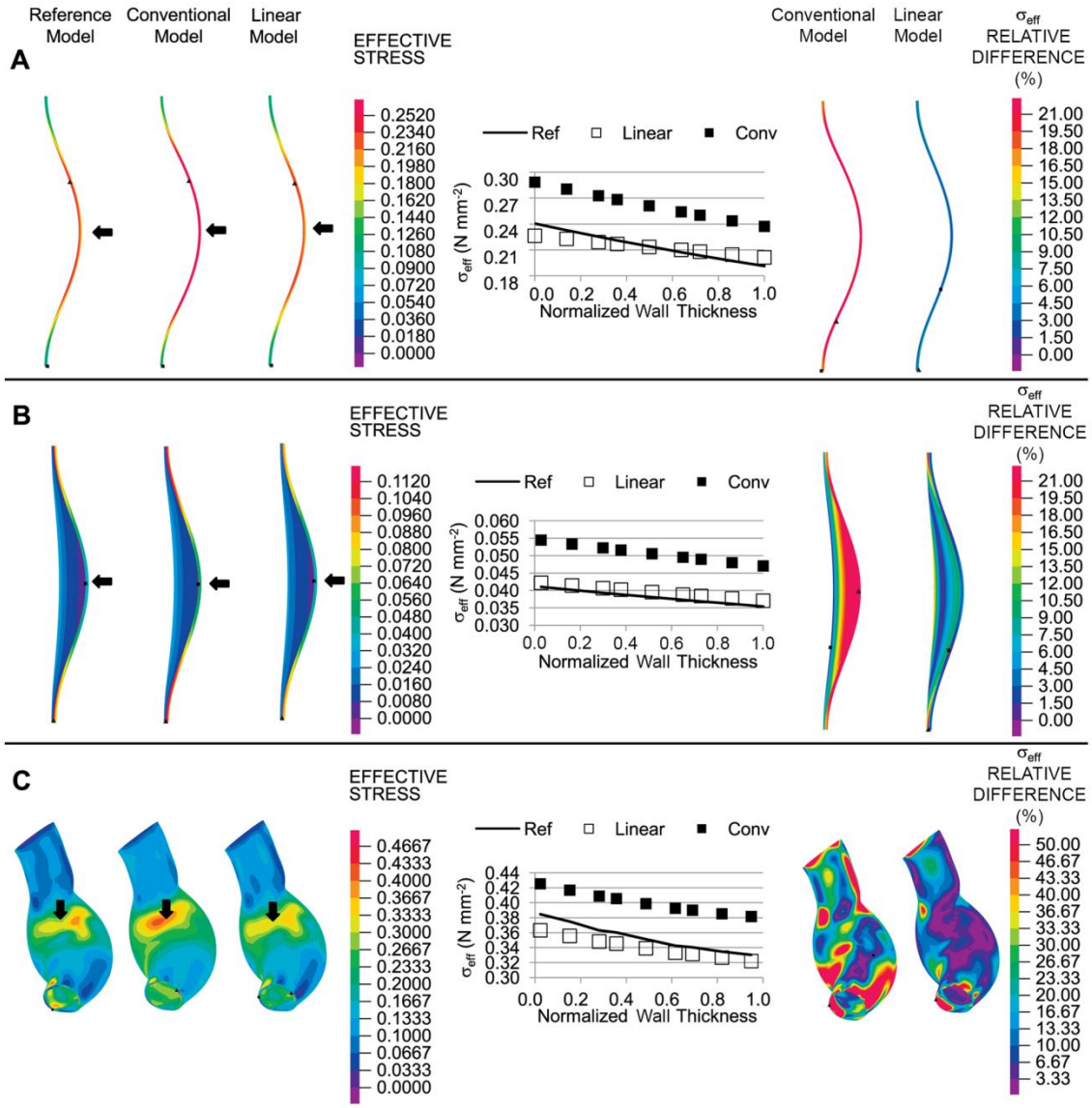

Figure 14. Effective wall stress distributions in different geometrical models of AAA. (A) Idealized bended-tubular axisymmetric model. (B) Idealized axisymmetric model of AAA with inclusion of thrombus. (C) Patient-specific model (anterior view of outer surface). In all cases, an internal pressure of 0.016 N/mm^2 (120 mmHg) was applied. For the geometries considered, effective wall stresses (in units of N/mm^2) are shown as computed using reference, conventional and linear models (left). Plots of the effective wall stress with respect to the normalized thickness in the regions indicated by

the black arrows are shown (middle). Differences in the effective wall stress with respect to reference wall stresses for the linear and conventional approaches are also shown (right). Obtained from [1].

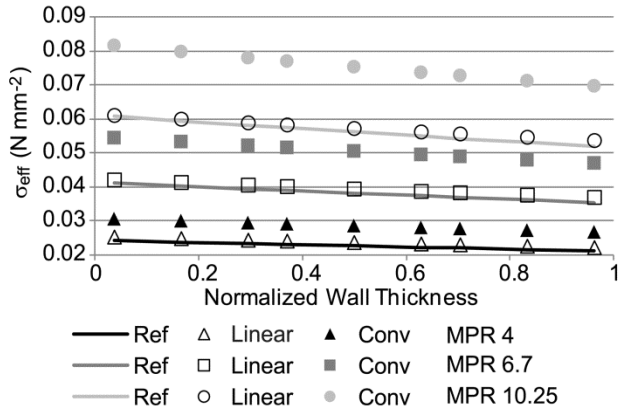

Figure 15. Effective stress distributions versus normalized wall thickness for the idealized AAA model with thrombus. Simulations were performed assuming a wall/thrombus material property ratio (MPR) of 4, 6.7 and 10.25, in the reference, conventional and linear models. In all cases, an internal pressure of 0.016 N/mm^2 (120 mmHg) was applied. Ref: reference model, Conv: conventional model. Obtained from [1].

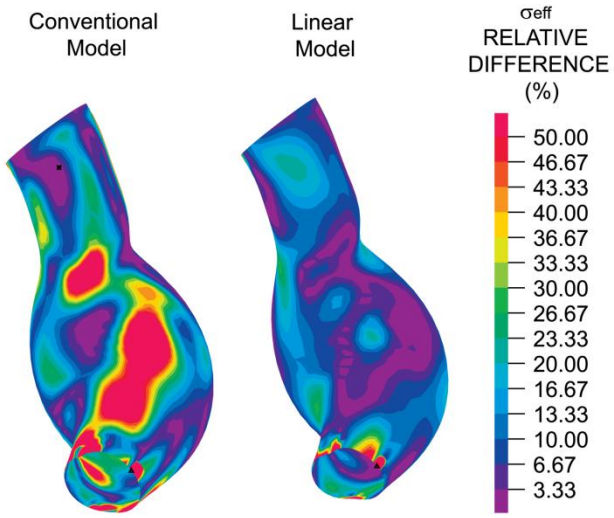

Figure 16. Relative differences in effective stress on the lumen surface of a patient-specific AAA model. Anterior view. Differences in effective wall stress for the linear and conventional models are with respect to the stresses in the reference model. RV material properties were employed in reference and conventional models. A systolic pressure of 0.016 N/mm^2 (120 mmHg) was applied to the lumen of the deformed configurations of the linear and conventional models. Obtained from [1].

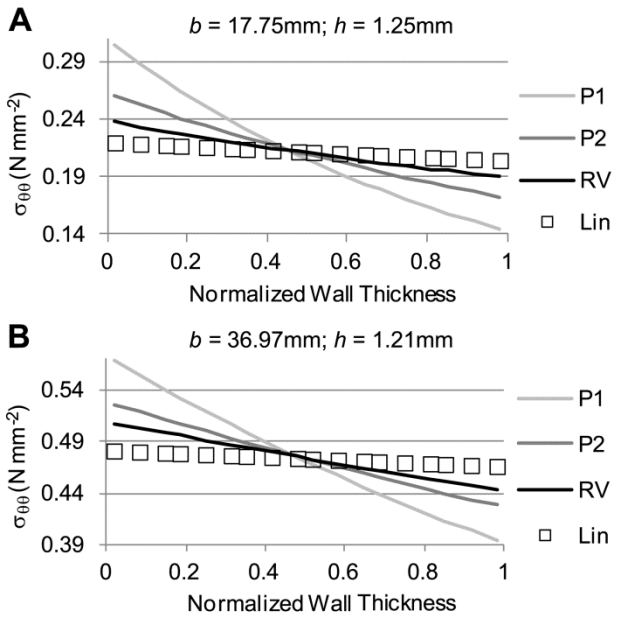

Figure 17. Comparison of circumferential stress distributions obtained using different tissue material properties in a tubular model. Material properties employed were those listed in **Table 3** (RV, P1, and P2), and results using the linear model (Lin) are also shown for comparison. For each panel shown, regardless of the material property employed in the model, the deformed configuration (described by the outer radius *b* and wall thickness *h*) was the same, while the initial, unstressed configuration was adjusted. (A) Circumferential stress distributions obtained for the case of a small aneurysm. (B) Circumferential stress distributions for a larger aneurysm model. Obtained from [1].

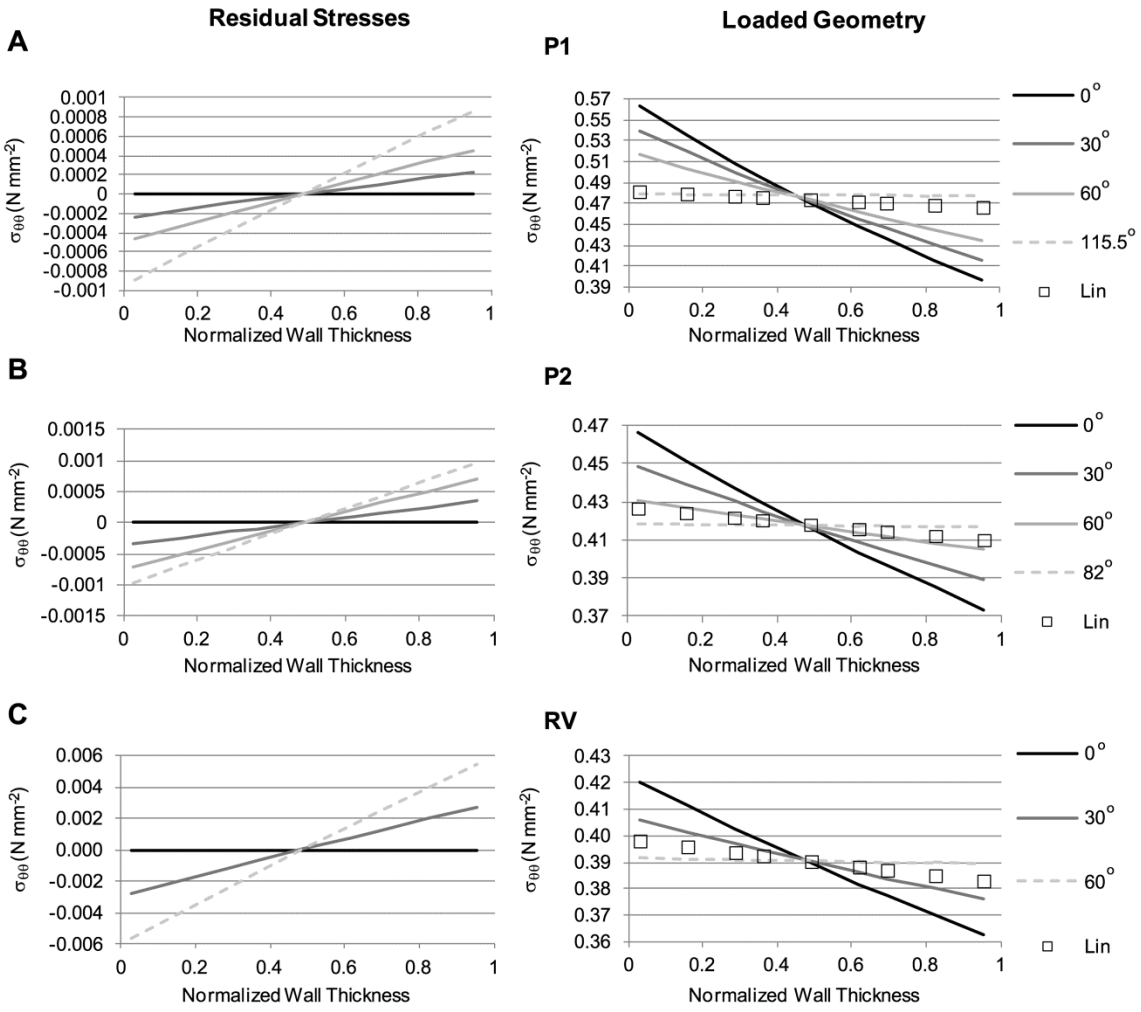

Figure 18. Effect of varying opening angle on circumferential residual stresses and loaded stress distributions. The model employed to compute residual stresses is schematically shown in **Fig. 7**. The angle θ was varied as indicated (with $\theta = 0^{\circ}$ corresponding to the case of no residual stresses), and results obtained from employing different tissue material properties, listed in **Table 3**, are presented: (A) P1; (B) P2; (C) RV material properties. Results show residual stresses (left panels) in the unloaded (closed) configuration; and wall stresses after applying an internal pressure, $p = 0.016$ N/mm^2 (right panels). Circumferential wall stresses obtained using the linear model are included for comparison. For the cases considered, the unloaded, closed configuration,

which exhibits residual stresses, was the same, and characterized by b_0 = 30 mm and a wall thickness of 1.5 mm. As the opening angle increased, the magnitude of residual stresses and gradient of stresses across the wall increased (right column). The magnitude of wall stresses in the loaded configuration, in contrast, decreased, and the gradient of wall stresses across the wall thickness decreased. Irrespective of the material properties employed, as θ increased, the magnitude of the stresses obtained using the nonlinear material properties (P1, P2, RV) approached the stress values obtained using the linear model. Dotted lines show the case at which a relatively uniform stress distribution across the wall was obtained. Obtained from [1].

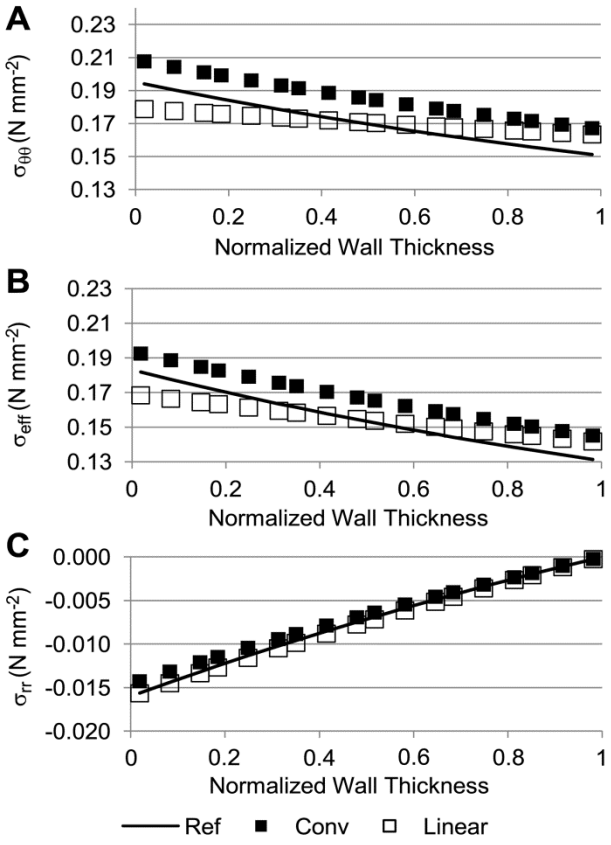

Figure 19. Stresses in a tubular model when pressure is imposed on the conventional model's undeformed configuration. For comparative purposes, wall stresses in the thick-wall tube are shown as obtained in the reference, conventional and linear models. Imposed internal pressure was 0.016 N/mm^2 (120 mmHg) and was applied to the initial, undeformed configuration in the conventional model. (A) Circumferential stress; (B) effective stress; and (C) radial stress distributions are plotted across the normalized wall thickness. For the reference model, the inner and outer radii of the deformed configuration were 14.8 mm and 16.1 mm, respectively; for the conventional model, the inner and outer radii of the deformed configuration were 16.18 mm and 17.45 mm, respectively; RV material properties were used for both the reference and conventional models; E = 8.4x10^9 N/mm^2 for the linear model. Conventional models more closely

approximated reference wall stresses than in the case in which pressure was applied to the deformed configuration of the conventional model. Obtained from [1].

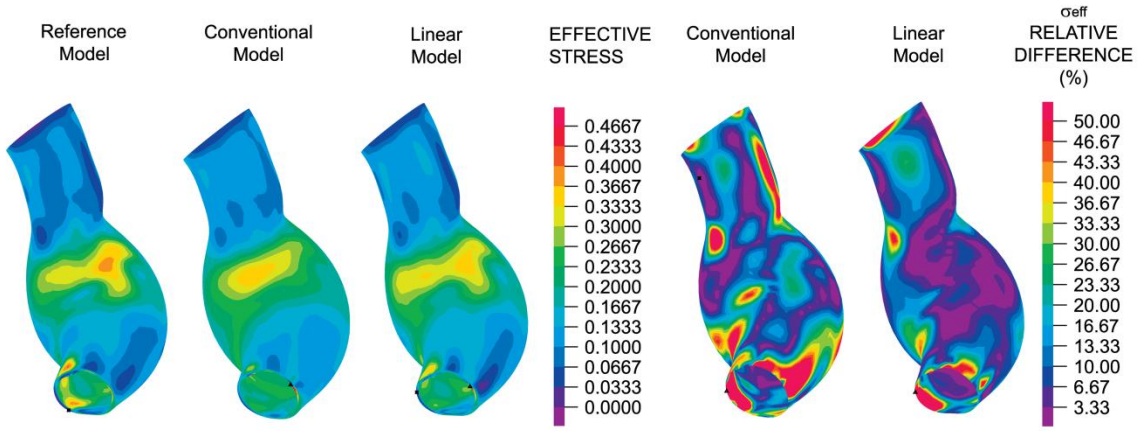

Figure 20. Patient-specific stress comparisons when internal pressure is imposed on the conventional model's undeformed configuration. Anterior view. Imposed intraluminal pressure was 0.016 N/mm^2 (120 mmHg). Effective wall stresses (in units of N/mm^2) are shown as computed using reference, conventional and linear models (left). Differences in the effective wall stress with respect to reference wall stresses for the linear and conventional approaches are also shown (right). Obtained from [1].

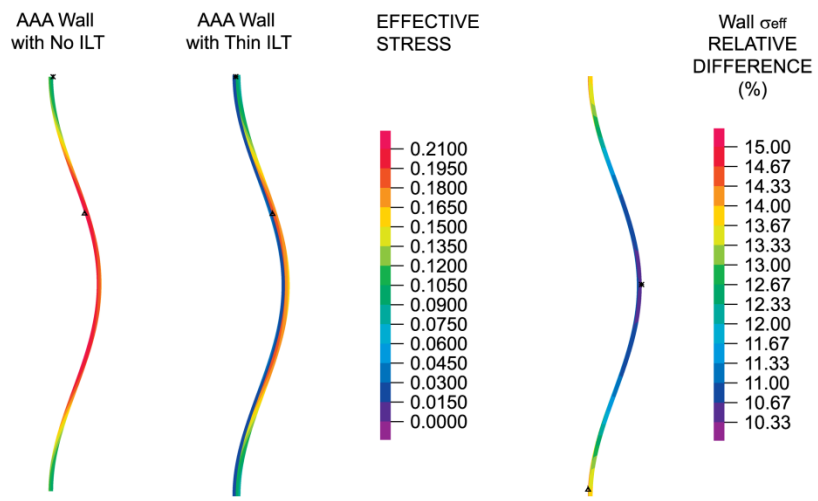

Figure 21. Inclusion of a thin thrombus attenuates wall stresses in an idealized, curved model of an AAA. The imposed intraluminal pressure was 0.016 N/mm^2 (120 mmHg), and the models were fixed in the longitudinal direction to simulate tethering of the AAA to the rest of the aorta. The thrombus was uniformly distributed with a thickness of 1 mm, and the wall was modeled with a uniform thickness of 1.5 mm. The outer radii of the wall at the middle and top of the AAA were 25.68 mm and 10.5 mm, respectively. The linear model was employed to compute wall stresses for both AAA models, E_{wall} = 8.4x10^9 N/mm^2; E_{ILT} = 1.25x10^9 N/mm^2. Effective wall stresses (in units of N/mm^2) are shown as computed in the axisymmetric curved models of an AAA in the absence and presence of a thrombus (left). Differences in the effective wall stress in the AAA-ILT model with respect to those of the ILT-free AAA are shown on the right. Including a thin, uniform thrombus in the FEA model attenuated the wall stresses slightly.